National Technical University of Athens

School of Mechanical Engineering
Fluids Department
Parallel CFD & Optimization Unit

Contribution to the Continuous Adjoint Method Applied to Shape Optimization in Turbulent Flows

Master Thesis
"Computational Mechanics
Joint Postgraduate Course"

Themistoklis Skamagkis

Supervisor:
Kyriakos C. Giannakoglou, Professor NTUA

Athens, January 2019

National Technical University of Athens
School of Mechanical Engineering
Fluids Department
Parallel CFD & Optimization Unit

Contribution to the Continuous Adjoint Method Applied to Shape Optimization in Turbulent Flows

Master Thesis
"Computational Mechanics
Joint Postgraduate Course"

Themistoklis Skamagkis

Supervisor: Kyriakos C. Giannakoglou, Professor NTUA

The scope of this thesis is to, firstly, investigate the existing continuous adjoint solver's capabilities in shape optimization problems concerning turbulent flows in simulations carried out using high-Re meshes, and secondly, to investigate possible extensions of the formulation/code in order to improve the accuracy of the computed sensitivity derivatives (SD). The adjoint solver has been developed by the PCOpt/NTUA within the OpenFOAM framework.

Applications are performed in external and internal aerodynamics, for incompressible flows. Turbulence was modelled using the Spalart-Allmaras turbulence model alongside Spalding's one-equation formula for the near-wall modelling of the flow on coarse (high-Re) meshes. The formulation of the adjoint to the high-Re Spalart-Allmaras turbulence model shows significant difficulties with regards to the differentiation of the wall function and the derivation and effective implementation of the so-called adjoint wall function. First, the adjoint solver is evaluated by comparing SD computed with the adjoint method against reference values computed using finite differences. Then, shape optimization is performed for an isolated airfoil, tagreting lift maximization and drag minimization as well as, ducts, including an industrial application (automotive application), targeting minimization of total pressure losses between the inlet and outlet. Also, the application of a boundary condition for the primal pressure, referenced in the literature as having positive a effect on the convergence of the adjoint equations, is tested. Finally, the SD expression, which contains terms resulting from the differentiation of the wall function, is revisited and the effect of a specific geometric term in the SD is investigated.

Εθνικό Μετσόβιο Πολυτεχνείο
Σχολή Μηχανολόγων Μηχανικών
Τομέας Ρευστών
Μονάδα Παράλληλης ΥΡΔ & Βελτιστοποίησης

Συνεισφορά στη Συνεχή Συζυγή Μέθοδο με Εφαρμογές στη Βελτιστοποίηση Μορφών σε Τυρβώδεις Ροές

Μεταπτυχιακή εργασία
''ΔΠΜΣ Υπολογιστική Μηχανική''

Θεμιστοκλής Σκαμάγκης

Επιβλέπων: Κ. Χ. Γιαννάκογλου, Καθηγητής ΕΜΠ

Σκοπός της μεταπτυχιακής εργασίας είναι πρωτίστως η διερεύνηση των δυνατοτήτων του υπάρχοντα συνεχούς συζυγούς επιλύτη σε εφαρμογές που αφορούν τη βελτιστοποίηση αεροδυναμικών μορφών σε πλέγματα όπως αυτά που χρησιμοποιούνται για την πρόλεξη τυρβωδών ροών με χρήση συναρτήσεων τοίχου, και, στη συνέχεια, η συνεισφορά στην επέκταση του συνεχούς συζυγούς επιλύτη με σκοπό τη βελτίωση της ακρίβειας των παραγώγων ευαισθησίας. Ο επιλύτης της συζυγούς ροής έχει αναπτυχθεί κατά την τελευταία 15ετία από τη ΜΠΥΡΒ/ΕΜΠ σε περιβάλλον OpenFOAM.

Πραγματοποιούνται εφαρμογές σε προβλήματα εξωτερικής και εσωτερικής αεροδυναμικής για ασυμπίεστες ροές. Η μοντελοποίηση της τύρβης έγινε με το μοντέλο των Spalart-Allmaras κάνοντας χρήση συναρτήσεων τοίχου, χρησιμοποιώντας κατάλληλα (όχι ιδιαίτερα πυκνά) πλέγματα, αυτά που συνήθως αναφέρονται ως πλέγματα υψηλών αριθμών Reynolds της τύρβης. Η μαθηματική διατύπωση του συζυγούς του μοντέλου Spalart-Allmaras παρουσιάζει ιδιαίτερες δυσκολίες που προκύπτουν από τη διαφόριση της συνάρτησης τοίχου και την ενσωμάτωση της επονομαζόμενης συζυγούς συνάρτησης τοίχου. Αρχικά, γίνεται επικύρωση του συζυγούς επιλύτη με σύγκριση παραγώγων ευαισθησίας που υπολογίζονται με τη συζυγή μέθοδο έναντι πεπερασμένων διαφορών. Έπειτα, γίνεται βελτιστοποίηση μεμονωμένης αεροτομής με στόχο τη μεγιστοποίηση της άνωσης και ελαχιστοποίηση οπισθέλκουσας και αγωγών, συμπεριλαμβανομένης και μιας βιομηχανικής εφαρμογής (της αυτοκινητοβιομηχανίας), με στόχο την ελάχιστη πτώση ολικής πίεσης μεταξύ εισόδου και εξόδου. Επίσης, γίνεται διερεύνηση των αποτελεσμάτων από την εφαρμογή μιας ανώτερης τάξης, από την υφιστάμενη στο OpenFOAM, οριακής συνθήκης για την πίεση η οποία, σύμφωνα με τη βιβλιογραφία, μπορεί να επιδράσει θετικά στη σύγκλιση των συζυγών εξισώσεων. Εδώ, πέρα από τη σύγκλιση διερευνάται, και η επίπτωση που έχει στην ακρίβεια των παραγώγων ευαισθησίας. Τέλος, επανεξετάζεται η έκφραση των παραγώγων ευαισθησίας, η οποία περιλαμβάνει όρους που προέρχονται από τη διαφόριση της συνάρτησης τοίχου, με έμφαση στην επίδραση ενός από τους όρους που την αποτελούν.

Acronyms

CFD	Computational Fluid Dynamics
NTUA	National Technical University of Athens
PCopt	Parallel CFD & Optimization unit
SD	Sensitivity Derivatives
FD	Finite Differences
BC	Boundary Condition
ATC	Transpose Convection Term

ΕΜΠ	Εθνικό Μετσόβιο Πολυτεχνείο
ΕΘΣ	Εργαστήριο Θερμικών Στροβιλομηχανών
ΜΠΥΡΒ	Μονάδα Παράλληλης Υπολογιστικής Ρευστοδυναμικής & Βελτιστοποίησης
ΥΡΔ	Υπολογιστική Ρευστοδυναμική

Contents

Chapter 1

Introduction

The use of CFD simulations, as an auxilliary tool, in industrial applications is gaining increasing attention in recent years. The majority of computational codes have matured, through years of research and refinement, and as a result CFD has gained credibility as a design tool for industrial products. In an attempt to adopt an integrated approach to product design, focus has shifted towards CFD-based optimization methods, with the overall goal being the improvement of products with minimal cost. In the present thesis, shape-optimization problems are of concern, wherein the goal is to find the shape of a component that yields an optimal desired quality in cases governed by the flow equations, hence the title: *CFD-based* optimization.

1.1 Shape Optimization

In shape optimization problems the optimal shape that is sought-after is controled by a number of design variables. By utilizing aspects of control theory and applying them to shape optimization the problem at hand is stated as seeking the optimal configuration of design variables that will yield the optimal shape. This process is driven by evaluating a quality of the flow that one seeks to minimize/maximize and which, from a mathematical viewpoint, is a function of the flow variables. This is called the objective function in shape optimization problems and usually, it is an integral defined along a boundary of the computational domain or over a specific volume inside the domain. As an example, consider the case of a duct flow, where the shape of the duct is parameterized using Bézier curves, and it is desirable to minimize the total pressure losses between the inlet and outlet of the duct. The design variables are the coordinates of the control points and the objective function

is the total pressure losses.

Two great categories of optimization methods exist, stochastic and deterministic. In deterministic optimization the algorithm is driven towards producing an improved shape by computing the gradient of the objective function w.r.t. to the design variables, also known as the sensitivity derivatives (SD). Based on this information the algorithm updates the values of the design variables in order to produce an improved shape and then march in the direction pointed to by the afforementioned gradient. At this point, a solution of the flow equations takes place, followed by an evaluation of the objective function's value and the process is repeated again until an optimized solution is obtained. Such an algorithm showcases increased efficiency because the direction in which the shape should be driven to is dictated by the gradient. One of the shortcomings of deterministic methods though, is their entrapment in local minima/extrema, since the values of the SD tend to zero close to those locations.

The question that arises is how are the SD ultimately computed. The most straightforward way of computing SD is through finite differences (FD), a computation performed by perturbating the objective function around each design variable $b_n, n \in [1, N]$ where N is the total number of design variables. Using a second-order scheme,

$$\frac{\delta F}{\delta b_n} = \frac{F(b_1, ..., b_n + \epsilon, ..., b_N) - F(b_1, ..., b_n - \epsilon, ..., b_N)}{2\epsilon} \tag{1.1}$$

The usage of FD poses significant concerns. First, there is uncertainty in the decision of an adequate value for ϵ since in fact, different values of ϵ may yield different results and there is no way to a priori determine a threshold for ϵ . Choosing a very small value for ϵ without consideration is not a viable option as it can result to round-off errors. Also, the flow equations must be fully converged as the subtraction performed in eq. 1.1 is between two very close values of F. A most serious issue though is the implications of the method, when it is applied to large scale problems, as the computation of the gradient needs $2 \times N$ evaluations of F by solving the flow equations; an infeasible scenario. An alternative to the FD method is the complex variables method where SD are computed as

$$\frac{\delta F}{\delta b_n} = \frac{Im[F(b_1, ..., b_n + i\epsilon, ..., b_N)]}{\epsilon} \tag{1.2}$$

where Im is the imaginary part of a function and $i = \sqrt{-1}$. This method is not as sensitive to the value of ϵ and it costs N number of evaluations. One other alternative, that is insensitive to the value of ϵ, as opposed to the FD method, is the direct differentiation method in which the flow equations are differentiated w.r.t. b_n. This differentiation results in N linear systems (as many as the design variables) whose solution yields the derivatives of flow variables w.r.t. to the design variables. Knowledge of these derivatives allows the computation of SD for the objective function at

hand. Direct differentiation is inevitably inadequate for large scale simulations as it depends upon the total number of design variables.

1.2 The Adjoint Method

There is one method for computing SD that is independent of N. This is the adjoint method. In this method, an augmented function is defined, by adding the flow equation residuals to the existing objective function. Inside the framework of the adjoint method, the flow equations are called the *primal* equations. The residuals are multiplied by the adjoint variable fields. After differentiating the objective function and rearranging the terms that exist in its expression, an adjoint system of equations is formulated, that once satisfied, the values of the SD can be obtained at a cost that is independent of N. In light of the above, there are two approaches that can be followed for the formulation of the adjoint equations. In *discrete* adjoint, the augmented function contains the discretized forms of the primal equations residuals and, thus, the differentiation of the objective function occurs on a discrete level. In *continuous* adjoint the primal equations are present in their continuous form and are discretized after the differentiation takes place. The two methods pose certain shortcomings and benefits, the most characteristic being that the discrete adjoint is more accurate in computing SD computationally more expensive [1, 2]. On the other hand, using continuous adjoint, there is a great challenge in accurately differentiating the flow equations, especially when using wall functions.

This thesis is concerned with the continuous variant of the adjoint equations in turbulent flows. When formulating the adjoint equations, a frequently made assumption is that the turbulence variables do not change w.r.t. the design variables. Such an assumption, also known as the "frozen turbulence" assumption can lead to significant errors in the computation of the SD. The turbulence variables can have an important contribution to the computation of SD, as has already been demonstrated in the literature [3, 4, 5]. Furthermore, the differentiation of the primal equations solved on high-Reynolds (not that fine) meshes poses an increased challenge because of the use of wall functions that also need to be differentiated [5, 3]. Adjoint methods that include the differentiation of turbulence models have already been developed at the Parallel CFD & Optimization Unit of the National Technical University of Athens (PCOpt/NTUA). The differentiation of the Spalart-Allmaras turbulence model was presented for the first time in Zymaris et al. [6] for low-Re meshes as well as the high-Re $k-\epsilon$ model [7], where the concept of adjoint wall functions was introduced for the first time. The differentiation of the $k-\epsilon$ turbulence model was extended to low-Re meshes in [8] and the adjoint to the high-Re Spalart-Allmaras turbulence model was presented for the first time in [3].

The adjoint solver that has been developed by PCOpt/NTUA has been implemented within the OpenFOAMframework. OpenFOAM (Open Source Field Operation and Manipulation) is a collection of C++ libraries developed primarily for computational fluid dynamics [9]. Based on the C++ language it boasts an array of usefull object oriented programming features that allow for code modularity and easy implementation of different objective functions and discretization schemes. Finally, the scope of this thesis is to investigate the existing capabilities of the optimization software in turbulent flows and specifically on high-Reynolds meshes where wall functions are used. Furthermore, the addition of certain terms in the SD computation has been implemented and tested.

Chapter 2

The Finite Volume Method in OpenFOAM

In this chapter, the flow (primal) equations for steady-state incompressible flows are presented, followed by a brief introduction to the finite volume method, for their discretization, as implemented in OpenFOAM. Focus is laid on the various discretization schemes used by the code.

2.1 Governing Flow Equations

The motion of a fluid is described by a set of partial differential equations (PDEs) known as the Navier-Stokes equations. These equations are derived from the application of conservation laws over a differential control volume within the flow domain. The resulting equations, referred to as the primal equations in the optimization problem, are presented below.

2.1.1 Continuity Equation

By applying the law of mass conservation over a differential control volume one can derive the continuity equation,

$$\frac{\partial \rho}{\partial t} + \frac{\partial (\rho v_i)}{\partial x_i} = 0 \tag{2.1}$$

where v_i and ρ are the fluid velocity components and density, respectively. For an incompressible fluid, the above equation is simplified to

$$\frac{\partial v_i}{\partial x_i} = 0 \tag{2.2}$$

2.1.2 Conservation of Momentum Equation

The momentum conservation equations are

$$\frac{\partial(\rho v_i)}{\partial t} + \frac{\partial\left(\rho v_i v_j\right)}{\partial x_j} = \frac{\partial}{\partial x_j}\left[\mu_{eff}\left(\frac{\partial v_i}{\partial x_j}+\frac{\partial v_j}{\partial x_i}\right)-\frac{2}{3}\mu_{eff}\frac{\partial v_i}{\partial x_i}\delta_{ij}\right]-\frac{\partial p}{\partial x_i} \quad , \quad i=1,2(,3) \tag{2.3}$$

where p is the pressure and μ_{eff} is the effective viscosity. In laminar flows, μ_{eff} is the bulk viscosity μ while in turbulent flows, it is the sum of the bulk and eddy viscosity μ_t. Combining eqs. 2.2 with 2.3 and assuming a steady state incompressible flow, the above equation is rewritten as

$$v_j\frac{\partial v_i}{\partial x_j}=\frac{\partial}{\partial x_j}\left[\nu_{eff}\left(\frac{\partial v_i}{\partial x_j}+\frac{\partial v_j}{\partial x_i}\right)\right]-\frac{\partial p}{\partial x_i} \quad , \quad i=1,2(,3) \tag{2.4}$$

Equation 2.4 has been divided by ρ and so p, from now on, denotes the quantity $\frac{p}{\rho}$ and ν_{eff} the effective kinematic viscocity. In the present study, only steady state incompressible flows are of concern. From this point onwards, any reference to the Navier-Stokes equations will be pointing to eqs. 2.2 and 2.4.

2.1.3 Spalart-Allmaras Turbulence Model

Modelling of turbulence is performed using the Spalart-Allmaras one-equation model [10] which solves the transport equation presented below for the turbulence variable $\widetilde{\nu}$,

$$v_j\frac{\partial\widetilde{\nu}}{\partial x_j}-\frac{\partial}{\partial x_j}\left[\left(\nu+\frac{\widetilde{\nu}}{\sigma}\right)\frac{\partial\widetilde{\nu}}{\partial x_j}\right]-\frac{c_{b2}}{\sigma}\left(\frac{\partial\widetilde{\nu}}{\partial x_j}\right)^2-\widetilde{\nu}\,P\left(\widetilde{\nu}\right)+\widetilde{\nu}\,D\left(\widetilde{\nu}\right)=0 \tag{2.5}$$

The eddy viscosity coefficient ν_t relates to $\widetilde{\nu}$ as

$$\nu_t = \widetilde{\nu} f_{v_1} \tag{2.6}$$

The production and dissipation terms are given by

$$P(\widetilde{\nu}) = c_{b1}\widetilde{Y} \ , \qquad D(\widetilde{\nu}) = c_{w1} f_w(\widetilde{Y}) \frac{\widetilde{\nu}}{\Delta^2} \tag{2.7}$$

and $\widetilde{Y}$ is computed through

$$\widetilde{Y} = Y f_{v3} + \frac{\widetilde{\nu}}{\Delta^2 \kappa^2} f_{v2} \ , \qquad Y = \left| e_{ijk} \frac{\partial v_k}{\partial x_j} \right| \tag{2.8}$$

where Y stands for the vorticity magnitude and Δ is the distance from the wall boundaries. The model functions read

$$\begin{aligned}
f_{v_1} &= \frac{\chi^3}{\chi^3 + c_{v_1}^3} \ , \quad f_{v_2} = \frac{1}{\left(1 + \frac{\chi}{c_{v_2}}\right)^3} \\
f_{v_3} &= \frac{(1 + \chi f_{v1})}{c_{v2}} \left[3\left(1 + \frac{\chi}{c_{v2}}\right) + \left(\frac{\chi}{c_{v2}}\right)^2 \right] \left(1 + \frac{\chi}{c_{v2}}\right)^{-3} \\
\chi &= \frac{\widetilde{\nu}}{\nu} \ , \quad f_w = g \left(\frac{1 + c_{w_3}^6}{g^6 + c_{w_3}^6} \right)^{1/6} \\
g &= r + c_{w_2}(r^6 - r) \ , \quad r = \frac{\widetilde{\nu}}{\widetilde{Y} \kappa^2 \Delta^2}.
\end{aligned} \tag{2.9}$$

The constants of the model are $c_{b1} = 0.1355$, $c_{b2} = 0.622$, $\kappa = 0.41$, $\sigma = 2/3$, $c_{w1} = \frac{c_{b1}}{\kappa^2} + \frac{(1+c_{b2})}{\sigma}$, $c_{w2} = 0.3$, $c_{w3} = 2$, $c_{v1} = 7.1$ and $c_{v2} = 5$. The Levi–Civita symbol, e_{ijk}, used in the vorticity magnitude, is

$$e_{ijk} = \begin{cases} +1 & (i,j,k) \in (1,2,3),\ (2,3,1),\ (3,1,2) \\ -1 & (i,j,k) \in (1,3,2),\ (3,2,1),\ (2,1,3) \\ 0 & i = j,\ j = k,\ k = i \end{cases} \tag{2.10}$$

In meshes which are not appropriately fine close to the solid walls (i.e. meshes used along with the wall function technique; these are usually referred to as meshes for high turbulent Reynolds number simulations or high-Re meshes in short), the computation of the normal (to the wall) derivative of the velocity, using finite differences, or any equivallent formula, is prone to important errors. This is due to the first cell center next to the wall (here, a cell-centered finite volume storage is used) being outside the viscous sublayer, lying within the log-law region, wherein velocity increases logarithmically with the distance from the wall. The wall function, that must be used in such a case, models the behaviour of the flow in the logarithmic area of the near-wall region of the flow, using empirical information, and this should

be used instead of the differentiation schemes.

The wall function technique, as programmed in OpenFOAM, makes use of the Spalding Wall Function [11] described by the equation

$$f_{WF} = y^+ - v^+ - e^{-\kappa B}\left[e^{\kappa v^+} - 1 - \kappa v^+ - \frac{(\kappa v^+)^2}{2} - \frac{(\kappa v^+)^3}{6}\right] = 0 \tag{2.11}$$

where the non-dimensional distance and velocity at cell-centre P at a distance Δ^P from the wall are,

$$y_P^+ = \frac{\Delta^P v_\tau}{\nu} \quad , \quad v_P^+ = \frac{|v_i|^P}{v_\tau} \tag{2.12}$$

Also, v_τ is the friction velocity, computed by

$$v_\tau^2 = -\left[(\nu + \nu_t)\left(\frac{\partial v_i}{\partial x_j} + \frac{\partial v_j}{\partial x_i}\right)\right]^f n_j t_i^I \tag{2.13}$$

where n_j and t_i^I are the normal to the wall and the parallel to the velocity at the first cell P (which is considered to be parallel to the wall) unit vectors. In eq. 2.11, $\kappa = 0.41$ is the von-Karman constant and $B \approx 5.5$. In eqs. 2.12 and 2.13, indices f and P denote quantities defined at the boundary wall face and the first cell centre off this boundary face, respectively.

In OpenFOAM, the viscous flux at this boundary face is computed through finite differences, namely

$$-\left[(\nu+\nu_t)\left(\frac{\partial v_i}{\partial x_j}+\frac{\partial v_j}{\partial x_i}\right)\right]^f n_j \approx -\left(\nu+\nu_t^f\right)\frac{v_i^f - v_i^P}{|Pf|} \tag{2.14}$$

Such a computation, as stated above, is prone to errors on a coarse mesh and ultimately results in a miscalculation of the velocity gradient close to the wall. As a remedy to this problem, the method proceeds with the computation of non-zero ν_t^f on the wall (at the aforesaid wall face) based on which the viscous flux across the boundary face is corrected.

$$\nu_t^f = -\frac{v_\tau^2}{\left(\frac{\partial v_i}{\partial x_j} + \frac{\partial v_j}{\partial x_i}\right)^f n_j t_i^I} - \nu \approx -|Pf|\frac{v_\tau^2}{(v_i^f - v_i^P)t_i^I} - \nu = |Pf|\frac{v_\tau^2}{v_i^P t_i^I} - \nu \tag{2.15}$$

The friction velocity involved in eq. 2.15 is calculated by solving the non-linear eq. 2.11 for v_τ using the Newton-Raphson method.

2.1.4 Integration of the Navier-Stokes Equations with the Finite Volume Method

The aforementioned flow equations are integrated over the fluid domain. Integrating the continuity, momentum and Spalart-Allmaras turbulence model equations, over a finite volume V, results to the expressions below,

$$\int_V \frac{\partial v_i}{\partial x_i} dV = 0 \tag{2.16a}$$

$$\int_V v_j \frac{\partial v_i}{\partial x_j} dV - \int_V \frac{\partial}{\partial x_j}\left[\nu\left(\frac{\partial v_i}{\partial x_j} + \frac{\partial v_j}{\partial x_i}\right)\right] dV + \int_V \frac{\partial p}{\partial x_i} dV = 0 \quad , \quad i = 1, 2(, 3) \tag{2.16b}$$

$$\int_V v_j \frac{\partial \widetilde{\nu}}{\partial x_j} dV - \int_V \frac{\partial}{\partial x_j}\left[\left(\nu + \frac{\widetilde{\nu}}{\sigma}\right)\frac{\partial \widetilde{\nu}}{\partial x_j}\right] dV - \int_V \frac{c_{b2}}{\sigma}\left(\frac{\partial \widetilde{\nu}}{\partial x_j}\right)^2 dV$$
$$- \int_V \widetilde{\nu}\, P\left(\widetilde{\nu}\right) dV + \int_V \widetilde{\nu}\, D\left(\widetilde{\nu}\right) dV = 0 \tag{2.16c}$$

The finite volume method is used to approximate the solution to a system of PDEs. At a preliminary stage, the continuous domain is split into a finite number of partitions, called control volumes, upon which the conservation laws of mass and momentum are applied. This process of splitting the domain is called domain or spatial discretization and yields a grid of points where the values of the flow variables are stored. In this regard, there are two approaches that can generally be followed. A cell-centered or a vertex-centered approach with each name pertaining to where the variable values are stored: either at the centroids of control volumes or their vertices. OpenFOAM exclusively relies upon cell-centered storage.

In essence, the discretized form of eqs. 2.16a, 2.16b and 2.16c are solved for every control volume. The volume integrals of divergence terms in this equation are transformed into surface integrals along the faces of each control volume. Through this process a system of algebraic equations is obtained that can be solved numerically. The discretization scheme of the volume integrals in this equation are of significant importance. Finally, the way these integrals are handled in OpenFOAMis described in the next section along with the schemes that are used for the interpolation of the variables at the faces of control volumes.

2.2 Implementation in OpenFOAM- Description of Main Discretization Schemes

In order to best describe the discretization schemes employed by OpenFOAMa general transport equation is considered for an arbitrary variable ϕ in steady state incompressible flows,

$$\int_V \frac{\partial(v_j\phi)}{\partial x_j}dV - \int_V \frac{\partial}{\partial x_j}\left[D^\phi \frac{\partial \phi}{\partial x_j}\right]dV + \int_V f^\phi dV \;=\; 0 \tag{2.17}$$

where D^ϕ is the diffusion coefficient and f^ϕ includes source terms.

In order to discretize the first two volume integrals that both contain the divergence operator, the Green-Gauss divergence theorem is used,

$$\int_V \frac{\partial F_i}{\partial x_i}dV = \oint_{\partial V} F_i n_i dS \tag{2.18}$$

where n_i is the unit vector normal to the finite volume boundary pointing outwards. The resulting surface integral results from the summation of surface integrals over the faces of the control volume. Each surface integral is then approximated by multiplying the flux of vector F_i, computed on the face centroid, with the face area and projecting it onto n_i, resulting to

$$\int_V \frac{\partial F_i}{\partial x_i}dV = \sum_{f=1}^{N_f} F_i^f n_i^f S^f \tag{2.19}$$

where S^f is the face area and F_i^f is defined at the centroid of each cell face. N_f is the total number of faces that surround a cell.

2.2.1 Interpolation at the Finite Volume Faces

During the discretization process, variables have to be interpolated at the faces separating two neighbour cells. A face is shared by two cells and, in the code, the one with the lower cell number, is the owner of the face and the other is referred to as the neighbour. Index P denotes the face owner cell and N the neighbour cell. The normal to the face unit vector n_i is pointing from P to N.

The most general interpolation scheme used for a quantity ϕ calculated at the face

of a cell is

$$\phi_f \;=\; \omega_f \phi_P + (1-\omega_f)\phi_N \tag{2.20}$$

In case of linear interpolation, the interpolation weight ω_f is calculated as

$$\omega_f \;=\; \frac{\vec{d}_{Nf}\cdot\vec{S}_f}{\vec{d}_{Pf}\cdot\vec{S}_f + \vec{d}_{fN}\cdot\vec{S}_f} \tag{2.21}$$

where $\vec{d}_{Pf}$ is the vector that joins the owner cell center P to the face center f and vector $\vec{d}_{fN}$ the face center f to the neighbour cell center P, respectively. Vector $\vec{S}$ is equall to $S\vec{n}$.

2.2.2 Gradient Discretization

For the computation of the gradient at a cell centroid P, the mean value theorem is used, in addition to eq. 2.19,

$$\overline{\frac{\partial\phi}{\partial x_j}}\bigg|_C V \;=\; \int_V \frac{\partial\phi}{\partial x_j} dV \tag{2.22}$$

and, finally, the gradient of ϕ at the cell centroid P is computed as

$$\overline{\frac{\partial\phi}{\partial x_j}}\bigg|_C \;=\; \frac{1}{V_P}\sum \phi_f S_j^f \tag{2.23}$$

where ϕ_f is computed using eq. 2.20. Through this method, it is assumed that the gradient at the cell centroid is equal to the average gradient over the control volume.

2.2.3 Convection Term

Using eq. 2.19, the convection term of the general transport equation is discretized as

$$\int_V \frac{\partial(v_j\phi)}{\partial x_j} dV = \sum_{f=1}^{N_f} (v_j\phi)^f n_j^f S^f \tag{2.24}$$

Two main interpolation schemes are effectively used for the calculation of ϕ at the cell faces. Using a first order upwind scheme, the value of ϕ at the face centroid of

a cell is

$$\begin{aligned} \phi_f &= \phi_P \quad if \quad \dot{m}_f \ > \ 0 \\ \phi_f &= \phi_N \quad if \quad \dot{m}_f \ < \ 0 \end{aligned} \tag{2.25}$$

A second-order upwind scheme can also be used that also takes into account the gradient of ϕ at the cell centroid,

$$\begin{aligned} \phi_f &= \phi_P + \left.\frac{\partial \phi}{\partial x_j}\right|_P \Delta_j \quad if \quad \dot{m}_f \ > \ 0 \\ \phi_f &= \phi_N + \left.\frac{\partial \phi}{\partial x_j}\right|_N \Delta_j \quad if \quad \dot{m}_f \ < \ 0 \end{aligned} \tag{2.26}$$

where Δ_j is the vector joining the cell-center (be it the owner or the neighbour cell) to the face center and $\dot{m}_f$ is the volume flux $(v_j n_j S)^f$ entering or leaving the control volume through the cell face. In OpenFOAM, this quantity is stored as a field that is computed by the SIMPLE algorithm during the pressure correction loop.

2.2.4 Diffusion Term

The integral containing the diffusion term is discretized as

$$\int_V \frac{\partial}{\partial x_j}\left[D^\phi \frac{\partial \phi}{\partial x_j}\right] dV = \sum_{f=1}^{N_f} \left[D^\phi \frac{\partial \phi}{\partial x_j}\right]^f n_j^f S^f \tag{2.27}$$

Note that the normal to the face directional derivative of ϕ, i.e. $\frac{\partial \phi}{\partial x_j} n_j$, is the one required. However, in a non-orthogonal unstructured mesh, the unit normal vector $\vec{n}$ may not be aligned with the vector that joins the two centroids of the elements straddling the face. For this reason, the surface vector S_j^f is split into two components

$$S_j^f = E_j^f + T_j^f \tag{2.28}$$

with vector T_j chosen to be perpendicular to S_j and E_j aligned with the vector connecting the two cell centers. The overall arangement is shown in fig. 2.1. From this point onwards, f, i.e. the index denoting quantities computed over the face of a cell, is dropped for simplicity of notation.

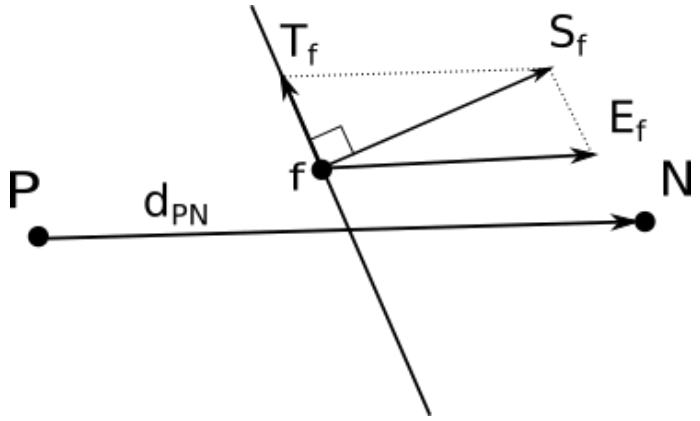

Figure 2.1: *Arrangement of vectors $\vec{S}_f$, $\vec{E}_f$ and $\vec{T}_f$. Vector $\vec{d}_{PN}$ joins the two cell-centers straddling the face f. Vector $\vec{S}_f$ is the surface normal vector (i.e. $\vec{n}S_f$ where S_f is the surface area). $\vec{E}_f$ is aligned with vector $\vec{d}_{PN}$ and $\vec{T}_f$ is perpendicular to $\vec{S}_f$.*

We, thus, get the following expression for the gradient

$$\left(\frac{\partial\phi}{\partial x_j}S_j\right)_f = \left(\frac{\partial\phi}{\partial x_j}\right)_f E_j + \left(\frac{\partial\phi}{\partial x_j}\right)_f T_j \tag{2.29}$$

The first term on the r.h.s. of eq. 2.29 is called the orthogonal part while the second term the non-orthogonal part. The computation of the first term is straightforward, since

$$e_j = \frac{(d_{PN})_j}{\left|\vec{d}_{PN}\right|} \quad and \quad E_j = |\vec{E}|e_j \tag{2.30}$$

meaning that

$$E_j = |\vec{E}|\frac{(d_{PN})_j}{\left|\vec{d}_{PN}\right|} \tag{2.31}$$

and, so, substituting E_j with the above expression results to

$$\left(\frac{\partial\phi}{\partial x_j}\right)_f E_j \;=\; |\vec{E}|\frac{\partial\phi}{\partial e} \;=\; |\vec{E}|\frac{\phi_P - \phi_N}{\left|\vec{d}_{PN}\right|} \tag{2.32}$$

Taking the dot product of S_j with eq. 2.28 the following expression is obtained (considering that $S_jT_j = 0$),

$$S_jS_j = E_jS_j \tag{2.33}$$

thus,

$$E_j S_j = |\vec{E}| \frac{(d_{PN})_j}{\left|\vec{d}_{PN}\right|} S_j \Rightarrow$$

$$\frac{(d_{PN})_j}{\left|\vec{d}_{PN}\right|} = \frac{E_j S_j}{(d_{PN})_i S_i} = \frac{S_j S_j}{(d_{PN})_i S_i} \tag{2.34}$$

Folowing this analysis, a final expression for the orthogonal term of eq. 2.29 is obtained

$$\left(\frac{\partial \phi}{\partial x_j}\right)_f E_j \;=\; (\phi_P - \phi_N) \frac{S_j S_j}{S_i \, (d_{PN})_i} \tag{2.35}$$

The non-orthogonal term is computed by taking into account that $T_j = S_j - E_j$.

$$\left(\frac{\partial \phi}{\partial x_j} T_j\right)_f = \left(\frac{\partial \phi}{\partial x_j}\right)_f S_j - \left(\frac{\partial \phi}{\partial x_j}\right)_f E_j = \overline{\frac{\partial \phi}{\partial x_j}}\bigg|_f \left(S_j \;-\; \frac{S_k S_k}{S_i \, (d_{PN})_i} (d_{PN})_j\right) \tag{2.36}$$

Now, the gradient of ϕ (i.e. $\overline{\frac{\partial \phi}{\partial x_j}}\Big|_f$) is calculated at the cell centers of the two elements straddling the face and is interpolated to the face using eq. 2.2.1.

Chapter 3

The Continuous Adjoint Method for Turbulent Flows

3.1 Primal Equations

The primal equations are the steady-state, Reynolds-Averaged Navier-Stokes for incompressible fluids, practically eqs. 2.2, 2.4 and 2.5. In residual form, the governing equations are written as

$$R^p = -\frac{\partial v_j}{\partial x_j} = 0 \tag{3.1a}$$

$$R_i^v = v_j \frac{\partial v_i}{\partial x_j} - \frac{\partial}{\partial x_j}\left[(\nu + \nu_t)\left(\frac{\partial v_i}{\partial x_j} + \frac{\partial v_j}{\partial x_i}\right)\right] + \frac{\partial p}{\partial x_i} = 0\ , \qquad i = 1, 2(, 3) \tag{3.1b}$$

$$R^{\widetilde{\nu}} = v_j \frac{\partial \widetilde{\nu}}{\partial x_j} - \frac{\partial}{\partial x_j}\left[\left(\nu + \frac{\widetilde{\nu}}{\sigma}\right)\frac{\partial \widetilde{\nu}}{\partial x_j}\right] - \frac{c_{b2}}{\sigma}\left(\frac{\partial \widetilde{\nu}}{\partial x_j}\right)^2 - \widetilde{\nu}\, P\left(\widetilde{\nu}\right) + \widetilde{\nu}\, D\left(\widetilde{\nu}\right) = 0 \tag{3.1c}$$

accompanied by the appropriate boundary conditions (BC). These are described in section 3.6 for external and internal aerodynamics.

3.2 Objective Function

Let F be the objective function to be minimized and $b_n, n \in [1, N]$ the vector of design variables w.r.t. which the sensitivities of F must be computed, using the

continuous adjoint method. In the present study, two different optimization problems are investigated, the minimization of total pressure losses in duct flows and the maximization/minimization of a force exerted on an airfoil.

3.2.1 Total Pressure Losses

The volume-averaged pressure losses between the inlet and outlet boundaries of the fluid domain are given by

$$\begin{aligned} F_{Pt} =& \int_{S_I} F_{S_{I,i}} n_i dS - \int_{S_O} F_{S_{O,i}} n_i dS \\ =& - \int_{S_I} \left(p + \frac{1}{2} v_m^2 \right) v_i n_i dS - \int_{S_O} \left(p + \frac{1}{2} v_m^2 \right) v_i n_i dS \end{aligned} \tag{3.2}$$

where n_i are the components of the outwards pointing unit normal vector. S_I and S_O denote the inlet and outlet boundaries respectively.

3.2.2 Force Exerted on a Body in Free Flow

A force exerted on the surface of an aerodynamic body, in an arbitrary direction $\vec{r}$, is given by the expression

$$F_L = \int_S \left[-(\nu + \nu_t) \left(\frac{\partial v_i}{\partial x_j} + \frac{\partial v_j}{\partial x_i} \right) + p \delta_i^j \right] n_j r_i dS \tag{3.3}$$

For the case of flow around an airfoil, choosing $\vec{r}$ to point in the direction perpendicular to the farfield flow, and upwards, will result in eq. 3.3 calculating the airfoil lift. It is desirable to maximize the airfoil lift, however, as the implemented shape optimization algorithm aims at minimizing an objective function, $\vec{r}$ is chosen to point downwards. Similarly, choosing the direction of $\vec{r}$ to be parallel to the farfield flow will result in eq. 3.3 expressing the drag force exerted on the airfoil.

3.3 Formulation of the Field Adjoint Equations

For the derivation of the field adjoint equations, an augmented objective function is defined by taking advantage of the fact that the residuals of the primal equations

are equal to zero as shown in section 3.1.

$$F_{aug} = F + \int_V u_i R_i^v dV + \int_V q R^p dV + \int_V \widetilde{\nu_a} R^{\widetilde{\nu}} dV \tag{3.4}$$

The multipliers of the aforementioned residuals are called the adjoint variables, namely u_i, the adjoint velocity, q the adjoint pressure and $\widetilde{\nu_a}$ the adjoint turbulence variable. In contrast to the assumption made by the majority of people developing continuous adjoint methods for turbulent flows, who make the assumption that changes in the design variables do not affect the eddy viscosity field (frozen turbulence assumption), it is herein considered that turbulence variations are important [5, 3, 4]. This is why the turbulence model equation has been added to the augmented objective function defined in eq. 3.4.
Differentiating the expression of the augmented function in 3.4 w.r.t. the design variables yields,

$$\begin{aligned} \frac{\delta F_{aug}}{\delta b_n} = \frac{\delta F}{\delta b_n} + \int_V \left(u_i \frac{\delta R_i^v}{\delta b_n} + q \frac{\delta R^p}{\delta b_n} + \widetilde{\nu_a} \frac{\delta R^{\widetilde{\nu}}}{\delta b_n} \right) dV \\ + \int_V \left(u_i R_i^v + q R^p + \widetilde{\nu_a} R^{\widetilde{\nu}} \right) \frac{\delta (dV)}{\delta b_n} \end{aligned} \tag{3.5}$$

Since the residuals of the primal equations are zero over the whole domain the last integral in eq. 3.5 vanishes and the equation becomes

$$\frac{\delta F_{aug}}{\delta b_n} = \frac{\delta F}{\delta b_n} + \int_V u_i \frac{\delta R_i^v}{\delta b_n} dV + \int_V q \frac{\delta R^p}{\delta b_n} dV + \int_V \widetilde{\nu_a} \frac{\delta R^{\widetilde{\nu}}}{\delta b_n} dV \tag{3.6}$$

In order to proceed further, a very usefull mathematical relation that forms the basis for the formulation to be presented, is the following [3, 12],

$$\frac{\delta}{\delta b_n} \left(\frac{\partial \phi}{\partial x_j} \right) = \frac{\partial}{\partial x_j} \left(\frac{\delta \phi}{\delta b_n} \right) - \frac{\partial \phi}{\partial x_k} \frac{\partial}{\partial x_j} \left(\frac{\delta x_k}{\delta b_n} \right) \tag{3.7}$$

In what follows, the proof of eq. 3.7 is demonstrated. Starting point is the relation between the total and partial derivatives of quantity ϕ w.r.t. b_n, which is

$$\frac{\delta \phi}{\delta b_n} = \frac{\partial \phi}{\partial b_n} + \frac{\partial \phi}{\partial x_k} \frac{\delta x_k}{\delta b_n} \tag{3.8}$$

The notion of the total derivative is similar to the material derivative of ϕ if a variable denoting time is substituted in place of b_n. A change in b_n will cause changes in the shape/geometry and, subsequently, in the flow variables. Thus, similar to the

material derivative of ϕ, $\frac{\delta\phi}{\delta b_n}$ is the total change in ϕ due to variations of b_n. It is comprised of a quantity that takes into acount only changes in the flow variables, the local term $\frac{\partial\phi}{\partial b_n}$, and a quantity that takes into account changes in the shape or geometry i.e. $\frac{\partial\phi}{\partial x_k}\frac{\delta x_k}{\delta b_n}$. The following inequality holds true

$$\frac{\delta}{\delta b_n}\left(\frac{\partial\phi}{\partial x_j}\right) \neq \frac{\partial}{\partial x_j}\left(\frac{\delta\phi}{\delta b_n}\right) \tag{3.9}$$

On the other hand, the partial derivatives permute

$$\frac{\partial}{\partial b_n}\left(\frac{\partial\phi}{\partial x_j}\right) = \frac{\partial}{\partial x_j}\left(\frac{\partial\phi}{\partial b_n}\right) \tag{3.10}$$

The differentiation of the gradient of ϕ, w.r.t. the design variables, takes place during the derivation of the adjoint equations. However, as the constraint posed by eq. 3.9 exists, eq. 3.8 is used instead, substituting ϕ with $\frac{\partial\phi}{\partial x_j}$, resulting in

$$\begin{aligned}\frac{\delta}{\delta b_n}\left(\frac{\partial\phi}{\partial x_j}\right) &= \frac{\partial}{\partial b_n}\left(\frac{\partial\phi}{\partial x_j}\right) + \frac{\partial}{\partial x_k}\left(\frac{\partial\phi}{\partial x_j}\right)\frac{\delta x_k}{\delta b_n} \\ &= \frac{\partial}{\partial b_n}\left(\frac{\partial\phi}{\partial x_j}\right) + \frac{\partial^2\phi}{\partial x_k\partial x_j}\frac{\delta x_k}{\delta b_n}\end{aligned} \tag{3.11}$$

Taking the gradient of eq. 3.8,

$$\begin{aligned}\frac{\partial}{\partial x_j}\left(\frac{\delta\phi}{\delta b_n}\right) &= \frac{\partial}{\partial x_j}\left(\frac{\partial\phi}{\partial b_n}\right) + \frac{\partial}{\partial x_j}\left(\frac{\partial\phi}{\partial x_k}\frac{\delta x_k}{\delta b_n}\right) \\ &= \frac{\partial}{\partial x_j}\left(\frac{\partial\phi}{\partial b_n}\right) + \frac{\partial^2\phi}{\partial x_k\partial x_j}\frac{\delta x_k}{\delta b_n} + \frac{\partial\phi}{\partial x_k}\frac{\partial}{\partial x_j}\left(\frac{\delta x_k}{\delta b_n}\right)\end{aligned} \tag{3.12}$$

Subtracting eq. 3.12 from 3.11 yields eq. 3.7.

3.3.1 Differentiation of the Flow Equations

Differentiation of the Continuity Equation

Differentiation of the continuity equation residual w.r.t. to the design variables yields

$$\frac{\delta R^p}{\delta b_n} = -\frac{\delta}{\delta b_n}\left(\frac{\partial v_j}{\partial x_j}\right) = 0 \tag{3.13}$$

and the corresponding term in eq. 3.6 becomes

$$-\int_V q\frac{\delta}{\delta b_n}\left(\frac{\partial v_i}{\partial x_i}\right)dV = -\int_S qn_i\frac{\delta v_i}{\delta b_n}dS + \int_V \frac{\partial q}{\partial x_i}\frac{\delta v_i}{\delta b_n}dV + \int_V q\frac{\partial v_i}{\partial x_k}\frac{\partial}{\partial x_i}\left(\frac{\delta x_k}{\delta b_n}\right)dV \tag{3.14}$$

Differentiation of the Momentum Equations

Differentiation of the residual of the momentum equation w.r.t. b_n yields

$$\frac{\delta R_i^v}{\delta b_n} = \frac{\delta v_j}{\delta b_n}\frac{\partial v_i}{\partial x_j} + v_j\frac{\delta}{\delta b_n}\left(\frac{\partial v_i}{\partial x_j}\right) + \frac{\delta}{\delta b_n}\left(\frac{\partial p}{\partial x_i}\right) - \frac{\delta}{\delta b_n}\left\{\frac{\partial}{\partial x_j}\left[(\nu+\nu_t)\left(\frac{\partial v_i}{\partial x_j}+\frac{\partial v_j}{\partial x_i}\right)\right]\right\} = 0 \tag{3.15}$$

and the corresponding terms in eq. 3.6, on a term-by-term analysis, become

$$\begin{aligned} termA: &\int_V u_i v_j\frac{\delta}{\delta b_n}\left(\frac{\partial v_i}{\partial x_j}\right)dV + \int_V u_i\frac{\delta v_j}{\delta b_n}\frac{\partial v_i}{\partial x_j}dV \\ &= \int_S u_i v_j n_j\frac{\delta v_i}{\delta b_n}dS - \int_V \frac{\partial(u_i v_j)}{\partial x_j}\frac{\delta v_i}{\delta b_n}dV - \int_V u_i v_j\frac{\partial v_i}{\partial x_k}\frac{\partial}{\partial x_j}\left(\frac{\delta x_k}{\delta b_n}\right)dV \\ &+ \int_V u_j\frac{\partial v_j}{\partial x_i}\frac{\delta v_i}{\delta b_n}dV \end{aligned} \tag{3.16}$$

$$termB: \int_V u_i\frac{\delta}{\delta b_n}\left(\frac{\partial p}{\partial x_i}\right)dV = \int_S u_i n_i\frac{\delta p}{\delta b_n}dS - \int_V \frac{\partial u_i}{\partial x_i}\frac{\delta p}{\delta b_n}dV - \int_V u_i\frac{\partial p}{\partial x_k}\frac{\partial}{\partial x_i}\left(\frac{\delta x_k}{\delta b_n}\right)dV \tag{3.17}$$

$$\begin{aligned} termC: &-\int_V u_i\frac{\delta}{\delta b_n}\left\{\frac{\partial}{\partial x_j}\left[(\nu+\nu_t)\left(\frac{\partial v_i}{\partial x_j}+\frac{\partial v_j}{\partial x_i}\right)\right]\right\}dV = \int_V u_i\frac{\delta}{\delta b_n}\left(\frac{\partial \tau_{ij}}{\partial x_j}\right)dV = \\ &-\int_S u_i n_j\frac{\delta\tau_{ij}}{\delta b_n}dS + \int_V \frac{\partial u_i}{\partial x_j}\left(\frac{\partial v_i}{\partial x_j}+\frac{\partial v_j}{\partial x_i}\right)\frac{\partial \nu_t}{\partial\widetilde{\nu}}\frac{\delta\widetilde{\nu}}{\delta b_n}dV \\ &+ \underbrace{\int_V \frac{\partial u_i}{\partial x_j}(\nu+\nu_t)\frac{\delta}{\delta b_n}\left(\frac{\partial v_i}{\partial x_j}+\frac{\partial v_j}{\partial x_i}\right)dV}_{T_D} + \int_V u_i\frac{\partial\tau_{ij}}{\partial x_k}\frac{\partial}{\partial x_j}\left(\frac{\delta x_k}{\delta b_n}\right)dV \end{aligned} \tag{3.18}$$

Term T_D can be developed further and yields quantities containing the adjoint stress tensor $\tau_{ij}^{\alpha} = (\nu + \nu_t)\left(\frac{\partial u_i}{\partial x_j} + \frac{\partial u_j}{\partial x_i}\right)$.

$$
\begin{aligned}
T_D &= \int_V \frac{\partial u_i}{\partial x_j}(\nu+\nu_t)\frac{\delta}{\delta b_n}\left(\frac{\partial v_i}{\partial x_j}+\frac{\partial v_j}{\partial x_i}\right) dV \\
&= \int_V (\nu+\nu_t)\frac{\partial u_i}{\partial x_j}\left[\frac{\delta}{\delta b_n}\left(\frac{\partial v_i}{\partial x_j}\right)+\frac{\delta}{\delta b_n}\left(\frac{\partial v_j}{\partial x_i}\right)\right] dV \\
&= \int_S (\nu+\nu_t)\left(\frac{\partial u_i}{\partial x_j}+\frac{\partial u_j}{\partial x_i}\right) n_j \frac{\delta v_i}{\delta b_n} dS - \int_V \frac{\partial}{\partial x_j}\left[(\nu+\nu_t)\left(\frac{\partial u_i}{\partial x_j}+\frac{\partial u_j}{\partial x_i}\right)\right]\frac{\delta v_i}{\delta b_n} dV \\
&- \int_V (\nu+\nu_t)\left(\frac{\partial u_i}{\partial x_j}+\frac{\partial u_j}{\partial x_i}\right)\frac{\partial v_i}{\partial x_k}\frac{\partial}{\partial x_j}\left(\frac{\delta x_k}{\delta b_n}\right) dV \\
&= \int_S \tau_{ij}^{\alpha} n_j \frac{\delta v_i}{\delta b_n} dS - \int_V \frac{\partial \tau_{ij}^{\alpha}}{\partial x_j}\frac{\delta v_i}{\delta b_n} dV - \int_V \tau_{ij}^{\alpha}\frac{\partial v_i}{\partial x_k}\frac{\partial}{\partial x_j}\left(\frac{\delta x_k}{\delta b_n}\right) dV
\end{aligned} \tag{3.19}
$$

It is important to note that the differentiation of the momentum equations leads to contributions to terms multiplying $\frac{\delta \widetilde{\nu}}{\delta b_n}$ as shown in eq 3.18. This means that the above development also contributes to the adjoint to the turbulence model equation.

Differentiation of the Spalart-Allmaras Turbulence Model

Differentiation of the Spalart-Allmaras model equation leads to

$$
\begin{aligned}
\frac{\delta R^{\widetilde{\nu}}}{\delta b_n} &= \frac{\delta v_j}{\delta b_n}\frac{\partial \widetilde{\nu}}{\partial x_j} + v_j \frac{\delta}{\delta b_n}\left(\frac{\partial \widetilde{\nu}}{\partial x_j}\right) - \frac{\delta}{\delta b_n}\left\{\frac{\partial}{\partial x_j}\left[\left(\nu + \frac{\widetilde{\nu}}{\sigma}\right)\frac{\partial \widetilde{\nu}}{\partial x_j}\right]\right\} \\
&- \frac{c_{b2}}{\sigma}\frac{\delta}{\delta b_n}\left[\left(\frac{\partial \widetilde{\nu}}{\partial x_j}\right)^2\right] + \widetilde{\nu}\left(-\frac{\delta P}{\delta b_n} + \frac{\delta D}{\delta b_n}\right) + (-P+D)\frac{\delta \widetilde{\nu}}{\delta b_n}
\end{aligned} \tag{3.20}
$$

The production and dissipation terms are equal to

$$
-\frac{\delta P}{\delta b_n} + \frac{\delta D}{\delta b_n} = \mathcal{C}_{\widetilde{\nu}}\frac{\delta \widetilde{\nu}}{\delta b_n} + \mathcal{C}_{\Delta}\frac{\delta \Delta}{\delta b_n} + \mathcal{C}_Y \frac{1}{Y} e_{mjk}\frac{\partial v_k}{\partial x_j} e_{mli}\frac{\delta}{\delta b_n}\left(\frac{\partial v_i}{\partial x_l}\right) \tag{3.21}
$$

where

$$\mathcal{C}_Y = \left(-c_{b_1} - c_{w_1}\mathcal{C}\frac{r}{\widetilde{\widetilde{Y}}}\right) f_{v_3} \tag{3.22}$$

$$\mathcal{C}_\Delta = -\frac{2}{\Delta^3}\left[c_{w_1} r\,\mathcal{C}\left(\Delta^2 - \frac{\widetilde{\nu} f_{v_2}}{\kappa^2 \widetilde{\widetilde{Y}}}\right) + c_{w_1} f_w \widetilde{\nu} - c_{b_1}\frac{f_{v_2}}{\kappa^2}\widetilde{\nu}\right] \tag{3.23}$$

$$\mathcal{C}_{\widetilde{\nu}} = \left(-c_{b_1} - c_{w_1}\mathcal{C}\frac{r}{\widetilde{\widetilde{Y}}}\right)\left(\frac{\partial f_{v_3}}{\partial \widetilde{\nu}} Y + \frac{f_{v_2}}{\kappa^2\Delta^2} + \frac{\partial f_{v_2}}{\partial \widetilde{\nu}}\frac{\widetilde{\nu}}{\kappa^2\Delta^2}\right) + c_{w_1}\mathcal{C}\frac{r}{\widetilde{\nu}} + c_{w_1}\frac{f_w}{\Delta^2} \tag{3.24}$$

$$C = \frac{c_{w_1}\widetilde{\nu}^2}{\Delta^2}\left[1 + c_{w_2}(6r^5 - 1)\right]\frac{c_{w_3}^6}{g^6 + c_{w_3}^6}\left(\frac{1 + c_{w_3}^6}{g^6 + c_{w_3}^6}\right)^{1/6} \tag{3.25}$$

$$\frac{\partial f_{v_2}}{\partial \widetilde{\nu}} = -\frac{3}{\nu c_{v_2}}\left(1 + \frac{\chi}{c_{v_2}}\right)^{-4} \tag{3.26}$$

$$\begin{aligned}\frac{\partial f_{v_3}}{\partial \widetilde{\nu}} = {} & \frac{1}{c_{v_2}}\left(\frac{f_{v_1}}{\nu} + \chi\frac{\partial f_{v_1}}{\partial \nu}\right)\left[3\left(1 + \frac{\chi}{c_{v_2}}\right) + \left(\frac{\chi}{c_{v_2}}\right)^2\right]\left(1 + \frac{\chi}{c_{v_2}}\right)^{-3} \\ & + \frac{1}{\nu c_{v_2}^2}(1 + \chi f_{v_1})\left(3 + 2\frac{\chi}{c_{v_2}}\right) c_{v_2}^2\left(1 + \frac{\chi}{c_{v_2}}\right)^{-3} \\ & - 3\frac{(1 + \chi f_{v_1})}{\nu c_{v_2}^2}\left[3\left(1 + \frac{\chi}{c_{v_2}}\right) + \left(\frac{\chi}{c_{v_2}}\right)^2\right]\left(1 + \frac{\chi}{c_{v_2}}\right)^{-4}\end{aligned} \tag{3.27}$$

Substituting expression 3.20 to eq. 3.6, the resulting volume integrals are developed as shown below,

$$\begin{aligned}term1 : & \int_V \widetilde{\nu_a}\frac{\partial \widetilde{\nu}}{\partial x_i}\frac{\delta v_i}{\delta b_n} dV + \int_V \widetilde{\nu_a} v_j \frac{\delta}{\delta b_n}\left(\frac{\partial \widetilde{\nu}}{\partial x_j}\right) dV \\ & = \int_V \widetilde{\nu_a}\frac{\partial \widetilde{\nu}}{\partial x_i}\frac{\delta v_i}{\delta b_n} dV + \int_S \widetilde{\nu_a} v_j n_j \frac{\delta \widetilde{\nu}}{\delta b_n} dS - \int_V \frac{\partial(\widetilde{\nu_a} v_j)}{\partial x_j}\frac{\delta \widetilde{\nu}}{\delta b_n} dV - \int_V \widetilde{\nu_a} v_j \frac{\partial \widetilde{\nu}}{\partial x_k}\frac{\partial}{\partial x_j}\left(\frac{\delta x_k}{\delta b_n}\right) dV\end{aligned} \tag{3.28}$$

$$\begin{aligned}term2 : & -\int_V \widetilde{\nu_a}\frac{\delta}{\delta b_n}\left\{\frac{\partial}{\partial x_j}\left[\left(\nu + \frac{\widetilde{\nu}}{\sigma}\right)\frac{\partial \widetilde{\nu}}{\partial x_j}\right]\right\} dV = \\ & - \int_S \widetilde{\nu_a} n_j \frac{1}{\sigma}\frac{\partial \widetilde{\nu}}{\partial x_j}\frac{\delta \widetilde{\nu}}{\delta b_n} dS - \int_S \widetilde{\nu_a} n_j \left(\nu + \frac{\widetilde{\nu}}{\sigma}\right)\frac{\delta}{\delta b_n}\left(\frac{\partial \widetilde{\nu}}{\partial x_j}\right) dS \\ & + \int_S n_j \frac{\partial \widetilde{\nu_a}}{\partial x_j}\left(\nu + \frac{\widetilde{\nu}}{\sigma}\right)\frac{\delta \widetilde{\nu}}{\delta b_n} dS + \int_V \frac{1}{\sigma}\frac{\partial \widetilde{\nu_a}}{\partial x_j}\frac{\partial \widetilde{\nu}}{\partial x_j}\frac{\delta \widetilde{\nu}}{\delta b_n} dV - \int_V \frac{\partial}{\partial x_j}\left[\frac{\partial \widetilde{\nu_a}}{\partial x_j}\left(\nu + \frac{\widetilde{\nu}}{\sigma}\right)\right]\frac{\delta \widetilde{\nu}}{\delta b_n} dV \\ & - \int_V \left(\nu + \frac{\widetilde{\nu}}{\sigma}\right)\frac{\partial \widetilde{\nu_a}}{\partial x_j}\frac{\partial \widetilde{\nu}}{\partial x_k}\frac{\partial}{\partial x_j}\left(\frac{\delta x_k}{\delta b_n}\right) dV + \int_V \widetilde{\nu_a}\frac{\partial}{\partial x_k}\left[\left(\nu + \frac{\widetilde{\nu}}{\sigma}\right)\frac{\partial \widetilde{\nu}}{\partial x_j}\right]\frac{\partial}{\partial x_j}\left(\frac{\delta x_k}{\delta b_n}\right) dV\end{aligned} \tag{3.29}$$

$$
\begin{aligned}
term3 : &- \int_V \widetilde{\nu_a} \frac{c_{b2}}{\sigma} \frac{\delta}{\delta b_n} \left[\left(\frac{\partial \widetilde{\nu}}{\partial x_j} \right)^2 \right] dV = - \int_V 2\widetilde{\nu_a} \frac{c_{b2}}{\sigma} \frac{\partial \widetilde{\nu}}{\partial x_j} \frac{\delta}{\delta b_n} \left(\frac{\partial \widetilde{\nu}}{\partial x_j} \right) dV \\
&= - \int_S 2\widetilde{\nu_a} n_j \frac{c_{b2}}{\sigma} \frac{\partial \widetilde{\nu}}{\partial x_j} \frac{\delta \widetilde{\nu}}{\delta b_n} dS + \int_V 2 \frac{c_{b2}}{\sigma} \frac{\partial}{\partial x_j} \left[\widetilde{\nu_a} \frac{\partial \widetilde{\nu}}{\partial x_j} \right] \frac{\delta \widetilde{\nu}}{\delta b_n} dV \\
&+ \int_V 2\widetilde{\nu_a} \frac{c_{b2}}{\sigma} \frac{\partial \widetilde{\nu}}{\partial x_j} \frac{\partial \widetilde{\nu}}{\partial x_k} \frac{\partial}{\partial x_j} \left(\frac{\delta x_k}{\delta b_n} \right) dV
\end{aligned} \tag{3.30}
$$

$$
\begin{aligned}
term4 : &\int_V \widetilde{\nu_a} \widetilde{\nu} \left(-\frac{\delta P}{\delta b_n} + \frac{\delta D}{\delta b_n} \right) dV + \int_V \widetilde{\nu_a} (-P + D) \frac{\delta \widetilde{\nu}}{\delta b_n} dV \\
&= \int_V \widetilde{\nu_a} \widetilde{\nu} \mathcal{C}_{\tilde{\nu}} \frac{\delta \widetilde{\nu}}{\delta b_n} dV + \int_V \widetilde{\nu_a} \widetilde{\nu} \mathcal{C}_{\Delta} \frac{\delta \Delta}{\delta b_n} dV + \int_S \widetilde{\nu_a} \widetilde{\nu} \mathcal{C}_Y \frac{1}{Y} e_{mjk} \frac{\partial v_k}{\partial x_j} e_{mli} n_l \frac{\delta v_i}{\delta b_n} dS \\
&- \int_V \frac{\partial}{\partial x_l} \left(\widetilde{\nu_a} \widetilde{\nu} \mathcal{C}_Y \frac{1}{Y} e_{mjk} \frac{\partial v_k}{\partial x_j} e_{mli} \frac{\partial}{\partial x_l} \right) \frac{\delta v_i}{\delta b_n} dV \\
&- \int_V \widetilde{\nu_a} \widetilde{\nu} \mathcal{C}_Y \frac{1}{Y} e_{mjd} \frac{\partial v_d}{\partial x_j} e_{mli} \frac{\partial v_i}{\partial x_k} \frac{\partial}{\partial x_l} \left(\frac{\delta x_k}{\delta b_n} \right) dV + \int_V \widetilde{\nu_a} \widetilde{\nu} (-P + D) \frac{\delta \widetilde{\nu}}{\delta b_n} dV
\end{aligned} \tag{3.31}
$$

Note that eq. 3.29 includes surface integrals that contain both $\frac{\delta \widetilde{\nu}}{\delta b_n}$ and $\frac{\delta}{\delta b_n} \left(\frac{\partial \widetilde{\nu}}{\partial x_j} \right)$. Their mutual existence is what ultimately leads to the derivation of different BCs for $\widetilde{\nu_a}$ between the inlet and outlet boundaries, as will be shown in a latter section, since one of the two needs to be eliminated where the other is fixed at zero.

3.3.2 Differentiation of the Objective Function

In the present study, two different objective functions are used (section 3.2), and for this reason, the differentiation of the objective function will follow a more generalized approach. The differences that occur between the two objectives, specifically in the adjoint BCs and the final expression of the SD, are outlined in the description of each test case. Both objective functions can be described as

$$
F = \int_S F_{S,i} n_i dS \tag{3.32}
$$

where the term $F_{S,i}$ is comprised solely of flow variables, excluding any geometrical terms. Differentiation of the objective fynction yields

$$
\frac{\delta F}{\delta b_n} = \frac{\delta}{\delta b_n} \int_S F_{S,i} n_i dS = \int_S \frac{\delta F_{S,i}}{\delta b_n} n_i dS + \int_S F_{S,i} \frac{\delta n_i}{\delta b_n} dS + \int_S F_{S,i} n_i \frac{\delta (dS)}{\delta b_n} \tag{3.33}
$$

Since term $F_{S,i}$ depends directly on the flow variables, which in turn, depend on the design variables, its differentiation follows the chain rule and results in

$$\frac{\delta F_{S,i}}{\delta b_n} = \frac{\partial F_{S,i}}{\partial v_j}\frac{\delta v_j}{\delta b_n} + \frac{\partial F_{S,i}}{\partial p}\frac{\delta p}{\delta b_n} + \frac{\partial F_{S,k}}{\partial \tau_{ij}}\frac{\delta \tau_{ij}}{\delta b_n} + \frac{\partial F_{S,i}}{\partial \widetilde{\nu}}\frac{\delta \widetilde{\nu}}{\delta b_n} \tag{3.34}$$

Concluding, the final expression for eq. 3.33 is

$$\begin{aligned}\frac{\delta F}{\delta b_n} = &\int_S \frac{\partial F_{S,i}}{\partial v_j}\frac{\delta v_j}{\delta b_n} n_i dS + \int_S \frac{\partial F_{S,i}}{\partial p}\frac{\delta p}{\delta b_n} n_i dS + \int_S \frac{\partial F_{S,k}}{\partial \tau_{ij}}\frac{\delta \tau_{ij}}{\delta b_n} n_k dS \\ &+ \int_S \frac{\partial F_{S,i}}{\partial \widetilde{\nu}}\frac{\delta \widetilde{\nu}}{\delta b_n} n_i dS + \int_S F_{S,i}\frac{\delta n_i}{\delta b_n} dS + \int_S F_{S,i} n_i \frac{\delta (dS)}{\delta b_n}\end{aligned} \tag{3.35}$$

3.3.3 The Adjoint Field Equations

By replacing eqs. 3.13, 3.15, 3.20 and 3.35 and substituting into eq. 3.6, a final expression for $\frac{\delta F_{aug}}{\delta b_n}$ is assembled,

$$\begin{aligned}\frac{\delta F_{aug}}{\delta b_n} = &\int_V R^q \frac{\delta p}{\delta b_n} dV + \int_V R^u_i \frac{\delta v_i}{\delta b_n} dV + \int_V R^{\widetilde{\nu_a}} \frac{\delta \widetilde{\nu}}{\delta b_n} dV + \int_S \left(SC^u_i + \frac{\partial F_{S,j}}{\partial v_i} n_j \right) \frac{\delta v_i}{\delta b_n} dS \\ &+ \int_S \left(SC^q + \frac{\partial F_{S,j}}{\partial p} n_j \right) \frac{\delta p}{\delta b_n} dS + \int_S \left(SC^{\widetilde{\nu_a}} + \frac{\partial F_{S,i}}{\partial \widetilde{\nu}} n_i \right) \frac{\delta \widetilde{\nu}}{\delta b_n} dS \\ &+ \int_S \left(-u_i n_j + \frac{\partial F_{S,k}}{\partial \tau_{ij}} n_k \right) \frac{\delta \tau_{ij}}{\delta b_n} dS + \int_S -\widetilde{\nu_a} n_j \left(\nu + \frac{\widetilde{\nu}}{\sigma} \right) \frac{\delta}{\delta b_n} \left(\frac{\partial \widetilde{\nu}}{\partial x_j} \right) dS \\ &+ \int_V \widetilde{\nu_a} \widetilde{\nu} C_\Delta \frac{\delta \Delta}{\delta b_n} dV + \int_S F_{S,i} \frac{\delta n_i}{\delta b_n} dS + \int_S n_i F_{S,i} \frac{\delta (dS)}{\delta b_n} \\ &+ \int_V \left(FI^L_{jk} + FI^T_{jk} \right) \frac{\partial}{\partial x_j} \left(\frac{\delta x_k}{\delta b_n} \right) dV\end{aligned} \tag{3.36}$$

where

$$SC^q = u_j n_j \tag{3.37}$$

$$SC^u_i = -q n_i + u_i v_j n_j + \tau^\alpha_{ij} n_j - \widetilde{\nu_a} \widetilde{\nu} \mathcal{C}_Y \frac{1}{Y} e_{mjk} \frac{\partial v_k}{\partial x_j} e_{mli} n_l \tag{3.38}$$

$$SC^{\widetilde{\nu_a}} = \widetilde{\nu_a} v_j n_j - \widetilde{\nu_a} n_j \frac{1}{\sigma} \frac{\partial \widetilde{\nu}}{\partial x_j} + \frac{\partial \widetilde{\nu_a}}{\partial x_j} \left(\nu + \frac{\widetilde{\nu}}{\sigma} \right) n_j - 2 \widetilde{\nu_a} n_j \frac{c_{b2}}{\sigma} \frac{\partial \widetilde{\nu}}{\partial x_j} \tag{3.39}$$

and

$$FI^L_{jk} = -\tau^{\alpha}_{ij}\frac{\partial v_i}{\partial x_k} + u_i\frac{\partial \tau_{ij}}{\partial x_k} - u_j\frac{\partial p}{\partial x_k} - u_i v_j\frac{\partial v_i}{\partial x_k} + q\frac{\partial v_j}{\partial x_k} \tag{3.40}$$

$$\begin{aligned} FI^T_{jk} = {} & 2\widetilde{\nu}_a\frac{c_{b2}}{\sigma}\frac{\partial\widetilde{\nu}}{\partial x_j}\frac{\partial\widetilde{\nu}}{\partial x_k} - \left(\nu + \frac{\widetilde{\nu}}{\sigma}\right)\frac{\partial\widetilde{\nu}_a}{\partial x_j}\frac{\partial\widetilde{\nu}}{\partial x_k} \\ & + \widetilde{\nu}_a\frac{\partial}{\partial x_k}\left[\left(\nu + \frac{\widetilde{\nu}}{\sigma}\right)\frac{\partial\widetilde{\nu}}{\partial x_j}\right] - \widetilde{\nu}_a v_j\frac{\partial\widetilde{\nu}}{\partial x_k} - \widetilde{\nu}_a\widetilde{\nu}\mathcal{C}_Y\frac{1}{Y}e_{mld}\frac{\partial v_d}{\partial x_l}e_{mji}\frac{\partial v_i}{\partial x_k} \end{aligned} \tag{3.41}$$

By setting the multipliers of $\frac{\delta v_i}{\delta b_n}$, $\frac{\delta p}{\delta b_n}$, $\frac{\delta\widetilde{\nu}}{\delta b_n}$ to zero in the field integrals of eq. 3.36, the adjoint field equations arise and the first three volume integrals of eq. 3.36 vanish. The field adjoint equations, including that corresponding to the adjoint turbulence model PDE are given below:

$$R^q = -\frac{\partial u_j}{\partial x_j} = 0 \tag{3.42a}$$

$$\begin{aligned} R^u_i = {} & u_j\frac{\partial v_j}{\partial x_i} - \frac{\partial(u_i v_j)}{\partial x_j} - \frac{\partial}{\partial x_j}\left[(\nu+\nu_t)\left(\frac{\partial u_i}{\partial x_j} + \frac{\partial u_j}{\partial x_i}\right)\right] + \frac{\partial q}{\partial x_i} \\ & - \frac{\partial}{\partial x_l}\left(\widetilde{\nu}_a\widetilde{\nu}\mathcal{C}_Y\frac{1}{Y}e_{mjk}\frac{\partial v_k}{\partial x_j}e_{mli}\frac{\partial}{\partial x_l}\right) + \widetilde{\nu}_a\frac{\partial\widetilde{\nu}}{\partial x_i} = 0 \end{aligned} \tag{3.42b}$$

$$\begin{aligned} R^{\widetilde{\nu_a}} = {} & \frac{\partial\nu_t}{\partial\widetilde{\nu}}\frac{\partial u_i}{\partial x_j}\left(\frac{\partial v_i}{\partial x_j} + \frac{\partial v_j}{\partial x_i}\right) - \frac{\partial(\widetilde{\nu}_a v_j)}{\partial x_j} + \frac{1}{\sigma}\frac{\partial\widetilde{\nu}_a}{\partial x_j}\frac{\partial\widetilde{\nu}}{\partial x_j} - \frac{\partial}{\partial x_j}\left[\frac{\partial\widetilde{\nu}_a}{\partial x_j}\left(\nu + \frac{\widetilde{\nu}}{\sigma}\right)\right] \\ & + 2\frac{c_{b2}}{\sigma}\frac{\partial}{\partial x_j}\left[\widetilde{\nu}_a\frac{\partial\widetilde{\nu}}{\partial x_j}\right] + \widetilde{\nu}_a\widetilde{\nu}C_{\widetilde{\nu}} + \widetilde{\nu}_a\widetilde{\nu}(-P+D) = 0 \end{aligned} \tag{3.42c}$$

3.3.4 Deriving the Adjoint Boundary Conditions

After satisfying the adjoint field equations, the remaining terms in eq. 3.36 are

$$\begin{aligned} \frac{\delta F_{aug}}{\delta b_n} = {} & \int_S\left(SC^u_i + \frac{\partial F_{S,j}}{\partial v_i}n_j\right)\frac{\delta v_i}{\delta b_n}dS + \int_S\left(SC^q + \frac{\partial F_{S,j}}{\partial p}n_j\right)\frac{\delta p}{\delta b_n}dS \\ & + \int_S\left(SC^{\widetilde{\nu_a}} + \frac{\partial F_{S,i}}{\partial\widetilde{\nu}}n_i\right)\frac{\delta\widetilde{\nu}}{\delta b_n}dS + \int_S\left(-u_i n_j + \frac{\partial F_{S,k}}{\partial\tau_{ij}}n_k\right)\frac{\delta\tau_{ij}}{\delta b_n}dS \\ & + \int_S -\widetilde{\nu}_a n_j\left(\nu + \frac{\widetilde{\nu}}{\sigma}\right)\frac{\delta}{\delta b_n}\left(\frac{\partial\widetilde{\nu}}{\partial x_j}\right)dS + \int_V\widetilde{\nu}_a\widetilde{\nu}C_\Delta\frac{\delta\Delta}{\delta b_n}dV \\ & + \int_S F_{S,i}\frac{\delta n_i}{\delta b_n}dS + \int_S n_i F_{S,i}\frac{\delta(dS)}{\delta b_n} + \int_V\left(FI^L_{jk} + FI^T_{jk}\right)\frac{\partial}{\partial x_j}\left(\frac{\delta x_k}{\delta b_n}\right)dV \end{aligned} \tag{3.43}$$

Variations in the flow variables, i.e. $\frac{\delta v_i}{\delta b_n}$, $\frac{\delta p}{\delta b_n}$, $\frac{\delta \widetilde{\nu}}{\delta b_n}$ and $\frac{\delta \tau_{ij}}{\delta b_n}$, still exist within the first five surface integrals on the r.h.s. of eq. 3.43. Depending on the boundary, these variations can be equal to zero, an example being the velocity at the inlet to the domain which may have a fixed value irrespectively of the values of the design variables. It is clear that the primal BCs fully influence the adjoint BCs. Through the process of setting the multipliers of the flow variables variations to zero, at the boundaries where they are not eliminated because of the primal BCs, the adjoint BCs are derived. The terms that need to be eliminated are

$$\Pi_v = \int_S \left(SC_i^u + \frac{\partial F_{S,j}}{\partial v_i} n_j \right) \frac{\delta v_i}{\delta b_n} dS \tag{3.44a}$$

$$\Pi_p = \int_S \left(SC^q + \frac{\partial F_{S,j}}{\partial p} n_j \right) \frac{\delta p}{\delta b_n} dS \tag{3.44b}$$

$$\Pi_{\widetilde{\nu}} = \int_S \left(SC^{\widetilde{\nu_a}} + \frac{\partial F_{S,k}}{\partial \widetilde{\nu}} n_k \right) \frac{\delta \widetilde{\nu}}{\delta b_n} dS \tag{3.44c}$$

$$\Pi_{\tau_w} = \int_S \left(-u_i n_j + \frac{\partial F_{S,k}}{\partial \tau_{ij}} n_k \right) \frac{\delta \tau_{ij}}{\delta b_n} dS \tag{3.44d}$$

$$\Pi_{\widetilde{\nu}_x} = \int_S \widetilde{\nu_a} n_j \left(\nu + \frac{\widetilde{\nu}}{\sigma} \right) \frac{\delta}{\delta b_n} \left(\frac{\partial \widetilde{\nu}}{\partial x_j} \right) dS \tag{3.44e}$$

Inlet

Along the inlet to the domain, $\frac{\delta v_i}{\delta b_n}$ and $\frac{\delta \widetilde{\nu}}{\delta b_n}$ are equal to zero, since Dirichlet BCs are imposed on v_i and $\widetilde{\nu}$. Thus, Π_v and $\Pi_{\widetilde{\nu}}$ vanish. In order to eliminate Π_p and Π_{τ_w}, the multipliers of $\frac{\delta p}{\delta b_n}$ and $\frac{\delta \tau_w^{ij}}{\delta b_n}$ in eqs. 3.44b and 3.44d are set to zero, leading to BCs for the adjoint velocity components. As described in [3] , the adjoint velocity vector is split into its normal and tangential components. Setting $SC^q + \frac{\partial F_{S_I,j}}{\partial v_i} n_j = 0$ and $u_i n_j = \frac{\partial F_{S_k}}{\partial \tau_{ij}} n_k$ leads to

$$u_{\langle n \rangle} = -\frac{\partial F_{S_I,j}}{\partial p} n_j \tag{3.45a}$$

$$u^I_{\langle t \rangle} = \frac{\partial F_{S_I,k}}{\partial \tau_{ij}} n_k t_i^I n_j + \frac{\partial F_{S_I,k}}{\partial \tau_{ij}} n_k t_j^I n_i \tag{3.45b}$$

$$u^{II}_{\langle t \rangle} = \frac{\partial F_{S_I,k}}{\partial \tau_{ij}} n_k t_i^{II} n_j + \frac{\partial F_{S_I,k}}{\partial \tau_{ij}} n_k t_j^{II} n_i \tag{3.45c}$$

In addition, integral $\Pi_{\widetilde{\nu}_x}$ contains $\frac{\delta}{\delta b_n} \left(\frac{\partial \widetilde{\nu}}{\partial x_j} \right)$ and, thus, a Dirichlet BC is imposed on $\widetilde{\nu_a}$ so that

$$\widetilde{\nu_a} = 0 \tag{3.46}$$

A zero Neumann condition is imposed on q.

Outlet

Along the outlet of the domain, pressure has a fixed value and so $\frac{\delta p}{\delta b_n} = 0$. Also, $\widetilde{\nu}$ has a zero Neumann BC and so $\frac{\delta}{\delta b_n}\left(\frac{\partial \widetilde{\nu}}{\partial n}\right)$ is zero. Taking into account that, on the outlet patch, which is a fixed boundary, $\frac{\delta n_j}{\delta b_n}$ is zero, the following equation holds

$$\frac{\delta}{\delta b_n}\left(\frac{\partial \widetilde{\nu}}{\partial x_j} n_j\right) = \frac{\delta}{\delta b_n}\left(\frac{\partial \widetilde{\nu}}{\partial x_j}\right) n_j \tag{3.47}$$

Thus, by rearranging terms in eq. 3.44e, $\Pi_{\widetilde{\nu}_x}$ vanishes. In order to eliminate $\Pi_{\widetilde{\nu}}$, a Robin type BC results for $\widetilde{\nu_a}$,

$$\widetilde{\nu_a} v_j n_j - \widetilde{\nu_a} n_j \frac{1}{\sigma}\frac{\partial \widetilde{\nu}}{\partial x_j} + \frac{\partial \widetilde{\nu_a}}{\partial x_j}\left(\nu + \frac{\widetilde{\nu}}{\sigma}\right) n_j - 2\widetilde{\nu_a} n_j \frac{c_{b2}}{\sigma}\frac{\partial \widetilde{\nu}}{\partial x_j} + \frac{\partial F_{S_{O,k}}}{\partial \widetilde{\nu}} n_k = 0$$

Special attention must be paid to term Π_v. In order to eliminate it the following equalities

$$-q n_i + u_i v_j n_j + \tau_{ij}^{\alpha} n_j + \widetilde{\nu_a}\widetilde{\nu}\mathcal{C}_Y \frac{1}{Y} e_{mjk}\frac{\partial v_k}{\partial x_j} e_{mli} n_l + \frac{\partial F_{S_O,j}}{\partial v_i} n_j = 0 \tag{3.48}$$

must be satisfied. Multiplying the above equation with n_i results in a Dirichlet condition for the adjoint pressure

$$q = u_i n_i v_j n_j + \tau_{ij}^{\alpha} n_j n_i + \widetilde{\nu_a}\widetilde{\nu}\mathcal{C}_Y \frac{1}{Y} e_{mjk}\frac{\partial v_k}{\partial x_j} e_{mli} n_l n_i + \frac{\partial F_{S_O,j}}{\partial v_i} n_j n_i \tag{3.49}$$

whereas multiplying it with t_i^I and t_i^{II} yields BCs for the tangential components of the adjoint velocity, namely

$$u_i t_i^z v_j n_j + \tau_{ij}^{\alpha} n_j t_i^z + \widetilde{\nu_a}\widetilde{\nu}\mathcal{C}_Y \frac{1}{Y} e_{mjk}\frac{\partial v_k}{\partial x_j} e_{mli} n_l t_i^z + \frac{\partial F_{S_O,j}}{\partial v_i} n_j t_i^z = 0 \quad , \quad z = 1, 2 \tag{3.50}$$

Finally, a zero Neumann BC is imposed on the normal component of the adjoint velocity.

Non-parameterized Walls

The BC imposed on $\widetilde{\nu}$ along a wall which is not controlled by the optimization method (i.e. is not parameterized) is a zero Dirichlet type and for this reason $\frac{\delta \widetilde{\nu}}{\delta b_n}$ is

equal to zero. However, the gradient of $\widetilde{\nu}$ is not and, so, in order to eliminate $\Pi_{\widetilde{\nu}_x}$ and make $\frac{\delta F_{aug}}{\delta b_n}$ independent of variations in $\frac{\partial \widetilde{\nu}}{\partial n}$ the following BC is imposed on $\widetilde{\nu}_a$,

$$\widetilde{\nu}_a = 0 \tag{3.51}$$

Furthermore $\frac{\delta v_i}{\delta b_n}$ is equal to zero due to the no-slip BC imposed on v_i. The BCs applied to u_i and q are written again only for the sake of completeness,

$$u_{\langle n \rangle} = -\frac{\partial F_{S_W,j}}{\partial p} n_j \tag{3.52a}$$

$$u^I_{\langle t \rangle} = \frac{\partial F_{S_W,k}}{\partial \tau_{ij}} n_k t^I_i n_j + \frac{\partial F_{S_W,k}}{\partial \tau_{ij}} n_k t^I_j n_i \tag{3.52b}$$

$$u^{II}_{\langle t \rangle} = \frac{\partial F_{S_W,k}}{\partial \tau_{ij}} n_k t^{II}_i n_j + \frac{\partial F_{S_W,k}}{\partial \tau_{ij}} n_k t^{II}_j n_i \tag{3.52c}$$

along with a zero Neumann BC for q.

Parameterized Wall

The BCs for the parameterized wall (i.e. those controlled by the optimization) are identical to those for the fixed wall boundary. In the present study, the flow variables variations w.r.t. the design variables are expressed through a material derivative of b_n. The only difference between fixed and parameterized walls are the variations in geometrical entities, such as the position vector and the unit vector, normal to the wall, which for a fixed (non-parameterized) boundary are zero. Their contributions to the SD computation is discussed in the next section.

This concludes the derivation of the adjoint BCs. Proceeding further, the BCs for the adjoint velocity are modified to account for the usage of the wall-function in the solution of the primal equations.

3.3.5 Adjoint Wall Functions

In high-Re meshes, where the wall-function technique is used to bridge the gap between the first cell center off the wall and the corresponding wall face, the differentiation of Spalding's wall function must be included in the derivation of the

adjoint equations. Consequently, the BCs for the adjoint velocity change into

$$u_{\langle n \rangle} = -\frac{\partial F_{S_W,j}}{\partial p} n_j \tag{3.53a}$$

$$u_\tau^2 = (\nu + \nu_t)\left(\frac{\partial u_i}{\partial x_j} + \frac{\partial u_j}{\partial x_i}\right) n_j t_i^I = -\frac{\partial F_{S_W,k}}{\partial v_i} n_k t_i^I \tag{3.53b}$$

$$u_{\langle t \rangle}^{II} = \frac{\partial F_{S_W,k}}{\partial \tau_{ij}} n_k t_i^{II} n_j + \frac{\partial F_{S_W,k}}{\partial \tau_{ij}} n_k t_j^{II} n_i \tag{3.53c}$$

for both the fixed and parameterized walls. In the above relation, eq. 3.53a is again obtained by setting $SC^q + \frac{\partial F_{S_{I,j}}}{\partial v_i} n_j = 0$ and eliminating Π_p. Eqs. 3.53b and 3.53c result by further developing Π_v and Π_{τ_w}, differentiating eq. 2.11 and combining them. Eq. 3.53b is the so-called adjoint law of the wall; this is an indispensable part of the adjoint system formulation when using wall functions. Using this formulation, the adjoint viscous fluxes at a solid wall face are computed using the expression provided by the adjoint friction velocity u_τ, which depends on the derivatives of the objective function w.r.t. v_i, eq. 3.53b.The differentiation of Spalding's law yields the following term,

$$\begin{aligned} T_{WF} = & \underbrace{\int_{S_{Wp}} 2 v_\tau C_v^{WF} \frac{v_i^P}{|\vec{v}|} \left(-u_i t_i^I + \frac{\partial F_{S_{Wp},k}}{\partial \tau_{ij}} n_k t_i^I n_j + \frac{\partial F_{S_{Wp},k}}{\partial \tau_{ij}} n_k t_j^I n_i\right) \frac{\delta v_i^P}{\delta b_n} dS}_{termWF_1} \\ & + \underbrace{\int_{S_{Wp}} C_\Delta^{WF} \left(-u_i t_i^I + \frac{\partial F_{S_{Wp},k}}{\partial \tau_{ij}} n_k t_i^I n_j + \frac{\partial F_{S_{Wp},k}}{\partial \tau_{ij}} n_k t_j^I n_i\right) \frac{\delta \Delta^P}{\delta b_n} dS}_{termWF_2} \\ & + \underbrace{\int_{S_{Wp}} \left(-u_i t_i^I + \frac{\partial F_{S_{Wp},k}}{\partial \tau_{ij}} n_k t_i^I n_j + \frac{\partial F_{S_{Wp},k}}{\partial \tau_{ij}} n_k t_j^I n_i\right) \tau_{ij} \frac{\delta \left(n_j t_i^I\right)}{\delta b_n} dS}_{termWF_3} \end{aligned} \tag{3.54}$$

which is added to the expression for $\frac{\delta F_{aug}}{\delta b_n}$. S_{W_p} stands for the parameteried wall. The first integral in T_{WF}, marked as $termWF_1$, contains variations in the velocity components at the cell centers adjacent to the wall. The multipliers of $\frac{\delta v_i^P}{\delta b_n}$ contribute as source terms to the discretized adjoint momentum equations in these cells. The second ($termWF_2$) and last ($termWF_3$) integrals contribute to the SD.

3.3.6 Sensitivity Derivatives

Having eliminated all terms that contain variations in the flow variables along all boundaries, the remaining terms constitute the SD. Consequently, the SD expression

is greatly simplified to

$$\begin{aligned}\frac{\delta F}{\delta b_n} =& \int_V \widetilde{\nu_a}\widetilde{\nu} C_\Delta \frac{\delta \Delta}{\delta b_n} dV + \int_V \left(FI^L_{jk} + FI^T_{jk}\right) \frac{\partial}{\partial x_j}\left(\frac{\delta x_k}{\delta b_n}\right) dV + \int_{S_{W_p}} F_{S_{W_p},i} \frac{\delta n_i}{\delta b_n} dS \\ &+ \int_{S_{W_p}} F_{S_{W_p},i} n_i \frac{\delta (dS)}{\delta b_n} + \int_{S_{Wp}} C^{WF}_\Delta \left(-u_i t^I_i + \frac{\partial F_{S_{W_p},k}}{\partial \tau_{ij}} n_k t^I_i n_j + \frac{\partial F_{S_{W_p},k}}{\partial \tau_{ij}} n_k t^I_j n_i\right) \frac{\delta \Delta^P}{\delta b_n} dS \\ &+ \int_{S_{Wp}} \left(-u_i t^I_i + \frac{\partial F_{S_{W_p},k}}{\partial \tau_{ij}} n_k t^I_i n_j + \frac{\partial F_{S_{W_p},k}}{\partial \tau_{ij}} n_k t^I_j n_i\right) \tau_{ij} \frac{\delta\left(n_j t^I_i\right)}{\delta b_n} dS + T_G \end{aligned} \tag{3.55}$$

Term T_G is,

$$\begin{aligned} T_G =& -\int_{S_{W_p}} \left(-u_k n_k + \frac{\partial F_{S_{W_p},k}}{\partial \tau_{lz}} n_k n_l n_z\right) \tau_{ij} \frac{\delta (n_i n_j)}{\delta b_n} dS - \int_{S_{W_p}} \frac{\partial F_{S_{W_p},k}}{\partial \tau_{lz}} n_k t^I_l t^I_z \tau_{ij} \frac{\delta (t^I_i t^I_j)}{\delta b_n} dS \\ &- \int_{S_{W_p}} \frac{\partial F_{S_{W_p},k}}{\partial \tau_{lz}} n_k t^{II}_l t^{II}_z \tau_{ij} \frac{\delta (t^{II}_i t^{II}_j)}{\delta b_n} dS - \int_{S_{W_p}} \frac{\partial F_{S_{W_p},k}}{\partial \tau_{lz}} n_k \left(t^{II}_l t^I_z + t^I_l t^{II}_z\right) \tau_{ij} \frac{\delta (t^{II}_i t^I_j)}{\delta b_n} dS \end{aligned} \tag{3.56}$$

The quantities that remain to be computed are

- $\frac{\delta n_i}{\delta b_n}$ and $\frac{\delta (dS)}{\delta b_n}$ along the parameterized boundary
- $\frac{\delta \Delta}{\delta b_n}$ for the whole domain
- $\frac{\partial}{\partial x_j}\left(\frac{\delta x_k}{\delta b_n}\right)$ for the whole domain

The fundamental prerequisite for the computation of the aforementioned terms is the computation of $\frac{\delta x_k}{\delta b_n}$. This procedure is further described in section 3.5 for two different shape parameterization methods. Terms $\frac{\delta n_i}{\delta b_n}$ and $\frac{\delta (dS)}{\delta b_n}$ can easily be computed since n_i and dS are functions of x_k. The computation of $\frac{\partial}{\partial x_j}\left(\frac{\delta x_k}{\delta b_n}\right)$ is performed using the discretization scheme for the gradient computation presented in section 2.2. More precisely, the discretization takes place as

$$\int_V \left(FI^L_{jk} + FI^T_{jk}\right) \frac{\partial}{\partial x_j}\left(\frac{\delta x_k}{\delta b_n}\right) dV = \left(FI^L_{jk} + FI^T_{jk}\right)_C \left(\frac{\sum_{f=1}^{N_f} \left[\frac{\delta x_k}{\delta b_n} n_j\right]_f}{V_C}\right) V_C \tag{3.57}$$

where V_C is the cell volume.

3.4 Adjoint to the Distance Equation

One way to compute the distance field (i.e. Δ) is through the solution of the Hamilton-Jacobi equation [3, 13], more specifically,

$$R^{\Delta} = \frac{\partial \left(c_j \Delta\right)}{\partial x_j} - \Delta \frac{\partial^2 \Delta}{\partial x_j^2} - 1 = 0 \tag{3.58}$$

where $c_j = \frac{\partial \Delta}{\partial x_j}$. This equation can be viewed as an additional primal PDE to be solved, meaning that it should be added to the augmented objective function which now becomes

$$F_{aug} = F + \int_V u_i R_i^v dV + \int_V q R^p dV + \int_V \widetilde{\nu_a} R^{\widetilde{\nu}} dV + \int_V \Delta_\alpha R^{\Delta} dV \tag{3.59}$$

where Δ_α is the adjoint to the distance field variable. The differentiation of eq. 3.59 leads to

$$\frac{\delta F_{aug}}{\delta b_n} = \frac{\delta F}{\delta b_n} + \int_V u_i \frac{\delta R_i^v}{\delta b_n} dV + \int_V q \frac{\delta R^p}{\delta b_n} dV + \int_V \widetilde{\nu_a} \frac{\delta R^{\widetilde{\nu}}}{\delta b_n} dV + \int_V \Delta_\alpha \frac{\delta R^{\Delta}}{\delta b_n} dV \tag{3.60}$$

and the last term on the r.h.s. of eq. 3.60 is further developed into

$$\int_V \Delta_\alpha \frac{\delta R^{\Delta}}{\delta b_n} dV = \int_V -2 \frac{\partial}{\partial x_j} \left(\Delta_\alpha \frac{\partial \Delta}{\partial x_j} \right) \frac{\delta \Delta}{\delta b_n} dV + \int_V -2 \frac{\partial \Delta}{\partial x_j} \frac{\partial \Delta}{\partial x_k} \frac{\partial}{\partial x_j} \left(\frac{\delta x_k}{\delta b_n} \right) dV \tag{3.61}$$

Keeping eq. 3.36 as a reference point, in order to make the SD expression independent of $\frac{\delta \Delta}{\delta b_n}$, the first term on the r.h.s. of eq. 3.61 contributes to the formulation of the adjoint to the distance field equation,

$$R^{\Delta_\alpha} = -2 \frac{\partial}{\partial x_j} \left(\Delta_\alpha \frac{\partial \Delta}{\partial x_j} \right) + \widetilde{\nu} \widetilde{\nu_a} C_\Delta = 0 \tag{3.62}$$

where the multipliers of $\frac{\delta \Delta^P}{\delta b_n}$ in $termWF_2$ (eq. 3.54) contribute as source terms to its discretized form at the cells adjacent to the walls. The terms inside the second integral on the r.h.s. of eq. 3.61 are added to FI_{jk}^T leading to a final expression for

the SD,

$$\frac{\delta F_{aug}}{\delta b_n} = \int_V \left(FI^L_{jk} + FI^T_{jk}\right) \frac{\partial}{\partial x_j}\left(\frac{\delta x_k}{\delta b_n}\right) dV + \int_{S_{W_p}} F_{S_{W_p},i} \frac{\delta n_i}{\delta b_n} dS + \int_{S_{W_p}} F_{S_{W_p},i} n_i \frac{\delta(dS)}{\delta b_n} + \int_{S_{Wp}} \left(-u_i t^I_i + \frac{\partial F_{S_{W_p},k}}{\partial \tau_{ij}} n_k t^I_i n_j + \frac{\partial F_{S_{W_p},k}}{\partial \tau_{ij}} n_k t^I_j n_i\right) \tau_{ij} \frac{\delta\left(n_j t^I_i\right)}{\delta b_n} dS + T_G \quad (3.63)$$

3.5 Design Variables and Mesh Parameterization

In shape optimization problems, the design variables control the shape to be optimized (e.g. the duct or airfoil). In the present study, two different parameterization techniques are employed. In the first method, the target boundary is parameterized using Bézier-Bernstein polynomials; in the second method a 3D structured lattice, consisting of volumetric B-splines control points, is used for the parameterization of the volume (shape and surrounding CFD grid) it encloses. Each method results in a different way to compute grid sensitivities. This section presents the two parameterization methods and, ultimately, the way that $\frac{\delta x_k}{\delta b_n}$ is computed in each one of them.

3.5.1 Shape Parameterization Using Bézier-Bernstein Curves

Using Bézier-Bernstein polynomials, the coordinates of the boundary nodes are given by

$$x_k(u) = \sum_{n=0}^{N-1} C_n(u) b_{n,k} \quad , \quad k = 1, 2(, 3) \quad (3.64)$$

where $b_{n,k}$ are control points' coordinates, $C_n(u)$ the Bernstein polynomials $u \in [0, 1]$ the curve parameter and N is the total number of control points used. The variation in the coordinates of boundary nodes w.r.t. to the design variables can be computed by directly differentiating eq. 3.64

$$\frac{\delta x_k}{\delta b_n} = \frac{\delta x_k}{\delta b_{m,l}} = \frac{\delta}{\delta b_{m,l}}\left(\sum_{n=0}^{N-1} C_n(u) b_{n,k}\right) = \sum_{n=0}^{N-1} C_n(u) \delta^m_n \delta^l_k = C_m(u) \delta^l_k \quad , \quad k = 1, 2(, 3) \quad (3.65)$$

Once SD have been computed, the design variables are updated and the parameterized boundary is displaced. Laplace equations are then solved to propagate the

displacement field to the interior of the domain. Consequently, $\frac{\delta x_k}{\delta b_n}$ which is simply computed on the parameterized boundary using eq. 3.65, is also propagated to the interior mesh by using the same Laplace equation model, one for each design variable.

3.5.2 Volumetric B-Splines

Using a parameterization based upon volumetric b-splines, a 3D structured lattice is constructed which encloses part of the geometry of interest. An example is shown in fig. 3.1. The nodes of the control lattice are the control points and their coordinates are the design variables. The coordinates of the control points are denoted as b_k^{IJL}

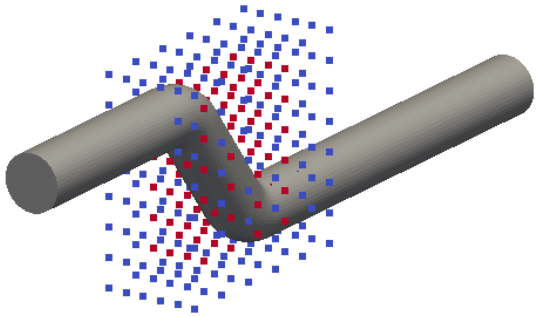

Figure 3.1: *Example of a 3D structured control box for the parameterization of a CFD grid using volumetric b-splines. Some control points may be chosen to be inactive, usually the boundary nodes of the control box, meaning that they are held stationary throughout the optimization loop. Moving the control points located on the boundary of the control lattice might result to the overlapping of grid elements in the viscinity of the control lattice boundaries.*

where $k \in [1, 3]$ and I,J,L are indices that correspond to the nodes in each direction of the 3D structured lattice. The cartesian coordinates of the CFD grid, within the bounds of the control grid, are mapped onto the parametric ones through the following relation

$$x_k(u, v, w) = U_{I,pu}(u)V_{J,pv}(v)W_{L,pw}(w)b_k^{IJL} \quad , \quad k = 1, 2(, 3) \tag{3.66}$$

where U, V, W are the b-splines polynomials in each of the 3 directions, pu, pv, pw their respective degrees and u, v, w the parametric coordinates defined in $[0, 1]$. The values of the polynomials also vary from $[0, 1]$ within the control box and their combination can exactly reproduce the coordinates of any CFD mesh.

At the beginning of the shape optimization loop, the coordinates of all mesh nodes

are known and for a given configuration of basis functions and polynomial degrees the corresponding parametric coordinates of each node of the CFD mesh can be computed by solving the system

$$x_k(u, v, w) - x_k = 0 \quad , \quad k = 1, 2(, 3) \tag{3.67}$$

These parametric coordinates (u, v, w) are invariant w.r.t. b_n, meaning that they do not depend upon the design variables and, thus, during each optimization cycle, the resultant mesh coordinates can easily be computed using eq. 3.66. The computation of the derivative $\frac{\delta x_k}{\delta b_n}$ is done by directly differentiating eq. 3.66 and following a similar procedure such as the one described in section 3.5.1, only this time, $\frac{\delta x_k}{\delta b_n}$ is directly computed for the whole domain.

3.6 BCs and SD for the Test Cases

In this section, the formulation of the primal and adjoint BCs is presented, as well as the final expression of the SD, for specific cases in external and internal aerodynamics which follow in chapter 4.

3.6.1 External Aerodynamics

The case concerning external aerodynamics that will be presented in the next chapter is the maximization of lift and the minimization of drag force acting on an airfoil. The primal BCs are summed up in table 3.1.

	inlet	***outlet***	***airfoil surface***
v_i	*Dirichlet* U_∞	*Zero Neumann*	*0*
p	*Zero Neumann*	*0*	*Zero Neumann*
$\widetilde{\nu}$	*Dirichlet*	*Zero Neumann*	*0*

Table 3.1: *Primal BCs in external aerodynamics. The farfield boundary is split into parts in which the flow enters and leaves the domain. The former will be mentioned as the inlet part of the farfield and the latter as the outlet.*

The differentiation of the objective function gives contributions to terms in the adjoint BCs, however, as described by eq. 3.3 it is defined only along the airfoil

surface i.e. the parameterized boundary. Thus, considering that

$$\frac{\partial F_{S,k}}{\partial p} n_k = r_j n_j \quad , \quad \frac{\partial F_{S_{W_p},k}}{\partial \tau_{ij}} n_k = -r_i n_j \tag{3.68}$$

the BCs are developed into

$$\begin{aligned}
Inlet: & \; u_{\langle n \rangle} = 0 \; , \; u^I_{\langle t \rangle} = 0 \; , \; u^{II}_{\langle t \rangle} = 0 \; , \; \frac{\partial q}{\partial n} = 0 \; , \; \widetilde{\nu}_a = 0 \\
Outlet: & \; \frac{\partial u_{\langle n \rangle}}{\partial n} = 0 \; , \; q = u_{\langle n \rangle} v_{\langle n \rangle} + \tau^{\alpha}_{ij} n_j n_i + \widetilde{\nu}_a \widetilde{\nu} \mathcal{C}_Y \frac{1}{Y} e_{mjk} \frac{\partial v_k}{\partial x_j} e_{mli} n_l n_i \; , \\
& \; u^z_{\langle t \rangle} v_{\langle n \rangle} + \tau^{\alpha}_{ij} n_j t^z_i + \widetilde{\nu}_a \widetilde{\nu} \mathcal{C}_Y \frac{1}{Y} e_{mjk} \frac{\partial v_k}{\partial x_j} e_{mli} n_l t^z_i = 0 \quad , \quad z = I, II \; , \\
& \; \widetilde{\nu}_a v_j n_j + \frac{\partial \widetilde{\nu}_a}{\partial x_j} \left(\nu + \frac{\widetilde{\nu}}{\sigma} \right) n_j = 0 \\
airfoil\ surface: & \; u_{\langle n \rangle} = -r_i n_i \; , \; \frac{\partial q}{\partial n} = 0 \; , \; \widetilde{\nu}_a = 0 \; , \; u^{II}_{\langle t \rangle} = -r_i t^{II}_i \\
& \; u^2_{\tau} \; = (\nu + \nu_t) \left(\frac{\partial u_i}{\partial x_j} + \frac{\partial u_j}{\partial x_i} \right) n_j t^I_i = 0
\end{aligned} \tag{3.69}$$

Taking also into account that $u_{\langle n \rangle} = -r_i n_i$ at the airfoil surface, term T_G in eq. 3.63 vanishes and the SD expression takes the following form

$$\begin{aligned}
\frac{\delta F}{\delta b_n} = & \int_V \left(F I^L_{jk} + F I^T_{jk} \right) \frac{\partial}{\partial x_j} \left(\frac{\delta x_k}{\delta b_n} \right) dV \\
& + \int_{S_{W_p}} \left[-(\nu + \nu_t) \left(\frac{\partial v_i}{\partial x_j} + \frac{\partial v_j}{\partial x_i} \right) + p \delta^j_i \right] r_i \frac{\delta n_j}{\delta b_n} dS \\
& + \int_{S_{W_p}} \left[-(\nu + \nu_t) \left(\frac{\partial v_i}{\partial x_j} + \frac{\partial v_j}{\partial x_i} \right) + p \delta^j_i \right] r_i n_j \frac{\delta (dS)}{\delta b_n} \\
& - \int_{S_{W_p}} \left(u^I_{\langle t \rangle} + r^I_{\langle t \rangle} \right) \tau_{ij} \frac{\delta \left(n_j t^I_i \right)}{\delta b_n} dS
\end{aligned} \tag{3.70}$$

3.6.2 Internal Aerodynamics

The cases concerning internal aerodynamics presented in the next chapter are concerned with the minimization of total pressure losses between the inlet and outlet of ducts. The primal BCs are summarized in table 3.2. The objective function, as described by eq. 3.2 is defined only along the inlet and outlet boundaries of the domain. Differentiation of the objective function with respect to pressure and velocity

	inlet	***outlet***	***wall***
v_i	*Dirichlet*	*Zero Neumann*	*0*
p	*Zero Neumann*	*0*	*Zero Neumann*
$\widetilde{\nu}$	*Dirichlet*	*Zero Neumann*	*0*

Table 3.2: *Primal BCs in internal aerodynamics.*

yields the following terms (along the inlte and outlet boundaries)

$$\frac{\partial F_{S,j}}{\partial p} n_j = -v_j n_j \tag{3.71a}$$

$$\frac{\partial F_{S,j}}{\partial v_i} n_j = -\left(p + \frac{1}{2} v_m^2\right) n_i - v_j n_j v_i \tag{3.71b}$$

which in turn contribute to the adjoint BCs at the inlet and outlet patches. The adjoint BCs are

$$\begin{aligned}
Inlet: & \; u_{\langle n \rangle} = v_j n_j \;,\; u^I_{\langle t \rangle} = 0 \;,\; u^{II}_{\langle t \rangle} = 0 \;,\; \frac{\partial q}{\partial n} = 0 \;,\; \widetilde{\nu}_a = 0 \\
Outlet: & \; \frac{\partial u_{\langle n \rangle}}{\partial n} = 0 \;,\; q = u_{\langle n \rangle} v_{\langle n \rangle} + \tau^{\alpha}_{ij} n_j n_i + \widetilde{\nu}_a \widetilde{\nu} \mathcal{C}_Y \frac{1}{Y} e_{mjk} \frac{\partial v_k}{\partial x_j} e_{mli} n_l n_i \;, \\
& \; u^z_{\langle t \rangle} v_{\langle n \rangle} + \tau^{\alpha}_{ij} n_j t^z_i + \widetilde{\nu}_a \widetilde{\nu} \mathcal{C}_Y \frac{1}{Y} e_{mjk} \frac{\partial v_k}{\partial x_j} e_{mli} n_l t^z_i \\
& - \left(p + \frac{1}{2} v_m^2\right) - v^2_{\langle n \rangle} = 0 \quad , \quad z = I, II \;, \\
& \; \widetilde{\nu}_a v_j n_j + \frac{\partial \widetilde{\nu}_a}{\partial x_j} \left(\nu + \frac{\widetilde{\nu}}{\sigma}\right) n_j = 0 \\
walls: & \; u_{\langle n \rangle} = 0 \;,\; \frac{\partial q}{\partial n} = 0 \;,\; \widetilde{\nu}_a = 0 \;,\; u^{II}_{\langle t \rangle} = 0 \\
& \; u^2_{\tau} \;\; = (\nu + \nu_t) \left(\frac{\partial u_i}{\partial x_j} + \frac{\partial u_j}{\partial x_i}\right) n_j t^I_i = 0
\end{aligned} \tag{3.72}$$

Taking the above BCs into consideration, in addition to the fact that, in this case, the objective function is not defined along the parameterized walls, term T_G in eq. 3.63 vanishes and the latter takes the following form

$$\frac{\delta F}{\delta b_n} = \int_V \left(F I^L_{jk} + F I^T_{jk}\right) \frac{\partial}{\partial x_j} \left(\frac{\delta x_k}{\delta b_n}\right) dV - \int_{S_{Wp}} u^I_{\langle t \rangle} \tau_{ij} \frac{\delta \left(n_j t^I_i\right)}{\delta b_n} dS \tag{3.73}$$

3.7 Design Variables Update Methods

In this section, the two optimization methods that have been utilized in this thesis are succintly described, based on [14].

3.7.1 Steepest Descent

The steepest descent method seeks to find an adequate direction, provided by $\frac{\delta F}{\delta b_n}$, in which to *move* inside the vector space of the design variables, by updating their values in each optimization iteration, in order to acquire a desired result on the function $F(b_n)$, be it reducing or increasing its value. Since the adjoint code, that has been developed by PCOpt/NTUA, incorporates optimization problems as minimization problems, the afforementioned direction will be refering only to a direction that minimizes F. In adjoint-based optimization, this direction is provided by $\frac{\delta F}{\delta b_n}$ and the expression that describes this process is

$$b_n^{new} = b_n^{old} - \eta \frac{\delta F}{\delta b_n} \tag{3.74}$$

In each iteration a *step* is taken towards the direction of the objective function's minimization within the vector space of the design variables. An important desicion to be made is the choice of the value of η, and this value decides the *step length* of the descent. In the current implementation, the choice of η is decided by providing a maximum allowed displacement for the values of the control points b_n. Initially, η is assumed to be equal to 1 for all design variables. However, once the displacement of b_n is computed (in the first iteration) and if the computed displacement is greater than the maximum threshold provided by the user, η is fixed to less or greater than 1, in order to limit the displacement accordingly. This value of η is kept and used during the rest of the optimization loop.

3.7.2 BFGS

In contrast to a line search method, there are methods that, apart from the gradient of F, also utilize the second derivative of F, known as the Hessian matrix $\nabla^2_{b_n} F$. The formula that is used for updating the design variables takes the form

$$b_n^{new} = b_n^{old} - \eta \left[\left(\frac{\delta^2 F}{\delta b_n \delta b_m} \right)^{-1} \frac{\delta F}{\delta b_m} \right]^{old} \tag{3.75}$$

However, the exact computation of the inverse of the Hessian matrix can be very inefficient and so, in large scale problems, an approximation B_{nm} is used instead

$$b_n^{new} = b_n^{old} - \eta \left[B_{nm}^{-1} \frac{\delta F}{\delta b_m} \right]^{old} \tag{3.76}$$

Choosing B_{nm} to be equal to the identity matrix yields eq. 3.74, while choosing B_{nm} to be an approximation of the Hessian matrix leads to a Quasi-Newton method. Quasi-Newton methods use an approximation of the Hessian matrix in contrast to a Newton method which uses the exact Hessian. The BFGS method computes the approximation B_k, for every iteration k (the nm index is dropped for simplicity), using the following equation

$$B_{k+1} = B_k - \frac{B_k s_k s_k^T B_k}{s_k^T B_k s_k} + \frac{y_k y_k^T}{y_k^T s_k} \tag{3.77}$$

where $s_k = x_{k+1} - x_k$ and $y_k = \nabla F_{k+1} - \nabla F_k$. Alternatively, the inverse of B_k can be computed through the following relation,

$$B_{k+1}^{-1} = \left(I - \rho_k s_k y_k^T \right) B_k^{-1} \left(I - \rho_k y_k^T s_k \right) + \rho_k s_k s_k^T \tag{3.78}$$

where $\rho_k = \frac{1}{s_k y_k^T}$.

Practically, the computation of ∇F_{k+1} is performed by solving the adjoint equations after updating the design variables. For the very first optimization step there is no information about the gradient of the objective function and so, a steepest descent is performed in order to drive the optimization forward. The value of η can be computed through line search methods or using the procedure that includes the maximum allowed displacement as previously described.

Chapter 4

Applications and Discussion

In this chapter, a variety of shape optimization test cases is presented, both in external and internal aerodynamics. Common characteristic among them is the fact that all of these cases are turbulent and computations are performed on high-Re meshes using wall functions. First, the use of the adjoint wall function is illustrated and the role it has as an indispensable part of the adjoint formulation is highlighted. More specifically, avoiding the use of the adjoint wall function means that, although the primal equations are solved by making use of Spalding's Law, the adjoint equations are solved using the BCs for wall boundaries provided by eq. 3.52 instead of 3.53. Once the adjoint solver's capacity for computing SD, with relative accuracy, is validated, shape optimization of an airfoil is performed, targeting lift maximization and drag minimization. Afterwards, focus is shifted towards internal aerodynamics and the minimization of total pressure losses in ducts. Shape optimization is performed on a 2D case and, then, extended to 3D cases.

4.1 External Aerodynamics

The NACA4415 airfoil surface was parameterized using volumetric B-splines, through the process described in section 3.5, resulting in a total of $6 \times 7 \times 3 = 126$ control points from which only 20 are allowed to move in the x and y directions. The boundary nodes of the control box remain fixed, throughout the shape optimization loop, in order to avoid the creation of overlapping mesh cells, between the parameterized and non-parameterized parts of the mesh, during the mesh displacement phase. Figure 4.1 illustrates these points. The mesh consists of 2×10^5 cells, the farfield flow angle is $\alpha = 3^o$ and the Reynolds number based on the airfoil chord length is $Re = 6 \times 10^6$. Two different meshes of approximately the same size have

been tested, one with a $y^+ \approx 10$ and the other with $y^+ \approx 50$ for the first cell-centers off the airfoil wall.

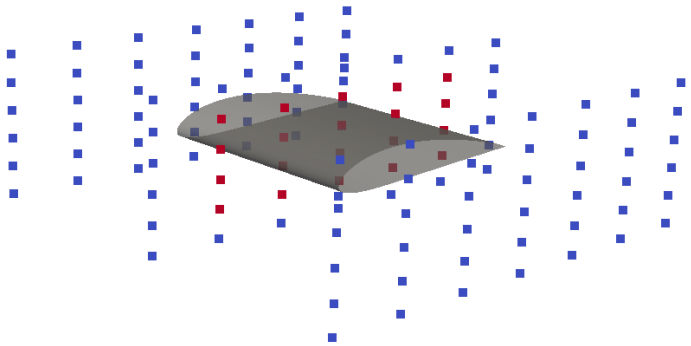

Figure 4.1: *Parameterization of airfoil surface using volumetric B-splines. Control points colored in red are the active ones that are allowed to move while the blue ones are fixed. Flow is purely 2D as velocity components are not solved for the z direction. Active control points do not move in the z direction. Even though the control lattice is 3D there is no stretching of the airfoil surface, in the z direction and this is ensured by the symmetry of the basis functions.*

4.1.1 Shape Optimization Results

Validation of SD Computation

Results comparing the adjoint method's capacity for computing SD, with and without using the adjoint wall function, are presented below, in figs. 4.2 and 4.3. The objective function is the lift force acting on the NACA4415 airfoil. Omission of the adjoint wall function results in miscalculation of SD, especially in the x direction, which happens to be the principal direction of the farfield flow. The contribution of the adjoint wall function is more pronounced with an increase in the value of y^+ from 10 to 50. A grid sensitivity study of the adjoint method is presented in fig. 4.4 performed on the two meshes with y^+ equal to 10 and 50.

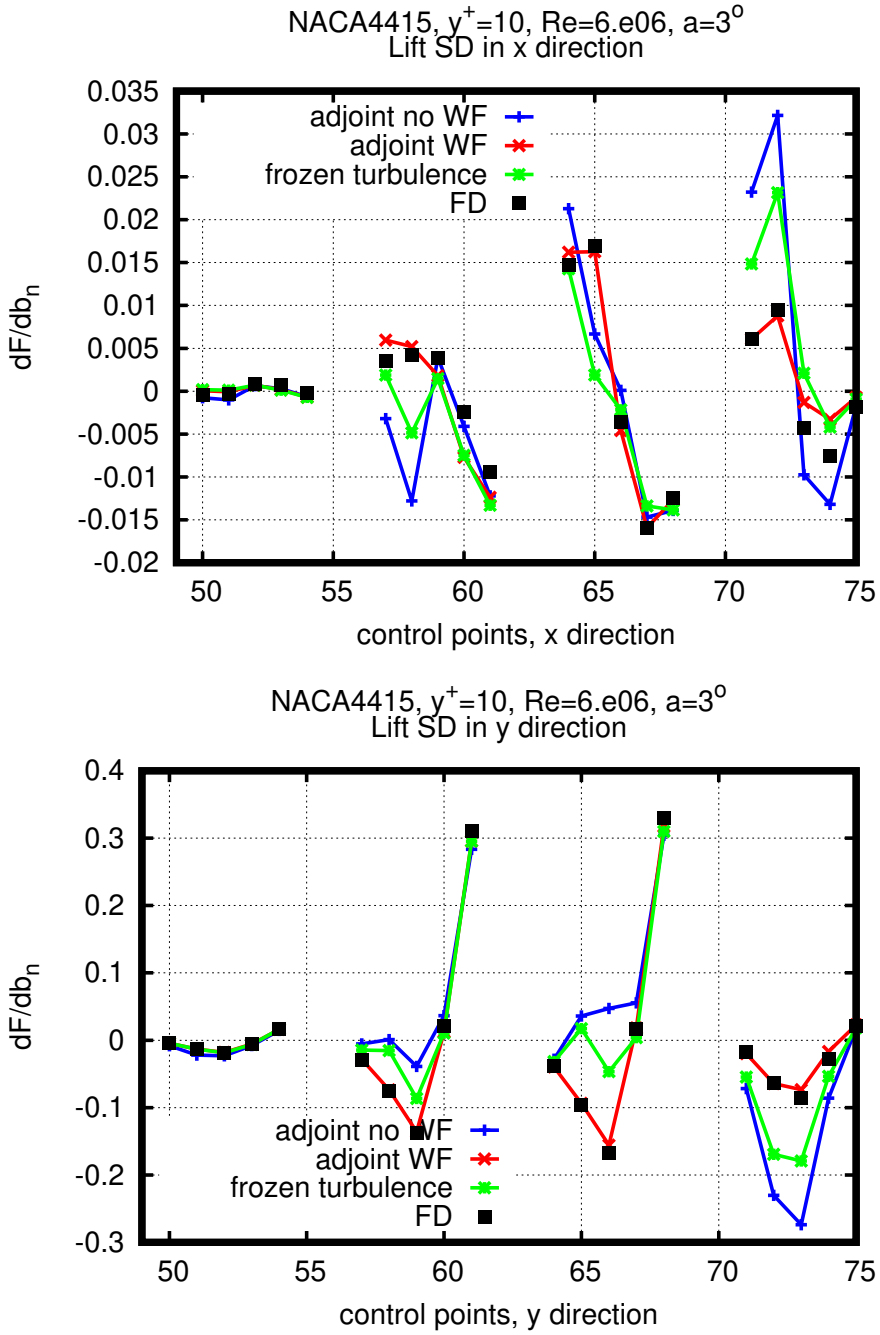

Figure 4.2: *NACA4415A airfoil, $y^+ = 10$, $Re = 6 \times 10^6$, a=3º. SD computed using the adjoint method without the adjoint wall function (adjoint no WF), including the adjoint WF, with the "frozen turbulence" assumption and using FD; the latter are considered to give "reference" SD. Derivatives w.r.t. to the x (top) and y (bottom) coordinates are shown.*

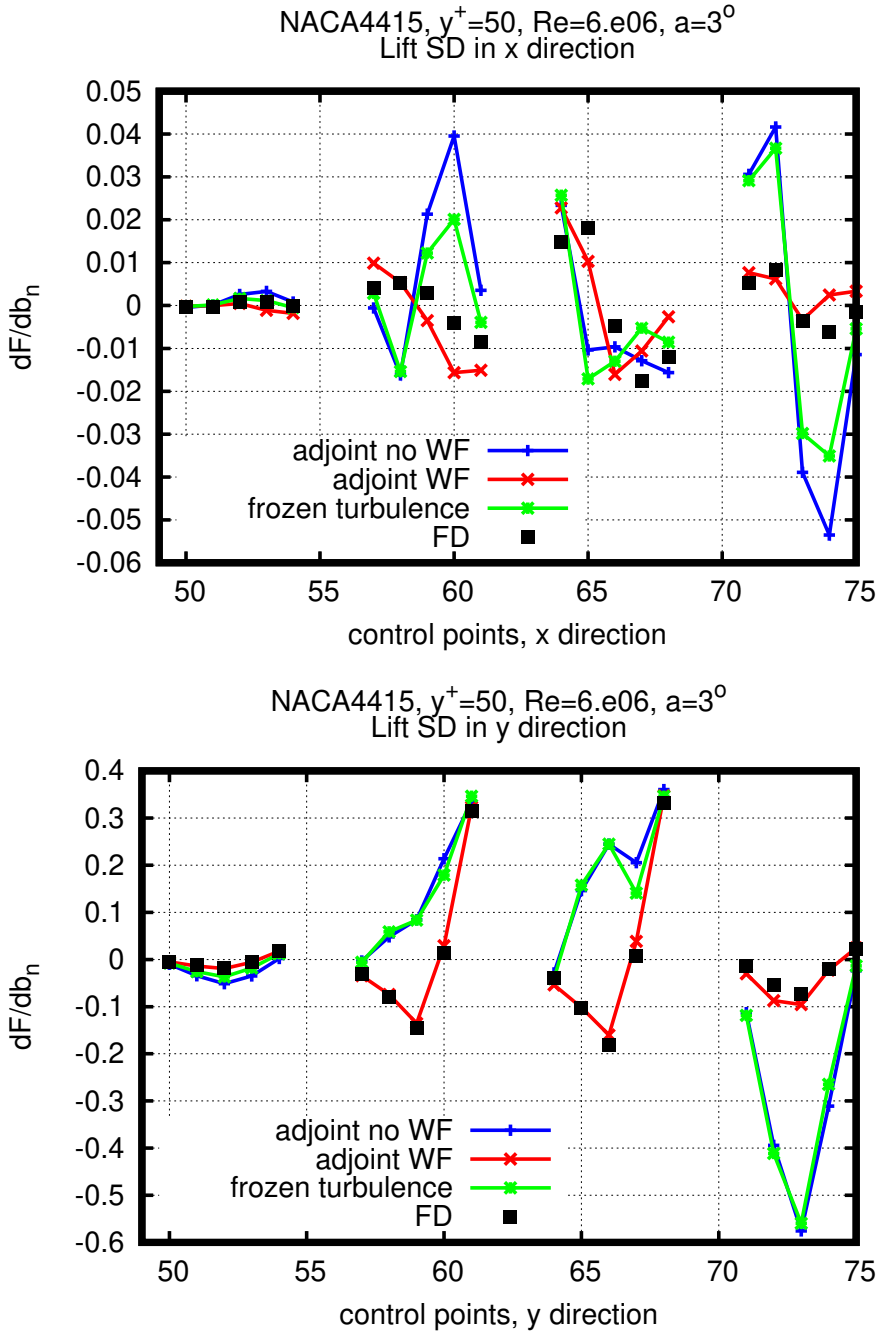

Figure 4.3: *NACA4415 airfoil, $y^+ = 50$, $Re = 6 \times 10^6$, a=3º. SD computed using the adjoint method without the adjoint wall function (adjoint no WF), including the adjoint WF, with the "frozen turbulence" assumption and using FD. Derivatives w.r.t. to the x (top) and y (bottom) coordinates are shown.*

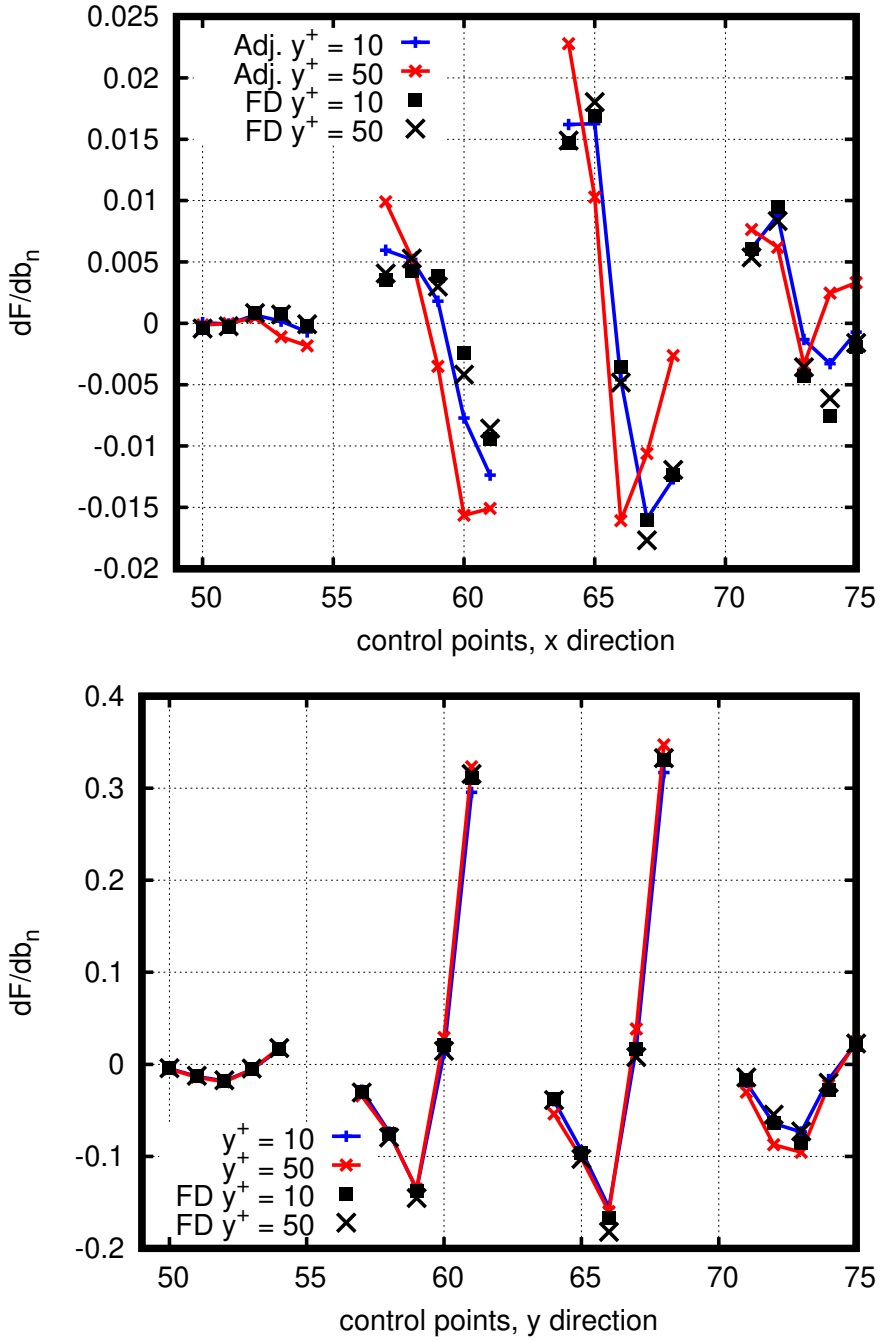

Figure 4.4: *NACA4415 airfoil, $Re = 6 \times 10^6$, a=3°. A comparison of lift SD computed using the adjoint method with the adjoint WF, on y^+=10 and y^+=50. Comparison is made with reference SD computed with FD. Derivatives w.r.t. to the x (top) and y (bottom) coordinates are shown.*

Lift Maximization

Using the previously validated code, a series of optimization cases are presented. The first case is dealing with the maximization of lift on the isolated airfoil presented in section 4.1, and the BCs are outlined in table 3.1. Optimization is performed using a steepest descent algorithm and the increase in the objective function is presented in fig. 4.5. Optimization is stopped after the 20th iteration as the goal of the presented results is solely the demonstration of the adjoint solver's capability to drive the optimization in the direction of increasing lift on high-Re meshes. A comparison of the initial and final shapes, is presented in fig. 4.7. The pressure distribution in the on the initial and optimized geometry can be seen in fig. 4.6. Lift force is increased by increasing the pressure on the rear side of the pressure side of the airfoil. For real-world applications, a constraint on the moment coefficient would have been necessary.

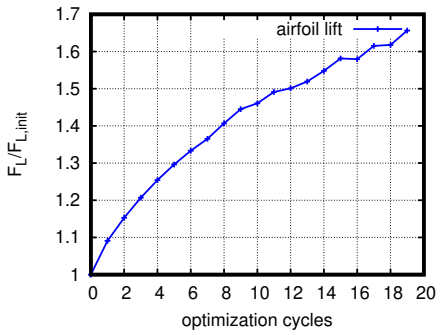

Figure 4.5: *NACA4415 airfoil, $y^+ = 10$, $Re = 6 \times 10^6$, a=3°. Lift maximization curve. The gain from the shape optimization of the airfoil surface is approximately 65%. The objective function's value is normalized based on the initial lift value.*

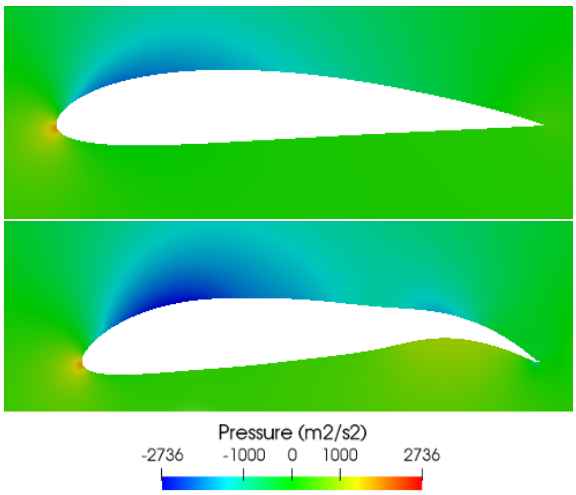

Figure 4.6: *NACA4415 airfoil,* $y^+ = 10$*,* $Re = 6 \times 10^6$*,* $a = 3^o$*. Pressure distribution around the airfoil in the initial (top) and optimized (bottom) airfoil geometry. Changes in the trailing part shape of the airfoil contribute the most to the increase in lift.*

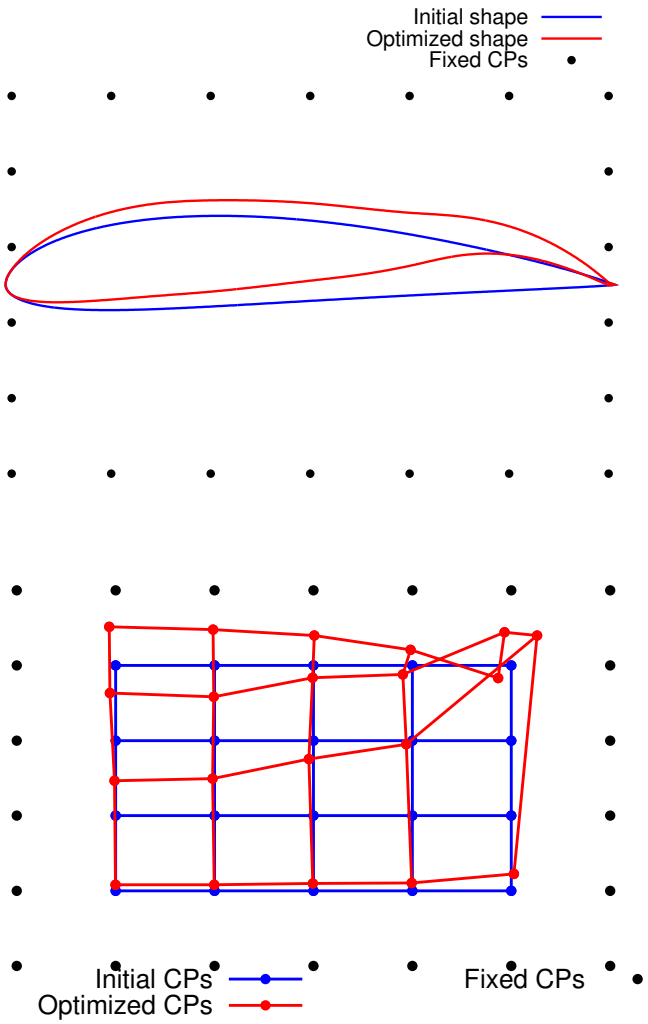

Figure 4.7: *NACA4415 airfoil,* $y^+ = 10$*,* $Re = 6 \times 10^6$*,* a*=3º. Initial (blue) and optimized (red) airfoil surface. The position of the control points (CPs) can also be seen (bottom) for the initial and optimez configurations.*

Drag Minimization

Shape optimization was also performed for the NACA4415 airfoil, this time targeting drag minimization. Convergence of the objective function is shown in fig. 4.8. Optimization is stopped after the 20th iteration, again, for the same reasons as discussed in section 4.1.1. A comparison of the initial and final shapes is presented in fig. 4.9. In table 4.1, the lift and drag coefficients computed on the initial and

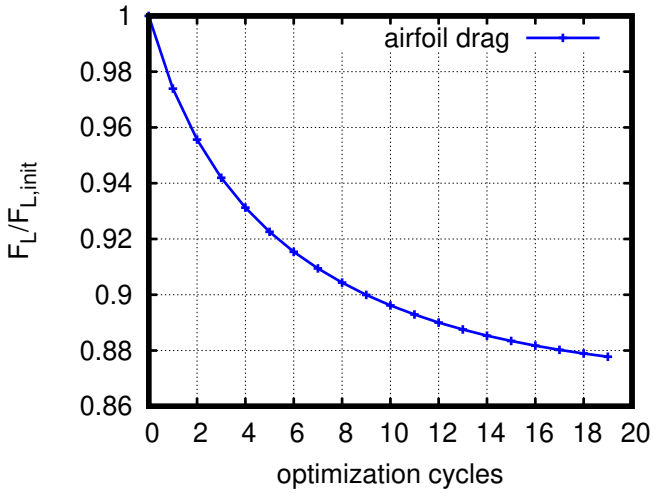

Figure 4.8: *NACA4415 airfoil, $y^+ = 10$, $Re = 6 \times 10^6$, $a=3^o$. Drag minimization curve. The gain from the shape optimization of the airfoil surface is approximately 12%. The objective function's value is normalized based on the initial drag value.*

optimized airfoil, for the two cases presented in this section, are presented.

	C_D	C_L
Initial	0.0123	0.7099
Lift maximization	0.02488	1.142
Drag minimization	0.01091	0.3692

Table 4.1: *Drag and lift coefficients computed on the initial and optimized geometry for lift maximization and drag minimization.*

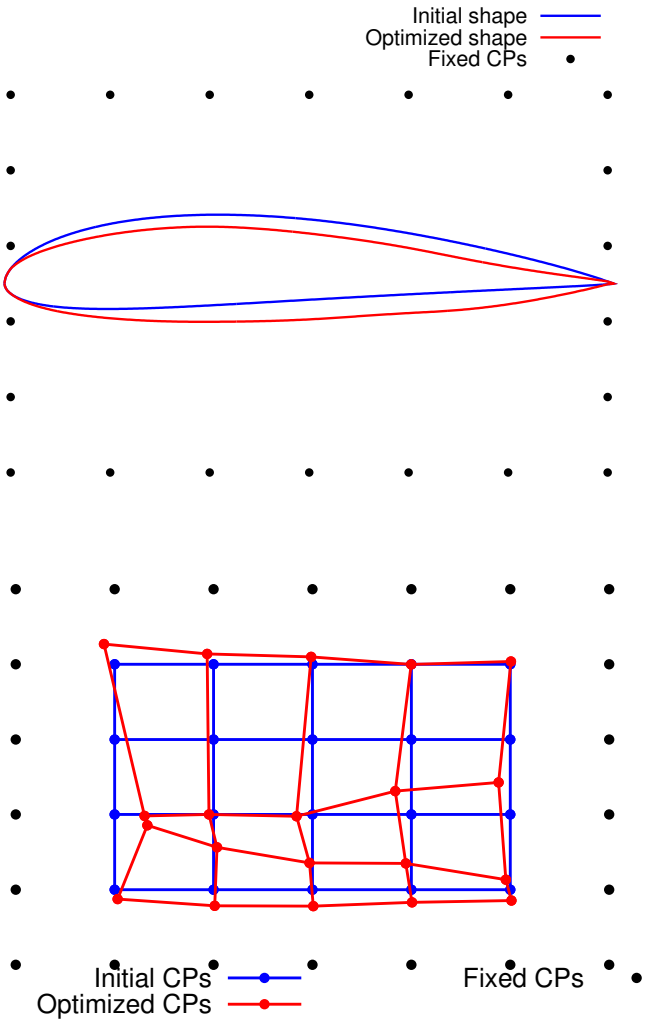

Figure 4.9: *NACA4415 airfoil, $y^+ = 10$, $Re = 6 \times 10^6$, a=3º. Initial (blue) and optimized (red) airfoil surface. The position of the control points (CPs) can also be seen (bottom) for the initial and optimized configurations.*

4.2 Minimization of Total Pressure Losses in Ducts

Next, the shape optimization software is tested in duct flow cases targeting minimum total pressure losses between the inlet and outlet.

4.2.1 2D Case of a U-bend Duct

The particular case of a 2D U-bend duct flow is investigated. The flow Reynolds number, based on the inlet height, is $Re = 1 \times 10^5$ and the mesh consists of 7000 cells with $y^+ \approx 10$. Comparison of SD computed with the adjoint method and FD is presented in fig. 4.11. The U-bend boundary was parameterized using Bézier curves, generated by utilizing 6 control points for each side of the parameterized wall (fig. 4.10). Throughout the optimization loop the outermost points on each side remain fixed. SD computed using the adjoint method complemented by the adjoint

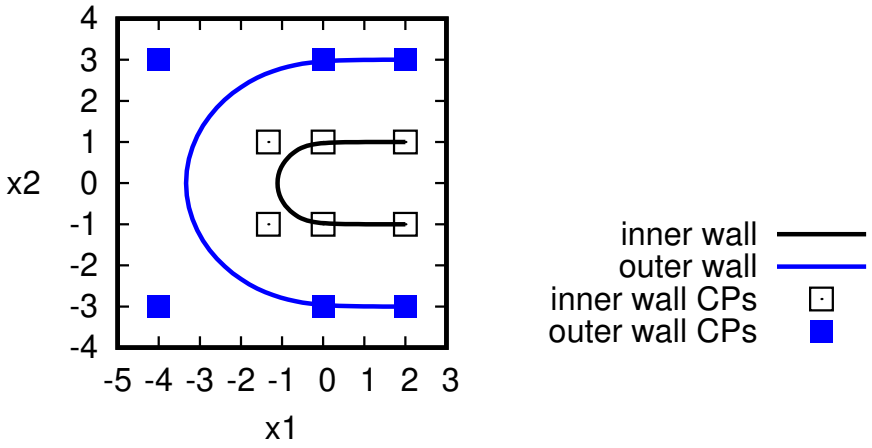

Figure 4.10: *U-bend duct, $y^+ \approx 10$, $Re = 1 \times 10^5$. Parameterization of the curved parts of the walls of the U-bend duct using Bézier curves, separately for the outer and inner wall. Six control points (CPs) have been used for each wall. The first and last control points of both walls remain fixed during the optimization.*

wall function are presented in fig. 4.11. Shape optimization is performed, using the steepest descent method, within 22 cycles (fig. 4.12), after which the objective function values practically stagnate. A comparison of the initial and optimized shapes of the U-bend duct is shown in fig. 4.13. Pressure losses have been reduced by 8% and the optimized shape, along with a comparison of the pressure and velocity magnitude fields between the initial and optimized geometry are presented in figs. 4.14 and 4.15. Streamlines indicating the locations of flow separation in the initial and optimized geometries are shown in fig. 4.16. Flow separation is reduced in the optimized duct.

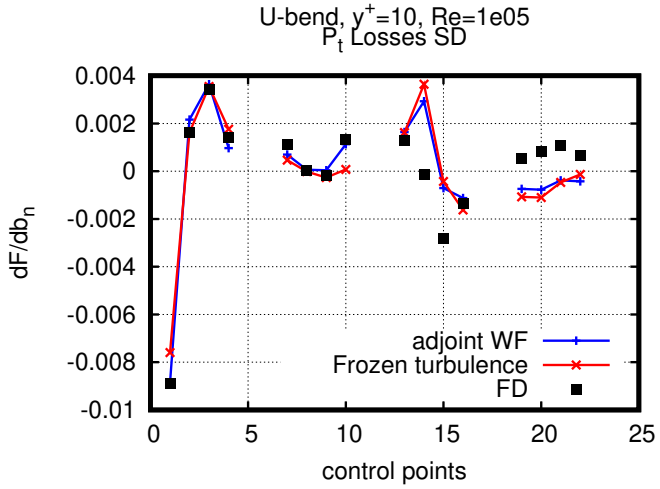

Figure 4.11: *U-bend, $y^+ \approx 10$, $Re = 1 \times 10^5$. SD computed on a high-Re mesh using the adjoint wall function (WF) compared to FD. The first 8 points pertain to derivatives of the bojective function w.r.t. the y-coordinates while the remaining points w.r.t. to the x-coordinates.*

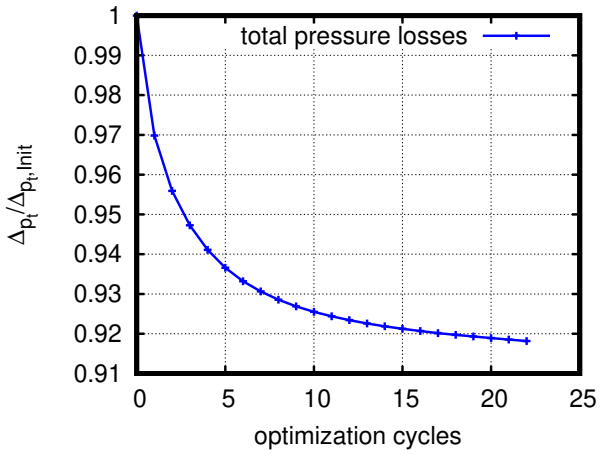

Figure 4.12: *U-bend, $y^+ \approx 10$, $Re = 1 \times 10^5$. Objective function convergence. Results shown are normalized based on the initial value of the objective function. The gain from the optimized shape is approximately 8%.*

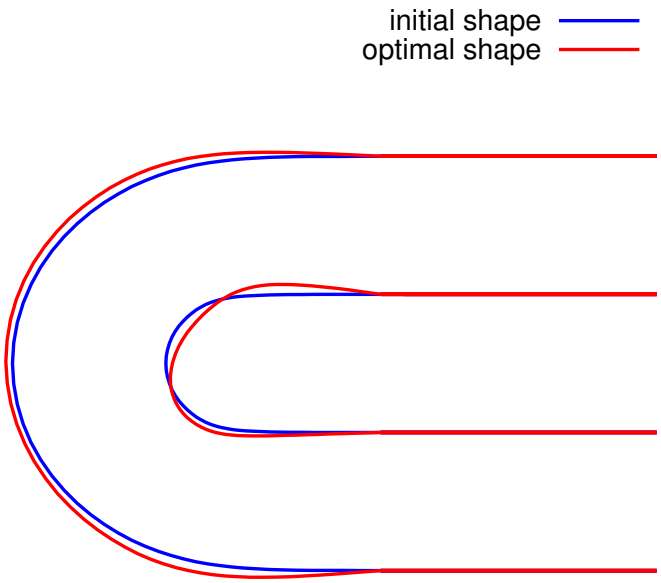

Figure 4.13: *U-bend, $y^+ \approx 10$, $Re = 1 \times 10^5$. A comparison of the initial (blue) and optimized (red) shape of the U-bend duct. Close-up view of the parameterized part of the duct.*

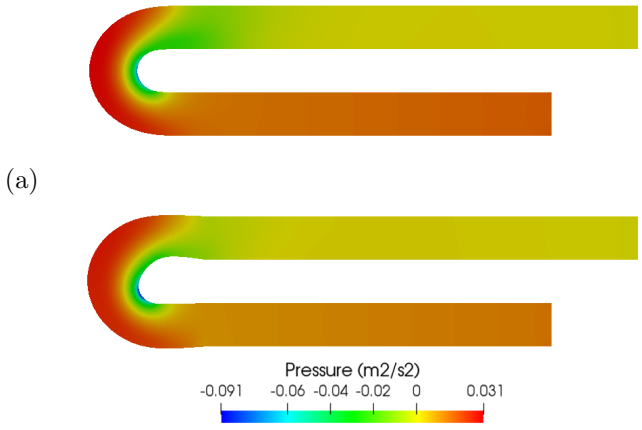

(a)

(b)

Figure 4.14: *U-bend, $y^+ \approx 10$, $Re = 1 \times 10^5$. Pressure distribution in the initial (a) and optimized (b) geometry.*

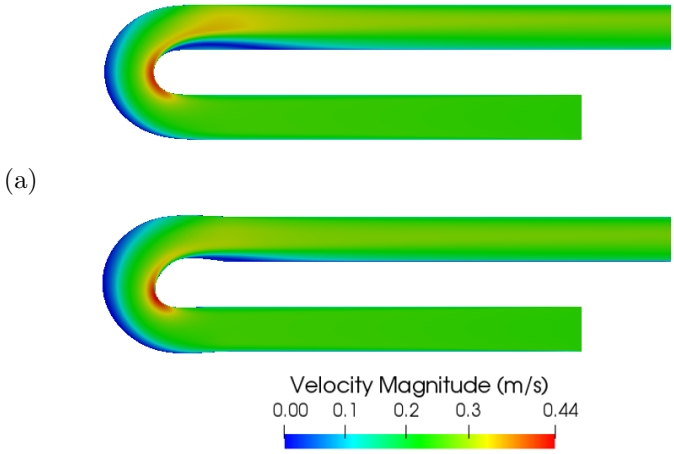

(a)

(b)

Figure 4.15: *U-bend, $y^+ \approx 10$, $Re = 1 \times 10^5$. Velocity magnitude field on the initial (a) and optimized (b) geometry.*

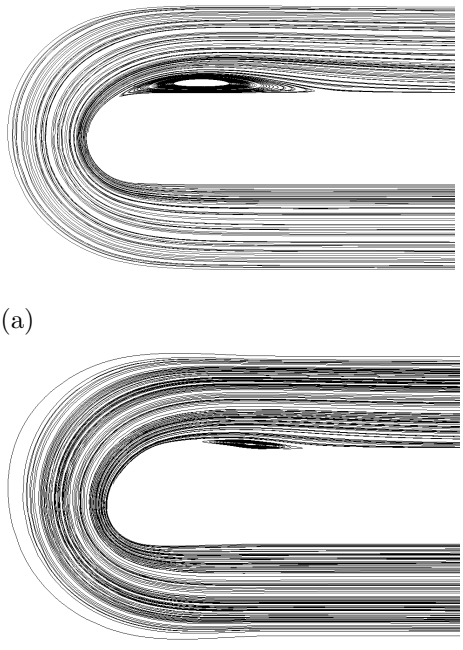

(a)

(b)

Figure 4.16: *U-bend, $y^+ \approx 10$, $Re = 1 \times 10^5$. Streamlines focused on the recirculation area of the U-bend duct in the initial (a) and optimized (b) geometry. Flow recirculation is reduced in the optimized geometry.*

4.2.2 3D Case of an S-Shaped Duct

The S-shaped duct flow was simulated using a mesh consisting of 92000 cells. The cross-section of the duct is circular, the Reynolds number based on the duct diameter is $Re = 1 \times 10^5$ and the average y^+ value is $y^+ \approx 22$. The geometry of the S-shaped duct and the location of the control lattice used for parameterization is shown in fig. 4.17. Shape optimization was performed using steepest descent and the convergence of the objective function is shown in fig. 4.18. The optimization loop was allowed to run for 19 cycles before mesh quality deterioration prevented further solution of the primal equations. A comparison of the original and optimized shape of the duct

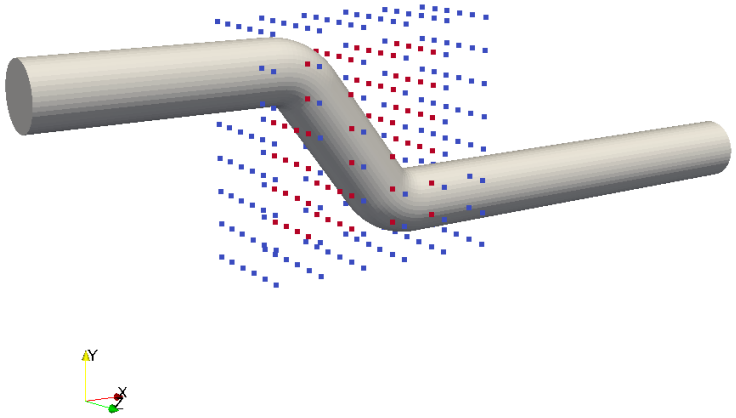

Figure 4.17: *S-shaped duct, $y^+ \approx 22$, $Re = 1 \times 10^5$. Parameterization of the S-shaped duct using volumetric B-splines.*

is presented in fig. 4.19. The optimization algorithm tends to create bulges on the overall shape, creating regions of flow separation and recirculation. Figs. 4.20 and 4.21 show the difference in the pressure and velocity magnitude fields between the initial and optimized geometry at the symmetry plane of the duct. Fig. 4.22 shows a cross-section of the duct close to the outlet illustrating velocity vectors, tangent to the cross-section surface, in the initial and optimized geometry respectively. This is an indication of the existence of secondary vortices in the duct. It was observed that the adjoint equations struggled to converge during certain steps of the optimization loop and the appearance of unsteady characteristics in the flow could be one of the reasons for this behaviour. In figs. 4.23 and 4.24 the adjoint pressure and the x and y components of the adjoint velocity are presented. It seems that the adjoint variables take their maximum values in the areas where flow separation occurs (locations with zero velocity magnitude in fig. 4.21). This could be interpreted as identifying the locations in which energy should be provided to the flow in order to avoid flow separation, therefore reducing pressure losses, and then reshaping the geometry accordingly to suit this need.

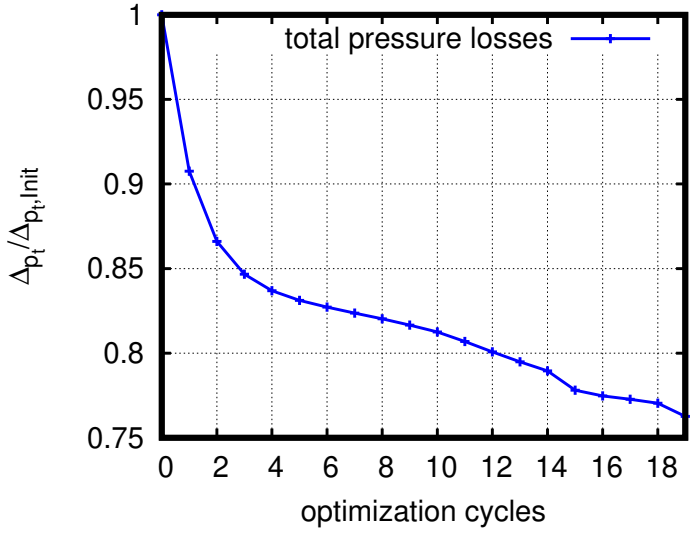

Figure 4.18: *S-shaped duct, $y^+ \approx 22$, $Re = 1 \times 10^5$. Convergence rate of the objective function. After 19 cycles the total pressure losses are by 25% less than in the initial geometry.*

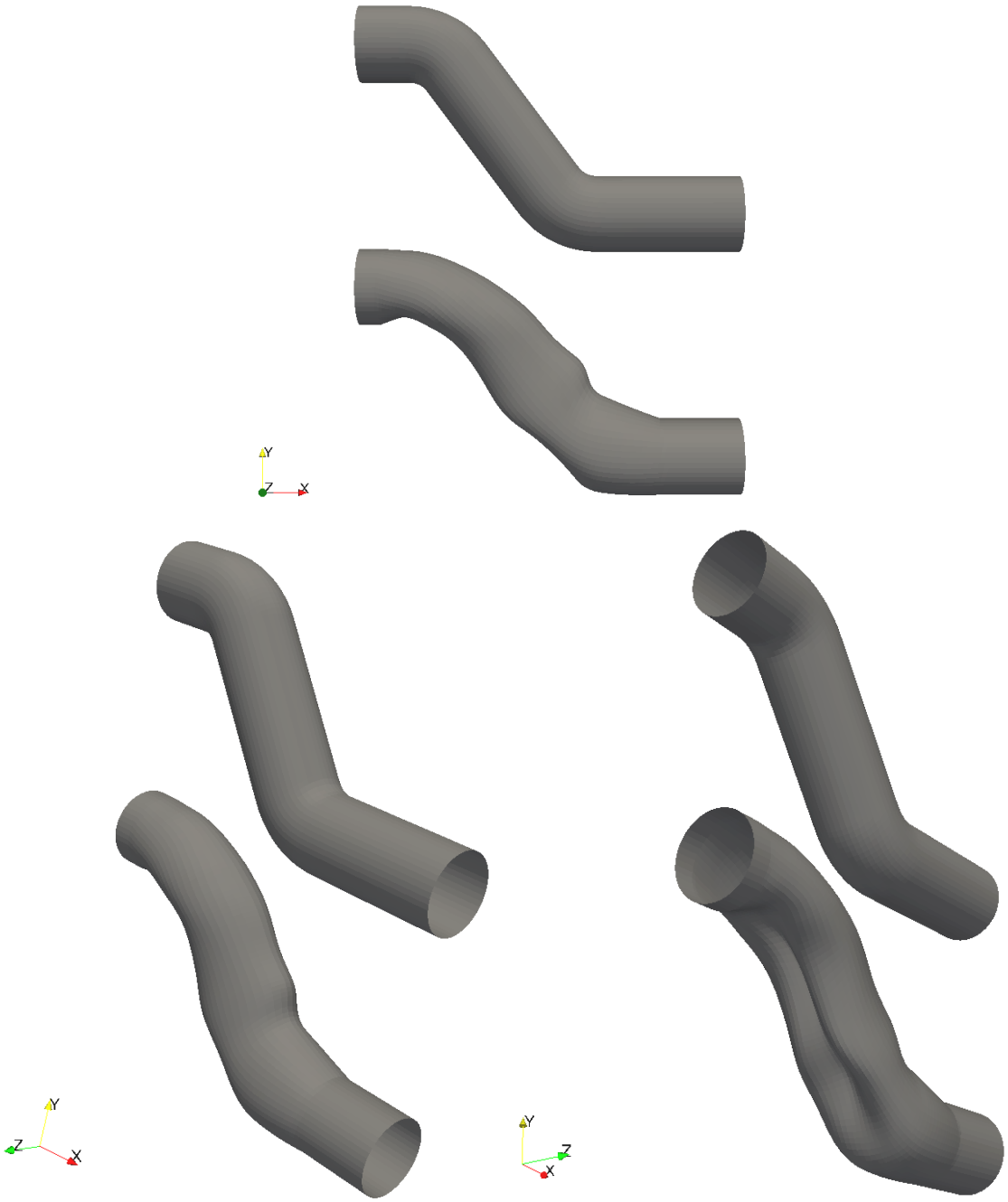

Figure 4.19: *S-shaped duct, $y^+ \approx 22$, $Re = 1 \times 10^5$. Initial (top) and optimized (bottom) geometry of the S-shaped duct, shown from different angles. Only the parameterized boundary is shown.*

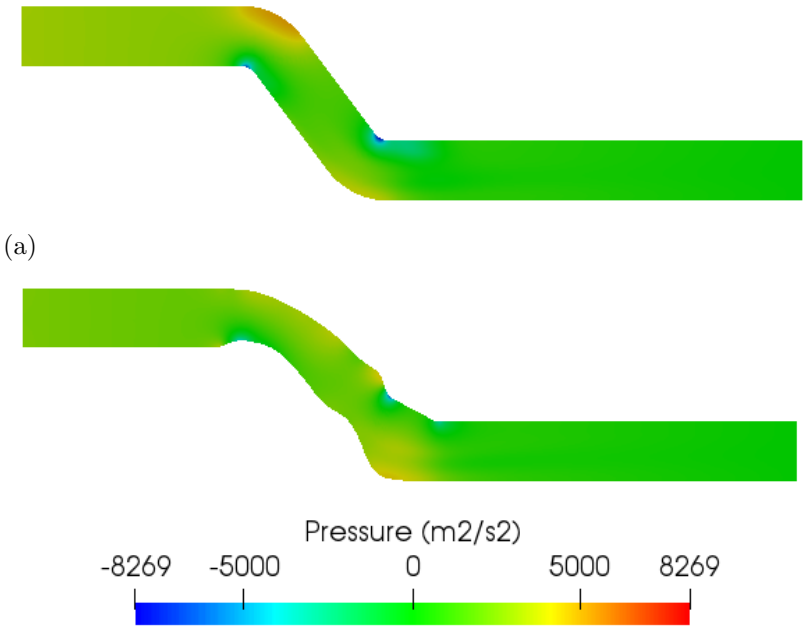

(a)

(b)

Figure 4.20: *S-shaped duct, $y^+ \approx 22$, $Re = 1 \times 10^5$. Pressure distribution on the initial (a) and optimized (b) geometry. Slice along the duct symmetry plane.*

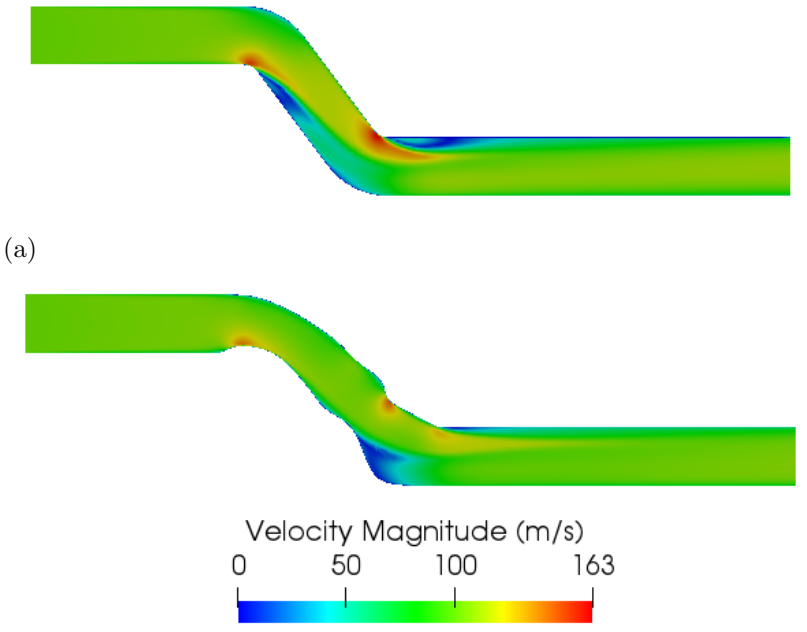

(a)

(b)

Figure 4.21: *S-shaped duct, $y^+ \approx 22$, $Re = 1 \times 10^5$. Velocity magnitude field on the initial (a) and optimized (b) geometry. Slice along the duct symmetry plane.*

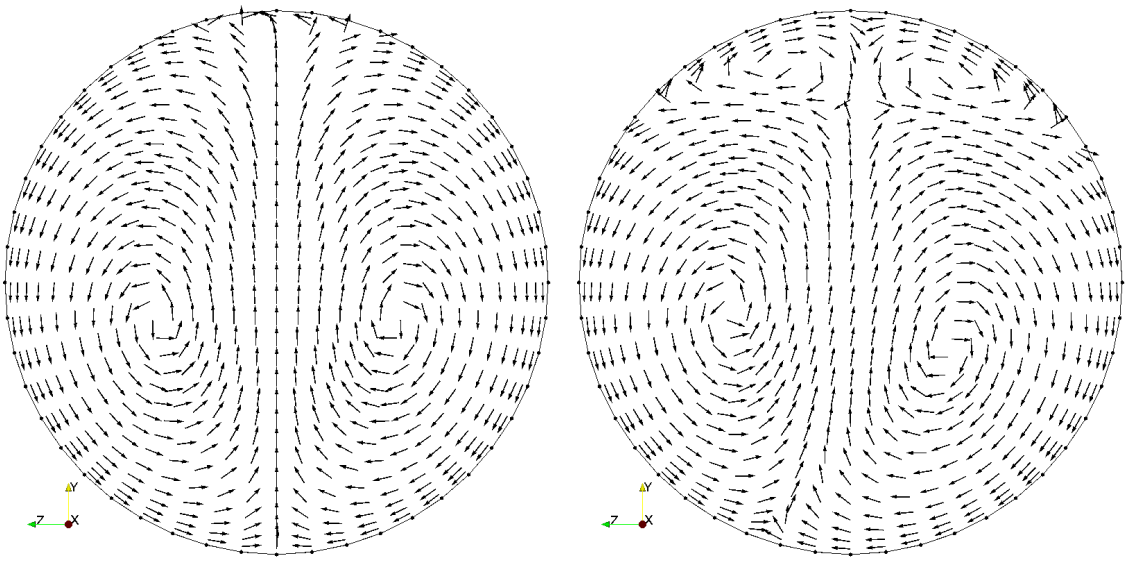

Figure 4.22: *S-shaped duct, $y^+ \approx 22$, $Re = 1 \times 10^5$. Surface vectors on a cross-section of the duct close to the outlet indicating the existence of secondary flows in the initial (left) and optimized (right) geometry.*

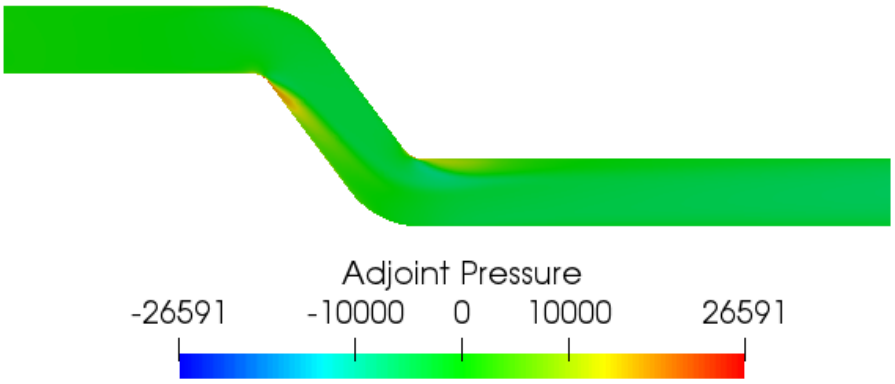

Figure 4.23: *S-shaped duct, $y^+ \approx 22$, $Re = 1 \times 10^5$. Adjoint pressure field computed on the initial geometry. Slice along the duct symmetry plane.*

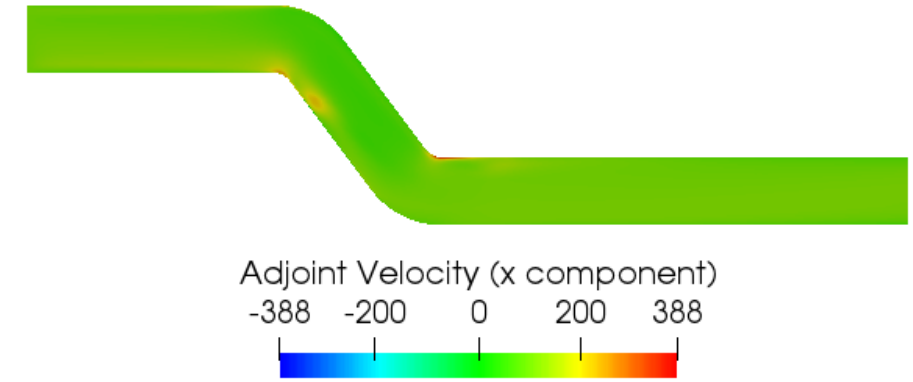

(a)

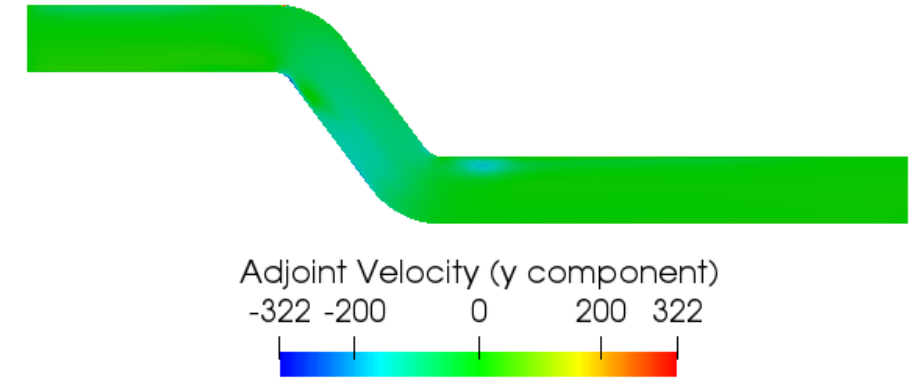

(b)

Figure 4.24: *S-shaped duct, $y^+ \approx 22$, $Re = 1 \times 10^5$. Adjoint velocity components x (a) and y (b) computed on the initial geometry. Slice along the duct symmetry plane.*

4.2.3 Minimization of Total Pressure Losses in an HVAC Duct

The final geometry that was optimized is that of an HVAC duct of a car (identical case as the one presented in Karoni 2018 [15] during her internship in BMW), again targeting the minimization of total pressure losses in a turbulent flow regime. The mesh is comprised of 2×10^6 cells, Reynolds number is $Re = 13800$, based on the hydraulic diameter of the inlet patch, and a greatly non-uniform y^+ ranges from 0.3 to 31 along the duct walls. Mesh parameterization is done using volumetric B-splines with 90 active control points. Design variables were updated using steepest descent and BFGS. The convergence rate is shown in fig. 4.25 and, as expected, BFGS converges faster. The optimization software drives the shape of the duct towards a geometry where the flow exhibits unsteady characteristics. As a result, the solution of the adjoint equations struggles to converge. The resulting geometry of the duct computed using steepest descent leads to approximately 9% less total pressure losses while the gain is 11% for the geometry generated with BFGS which reaches the objective minimum faster than steepest descent. A comparison of the initial and optimized shape is presented in fig. 4.26.

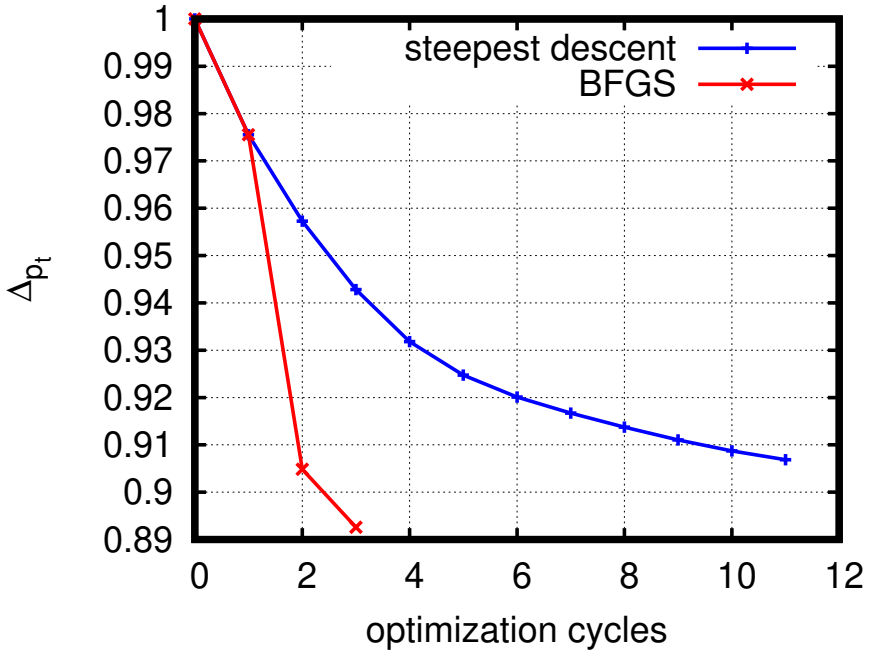

Figure 4.25: *HVAC duct, $Re = 13800$. Convergence rate of the objective function. The two optimization methods, steepest descent and BFGS are compared.*

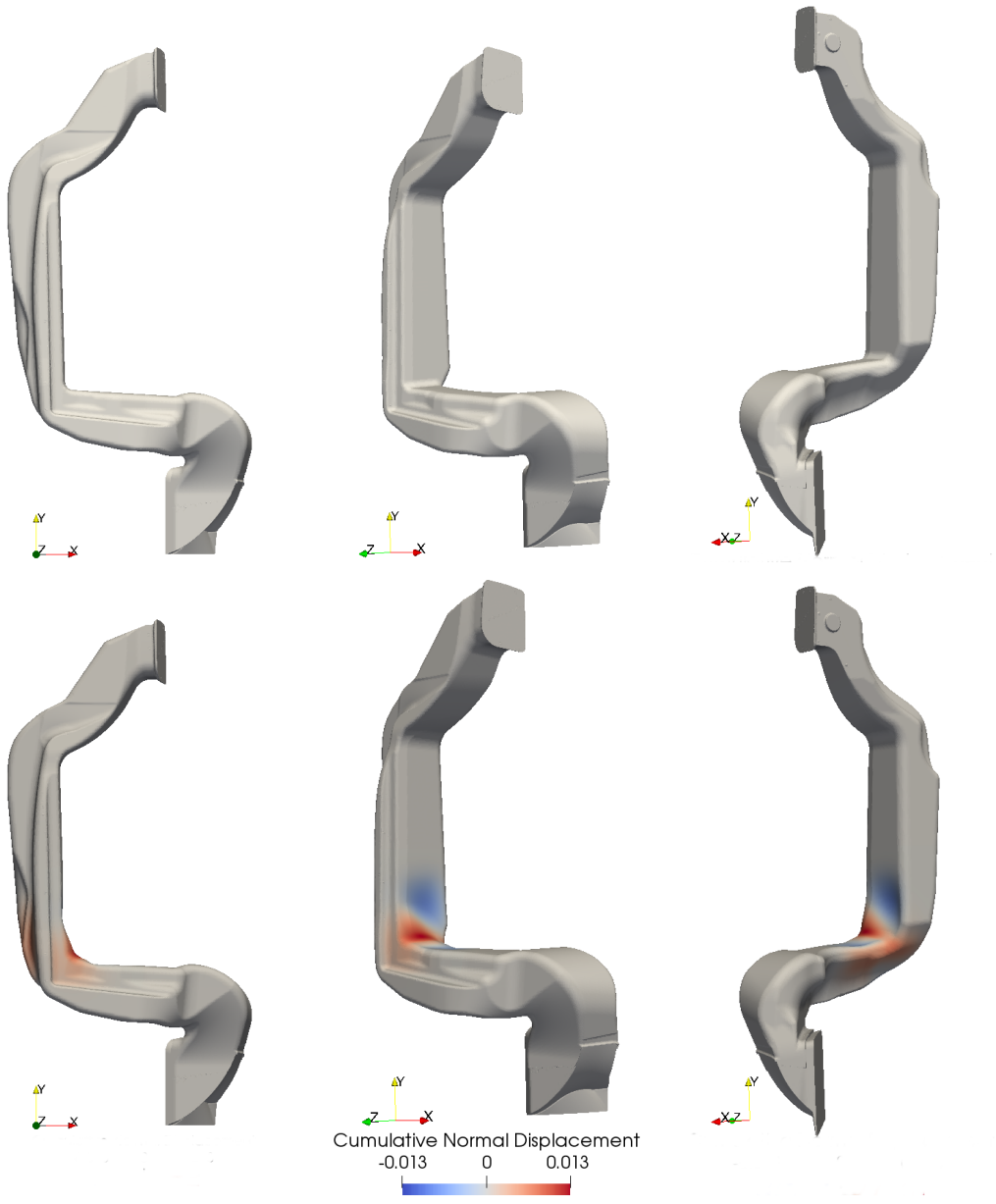

Figure 4.26: *HVAC duct, Re = 13800. Initial (top) and optimized (bottom) geometry. The cumulative normal displacement field indicates the direction in which the duct surface points moved, either outwards (red) or inwards (blue).*

Chapter 5

Various Implementation Studies

5.1 Higher-order pressure extrapolation at the wall

In OpenFOAM, a so-called zero Neumann condition is applied to pressure on certain boundary patches among which are solid walls. This study focuses on solid walls. The expression describing the behavior of pressure on such a boundary is given by

$$\frac{\partial p}{\partial n} = 0 \tag{5.1}$$

If the c index denotes a quantity stored at the center of the first cell adjacent to the boundary wall and the b index a quantity stored at the face of the cell that belongs to the boundary, then eq. 5.1 is discretized (with first-order accuracy) as

$$p_b = p_c \tag{5.2}$$

meaning that the pressure value on the wall where the zero gradient BC is imposed is the value of the adjacent cell. This is a zero-order accuracy extrapolation and, as discussed in [16], this badly reflects on the velocity vector orientation close to a wall boundary. With regards to the adjoint equations, this effect may result in high ATC (transpose convection term) values at the cells close to the wall [16] and as a result the adjoint equations may diverge. To circumvent this, a first order extrapolation is used to obtain the wall pressure field. The new BC is

$$p_b = p_c + \left.\frac{\partial p}{\partial x_i}\right|_c \Delta_i \tag{5.3}$$

where Δ_i is the vector joining the cell center to the face center.

5.2 Test Cases Revisited

5.2.1 The NACA4415 Airfoil Case - Revisited

The NACA4415 airfoil case presented in section 4.1 is revisited with the inclusion of the first order BC (eq. 5.3). Focus is laid on areas like the leading edge or areas with increased curvature (the exact location can be seen in fig. 5.2) as these locations are expected to actually show a change in the velocity vectors orientation. The change in the direction of the velocity vectors close to the leading edge is shown in fig. 5.1 and, in a different area of the airfoil surface, in fig. 5.2. The zero-order BC refers to using eq. 5.1 while the first-order BC refers to eq. 5.3. In what follows, a parametric study is performed for the SD computations. First, the adjoint equations are solved using eq. 5.1 for the adjoint pressure q and then, SD are computed using eqs. 5.1 and 5.3 both with the adjoint method and finite differences. The results are shown in fig. 5.3. No significant difference can be observed between the two cases. Then, the same study is performed for the adjoint pressure, once solving the primal equations with eq. 5.1 for the pressure at the wall and once using eq. 5.3. The latter are presented in fig. 5.4 and 5.5. It seems the use of eq. 5.3 for the adjoint pressure at the wall worsens the accuracy of the SD.

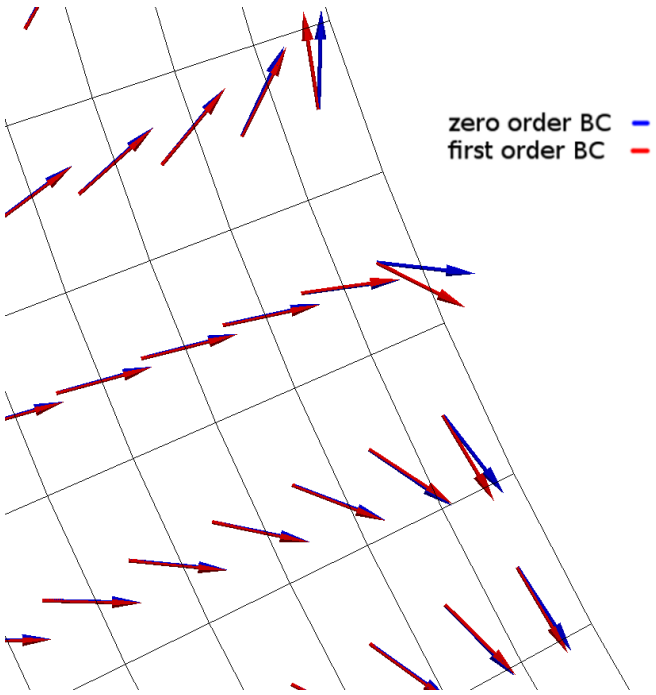

Figure 5.1: *NACA4415 airfoil,* $y^+ = 10$*,* $Re = 6 \times 10^6$*,* $a = 3^o$*. Velocity vectors computed by applying a zero-order BC for pressure (blue) compared to the first-order BC described by eq. 5.3 (red). The location shown is the leading edge of the airfoil.*

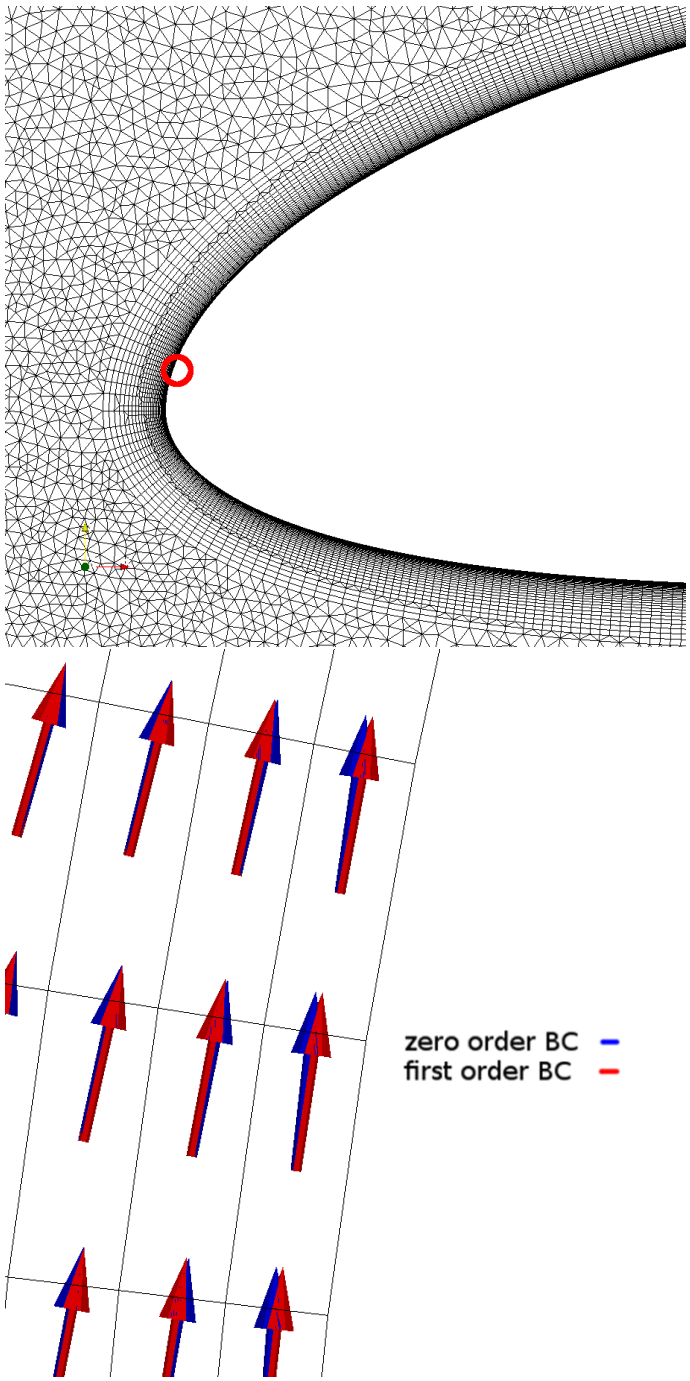

Figure 5.2: *NACA4415 airfoil, $y^+ = 10$, $Re = 6 \times 10^6$, $a = 3^o$. Velocity vectors computed by applying a zero-order BC for pressure (blue) compared to the first-order BC described by eq. 5.3 (red). The exact location of the flow is clearly marked.*

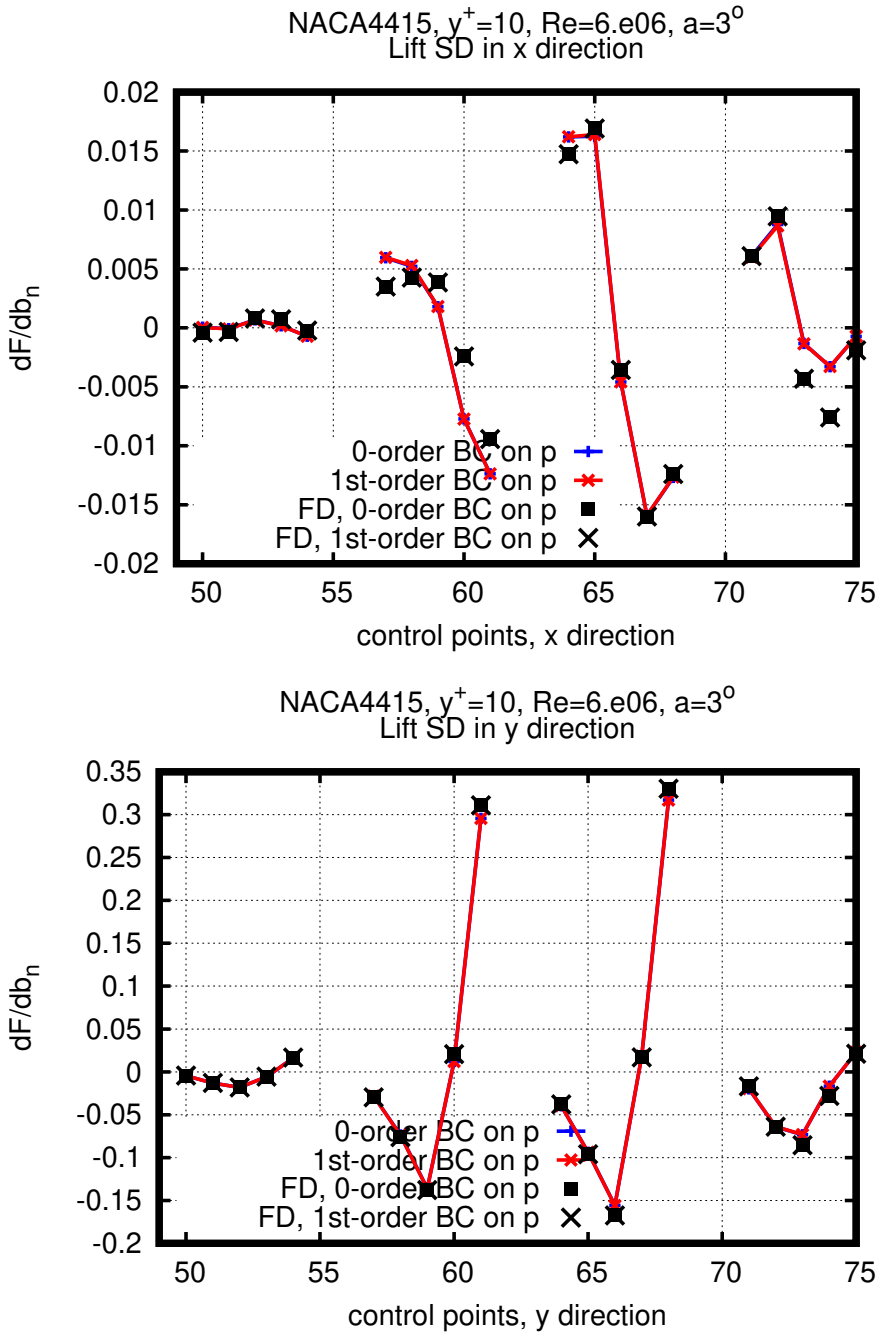

Figure 5.3: *NACA4415 airfoil, $y^+ = 10$, $Re = 6 \times 10^6$, a=3º. SD computed with the adjoint method, using a zero-order BC on pressure (red) and a first-order BC (blue) while a zero-order BC is applied on the adjoint pressure (p) at the wall. Reference SD are computed with finite differences, once using eq. 5.1 and once 5.3. Control points move in directions x (top) and y (bottom).*

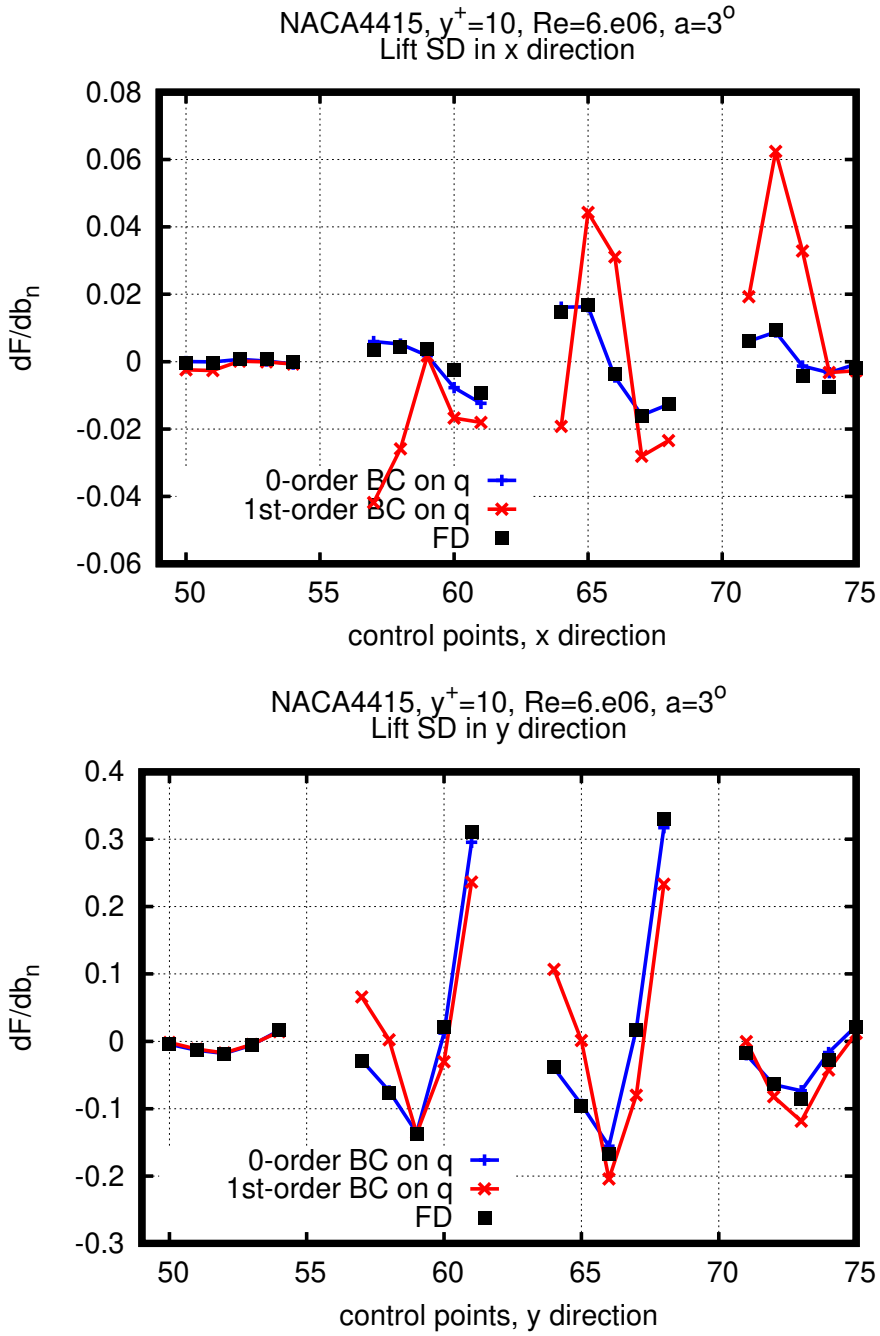

Figure 5.4: *NACA4415 airfoil, $y^+ = 10$, $Re = 6 \times 10^6$, a=3º. The primal equations are solved using eq. 5.1 for the pressure at the wall. SD are computed with the adjoint method using eq. 5.1 for the adjoint pressure (q) at the wall (blue) and eq. 5.3 (red). Control points move in directions x (top) and y (bottom).*

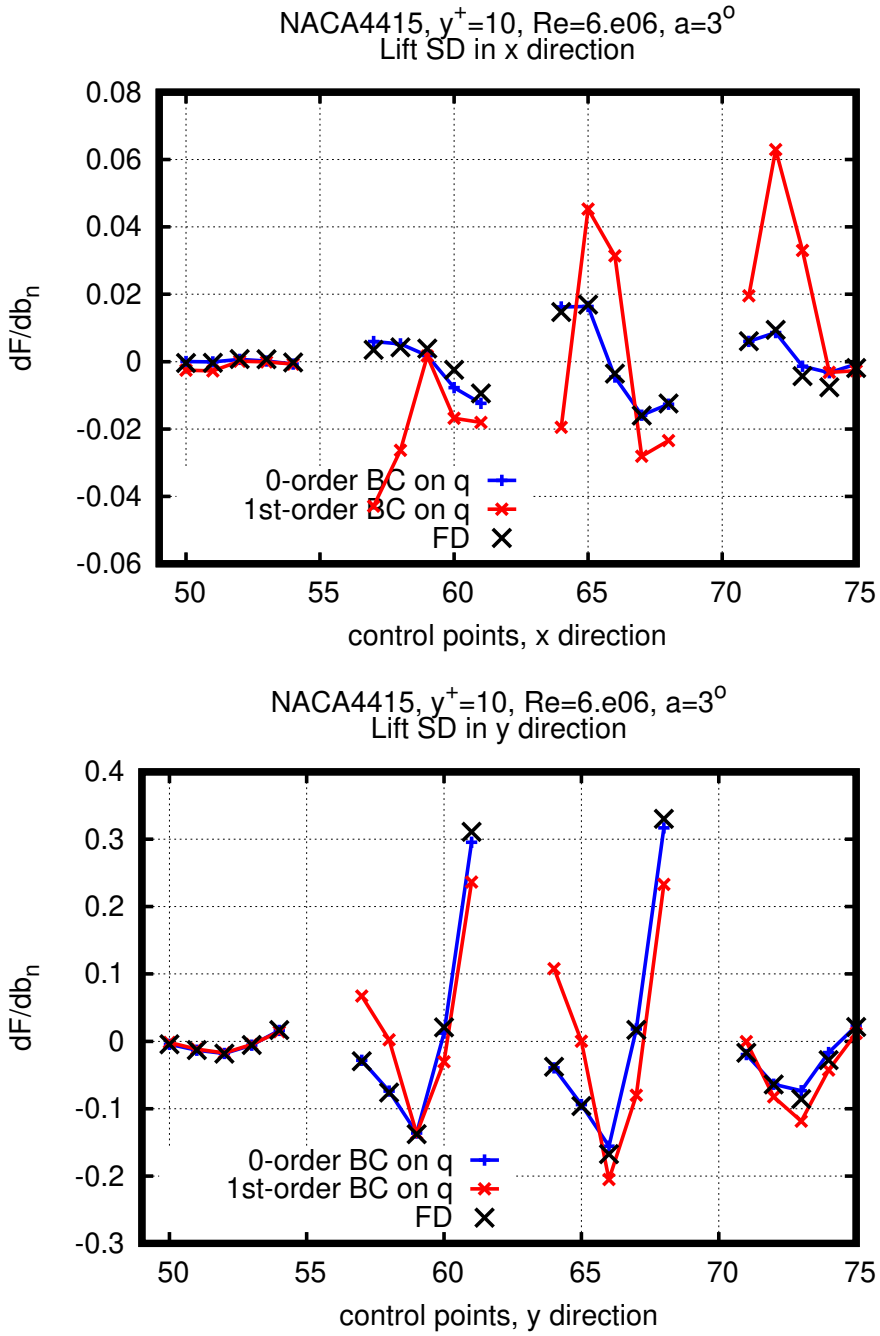

Figure 5.5: *NACA4415 airfoil, $y^+ = 10$, $Re = 6 \times 10^6$, a=3º. The primal equations are solved using eq. 5.3 for the pressure at the wall. SD are computed with the adjoint method using eq. 5.1 for the adjoint pressure (q) at the wall (blue) and eq. 5.3 (red). Control points move in directions x (top) and y (bottom).*

5.2.2 U-bend - Revisited

The U-bend case presented in section 4.2.1 with the inclusion of the first-order BC (eq. 5.3) is revisited. Results are focused on locations with increased surface curvature and the flow recirculation area, for the same reasons discussed in the previous case. The change in direction of the velocity vectors is minimal for the greatest part of the duct walls (fig. 5.6. Close to the flow recirculation area though this new BC influences the velocity field even at a distance from the walls, as shown in fig. 5.7. The same parametric study as the one described in the previous section is performed for the U-bend case. The results are presented in figs. 5.8 and 5.9. As is the case with the NACA4415 airfoil, using this BC on the adjoint pressure worsens the accuracy of the sensitivity derivatives computation. As a conclusion, it cannot

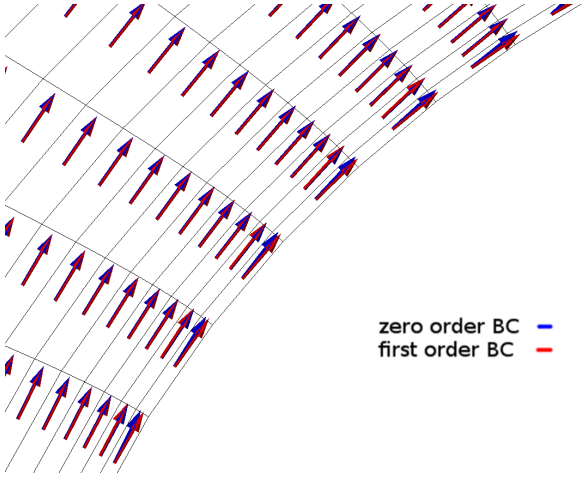

Figure 5.6: *U-bend, $y^+ = 10$, $Re = 1 \times 10^5$. Velocity vectors computed by applying a zero-order BC for the pressure gradient (blue) compared to a first-order BC (red). The location shown is the inner wall of the U-bend duct*

be said that the first-order extrapolation scheme improved the accuracy of the SD computations. Also, using the first-order extrapolation on the adjoint pressure yields poor results. However, this is not a conclusive statement as the effects of the first-order extrapolation seem to be case dependent. In [16], in the case presented there, flow separation occurs in certain areas close to the wall boundary, which appear only if the zero-order extrapolation scheme is used. This resulted in the generation of high ATC values that lead to the divergence of the adjoint equations and the remedy proposed was the use of the first-order scheme. This is not the case for the results presented herein, as in these examples there are no instances of flow separation occuring when using the zero-order scheme, that are also removed by applying the first-order extrapolation scheme.

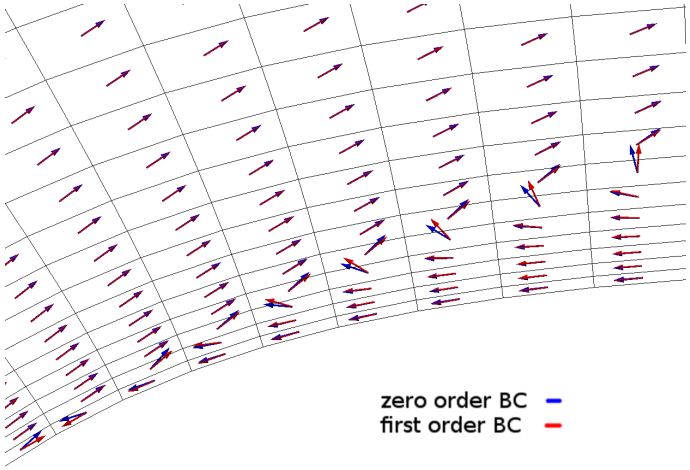

Figure 5.7: *U-bend, $y^+ = 10$, $Re = 1 \times 10^5$. Velocity vectors computed by applying a zero-order BC for the pressure gradient (blue) compared to a first-order BC (red). The location shown is close to the recirculation area, also shown in fig. 4.16.*

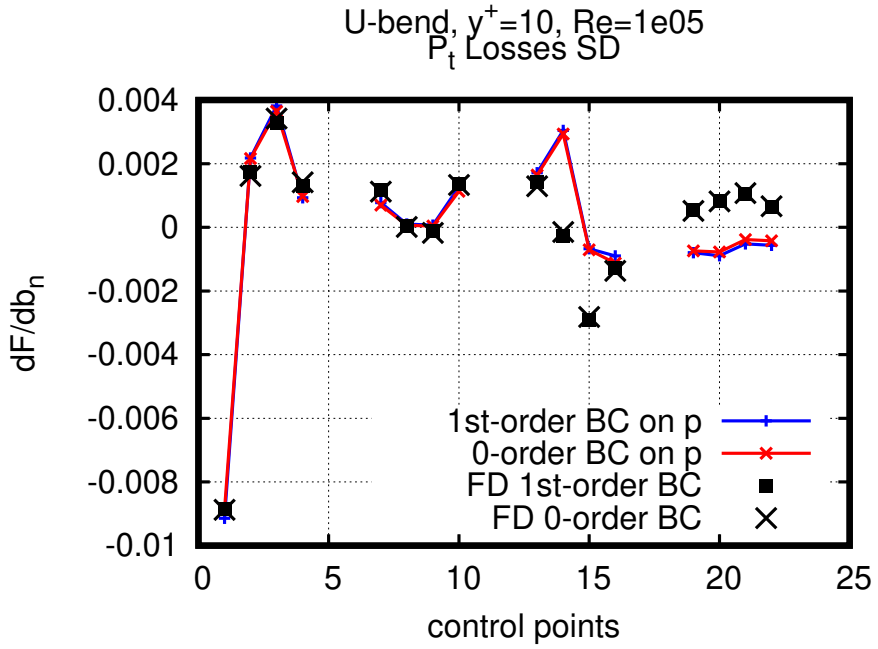

Figure 5.8: *U-bend, $y^+ = 10$, $Re = 1 \times 10^5$. SD computed with the adjoint method using a zero-order BC for the adjoint pressure. The primal equations are once solved with a zero-order BC for pressure (p) (red) and then, a first-order BC (blue). Reference SD computed with finite differences follow the same pattern. The first 8 points pertain to derivatives w.r.t. the y- coordinate while the remaining points w.r.t. to the x-coordinate of the control points.*

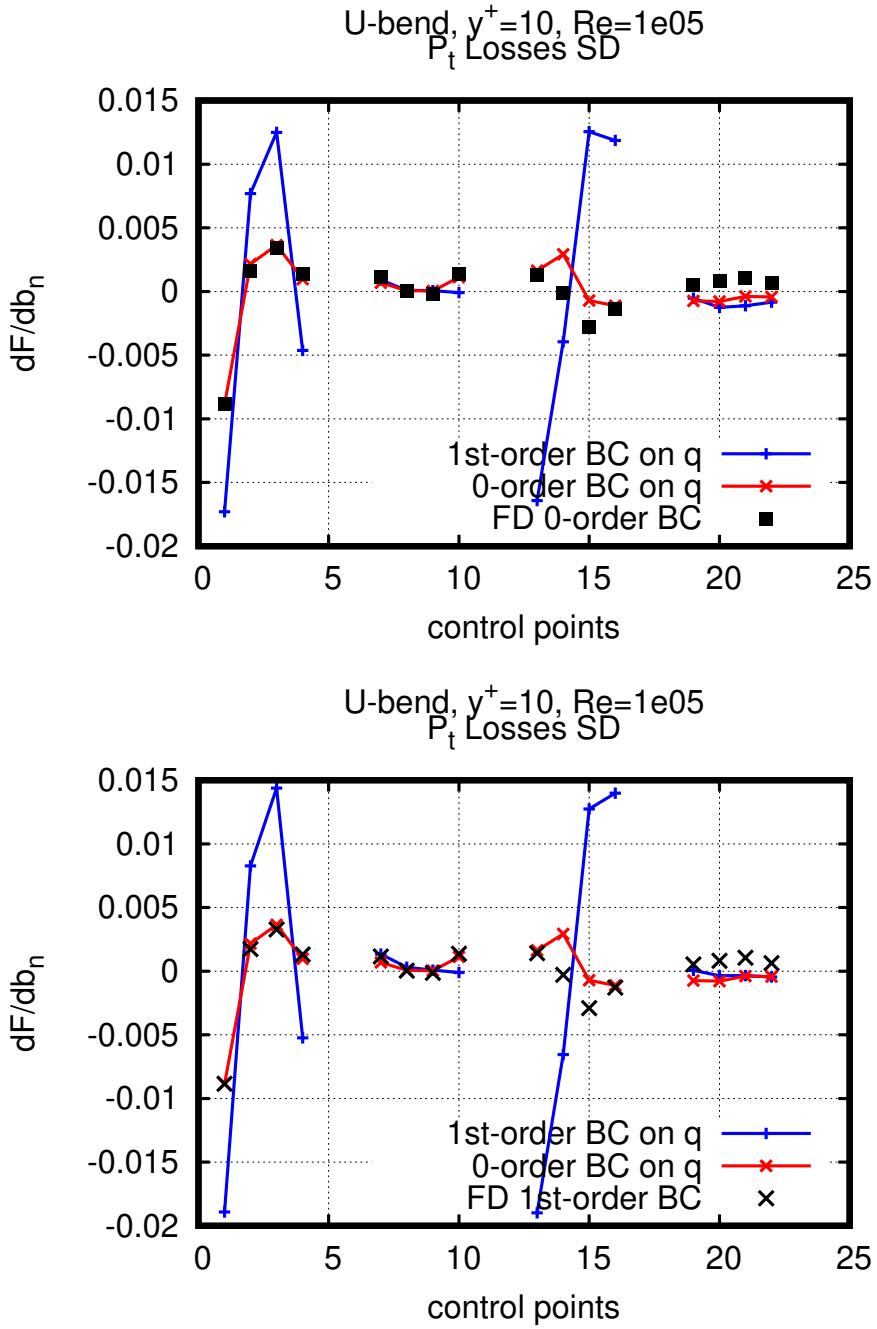

Figure 5.9: *U-bend, $y^+ = 10$, $Re = 1 \times 10^5$. Parametric study performed for the adjoint pressure BC while using a zero-order BC for the primal pressure at the wall (top) and then, a first-order BC for p (bottom). The first 8 points pertain to derivatives w.r.t. the y-coordinate while the remaining points w.r.t. to the x-coordinate of the control points.*

5.3 Revisiting the SD Expression

Upon revisiting eq. 3.55, focus is laid on one specific term found in T_{WF} which originates from the differentiation of the wall function and is written again here for the sake of completeness,

$$T_{SD} = \int_{S_{Wp}} \left(-u_i t_i^I + \frac{\partial F_{S_{Wp},k}}{\partial \tau_{ij}} n_k t_i^I n_j + \frac{\partial F_{S_{Wp},k}}{\partial \tau_{ij}} n_k t_j^I n_i \right) \tau_{ij} \frac{\delta \left(n_j t_i^I \right)}{\delta b_n} dS \tag{5.4}$$

where the normal and tangential to the wall unit vector components, n_i and t_i^I, are defined as in [3]. From now on, this term will be referred to as T_{SD}. Following an analysis of this term, it is safe to assume that it should be close to zero. Since

$$n_i \frac{\delta t_i^I}{\delta b_n} = -t_i^I \frac{\delta n_i}{\delta b_n} \tag{5.5}$$

$$n_j \frac{\delta n_j}{\delta b_n} = t_j^I \frac{\delta t_j^I}{\delta b_n} \tag{5.6}$$

and

$$\tau_{ij} \frac{\delta (n_j t_i^I)}{\delta b_n} = \underbrace{\tau_{ij} n_j \frac{\delta t_i^I}{\delta b_n}}_{\Phi_1} + \underbrace{\tau_{ij} t_i^I \frac{\delta n_j}{\delta b_n}}_{\Phi_2} \tag{5.7}$$

terms Φ_1 and Φ_2 in eq. 5.7 can further be developed into, by also taking into account eqs. 5.5 and 5.6,

$$\Phi_1 = n_k \tau_{kj} n_j n_i \frac{\delta t_i^I}{\delta b_n} + t_k^I \tau_{kj} n_j \underbrace{t_i^I \frac{\delta t_i^I}{\delta b_n}}_{=0} = -n_k \tau_{kj} n_j t_i^I \frac{\delta n_i}{\delta b_n} = -2\nu_{eff} \frac{\partial v_j}{\partial n} n_j t_i^I \frac{\delta n_i}{\delta b_n} \tag{5.8}$$

$$\Phi_2 = t_i^I \tau_{ik} n_k \underbrace{n_j \frac{\delta n_j}{\delta b_n}}_{=0} + t_i^I \tau_{ik} t_k^I t_j^I \frac{\delta n_j}{\delta b_n} = t_k^I \tau_{kj} t_j^I t_i^I \frac{\delta n_i}{\delta b_n} = 2\nu_{eff} \frac{\partial v_j}{\partial t^I} t_j^I t_i^I \frac{\delta n_i}{\delta b_n} \tag{5.9}$$

Terms Φ_1 and Φ_2 should both be close to zero, as the normal and tangential velocity components are not expected to drastically change in the normal and tangential directions respectively. Thus, term T_{SD} had, as of now, not been implemented in the code. However, in this thesis, a hypothesis was made, that the aforementioned two terms could make a noticeable difference to the SD values in sections of the flow with increased boundary curvature (such as the curved section of a U-bend duct). This hypothesis has been tested on the U-bend duct presented in section 4.2.1 and the result is presented in fig. 5.10. The addition of T_{SD} term does not

have a noticeable effect on the SD computations.

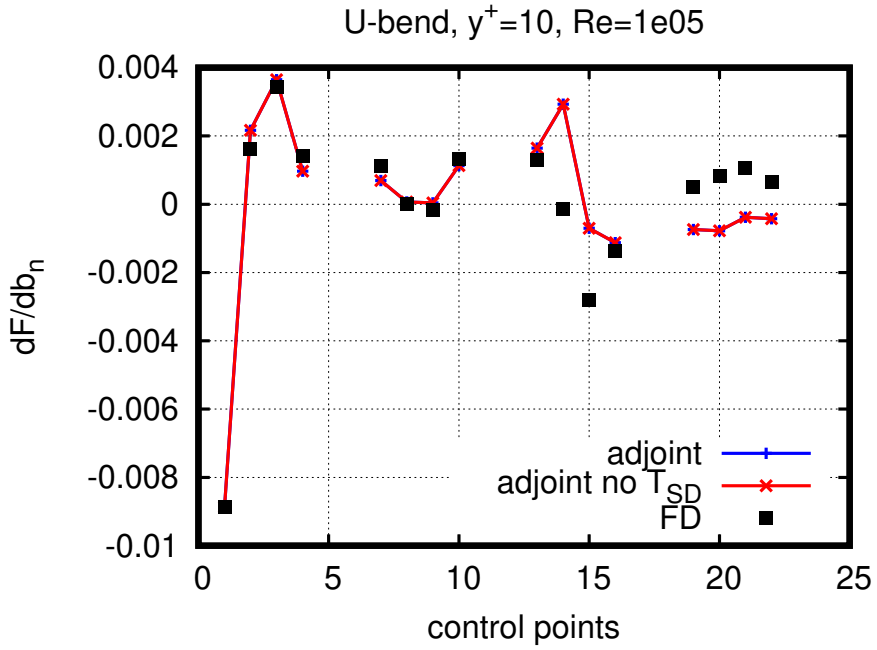

Figure 5.10: *U-bend, $y^+ \approx 10$, $Re = 1 \times 10^5$. Evaluation of the addition of term T_{SD} to the sensitivity derivatives computation.*

Chapter 6

Conclusions

The first part of this thesis is focused on the validation of SD computations with the adjoint method on high-Re meshes. The adjoint solver has been succesfully tested on the NACA4415 isolated airfoil, on two meshes with y^+ values of 10 and 50. On a $y^+ = 10$ mesh, the computations are more accurate when compared with reference SD computed with FD. Afterwards, shape optimization has been succesfully performed on the NACA4415 airfoil targeting lift maximization and drag minimization. The shape optimization software was capable of handling the two optimization problems in a turbulent flow solved on a high-Re mesh. For lift maximization, a constrain on the moment coefficient would be necessary for an industrial application. Focus was then shifted towards internal aerodynamics, where, this time, shape optimization targeting minimization total pressure losses, between the inlet and outlet (Δ_{P_t}), was performed on three test cases, a 2D U-bend duct, a 3D S-shaped duct and an HVAC duct (automotive industry application). Unsteady flow characteristics were observed during the optimization loop in both of the two 3D cases (S-shaped duct and HVAC). As a result, the optimization process was hindered, either due to an inability for further evolution of the primal equations or divergence of the adjoint equations. The gain in Δ_{P_t} was 25% in the S-shaped duct case and 11% for the HVAC duct, without though imposing other constrains. An additional problem that was encountered was the deterioration of mesh quality through each optimization iteration due to the use of a Laplace model used displacing the inner mesh. During shape optimization of the HVAC duct, two optimization methods were used, steepest descent and BFGS, achieving 9% and 11% reduction in Δ_{P_t} respectively. BFGS exhibited convergence at a much higher rate than steepest descent, as expected. In both methods, further evolution of the optimization algorithm was stopped due to the divergence of the adjoint equations. It could be likely that BFGS reached the final geometry, before failing, through taking a slightly different route or by taking larger steps, generating intermediate geometries that did not exhibit unsteadiness and were closer to the minimum of the objective function, while steepest descent

reached a geometry that did not favor further evolution of the adjoint equations at an intermediate step. Hence the resulting difference in the optimization results w.r.t. to the minimum Δ_{P_t}.

The second part of the thesis focuses on various implementation studies for the primal and adjoint solvers of OpenFOAM. First, a first-order extrapolation scheme was adopted for the primal pressure at the wall (instead of the zero-order scheme already implemented in OpenFOAM), and its effects on the SD computations were evaluated. Reportedly, a higher order scheme for the extrapolation of pressure at the wall boundary can have a benefficial effect on the adjoint equations convergence [16]. However, this seems to be case-dependent and mostly pertains to flows where flow separation occurs and large ATC values appear in the adjoint equations on cells close to the wall. In the cases presented herein, there was no improvement to the accuracy of SD computations. Secondly, a study was performed concerning one term in the SD expression, labeled T_{SD} in this thesis, that was assumed to have a negligible effect on the final SD value. This hypothesis was revisited on the U-bend test case and it seems that this term is in fact close to zero.

Concluding this thesis, the adjoint-based optimization tool, developed by PCOpt/NTUA, was capable of handling shape optimization problems in turbulent flows by making use of the so-called adjoint wall functions. Additional research could be performed in areas regarding the stability of the adjoint equations and the restriction of the optimization process to generating geometries that keep the flow in steady state conditions.

Appendix A

Pressure-based Solution Algorithms

A.1 SIMPLE Algorithm

In SIMPLE, the semi-discretized momentum equations are written down for the cell with index P as

$$\alpha_P v_{P,i} = \sum_{N=1}^{NB(P)} \alpha_N v_{N,i} - \frac{\partial p}{\partial x_i} + b_i \tag{A.1}$$

where α_P and α_N are discretization coefficients that result from the discretization of the diffusion and convection terms, b_i denotes any source terms that may appear in momentum equations and NB(P) symbolizes the adjacent cells to P.
SIMPLE is a segregated algorithm which means that the momentum equations are solved separately from the continuity equation, yielding an intermediate velocity field denoted as v_i^*. This tentative velocity field is computed using the existing pressure field, denoted as p^* and, at this preliminary stage, it does not satisfy the continuity equation. So, the semi-discretized momentum equations are written again as

$$\alpha_P v_{P,i}^* = \sum_{N=1}^{NB(P)} \alpha_N v_{N,i}^* - \frac{\partial p^*}{\partial x_i} + b_i^* \tag{A.2}$$

Solving eq. A.2, a predicition for the velocity field is derived

$$\alpha_P v_{P,i}^* = H_{P,j} - \frac{\partial p^*}{\partial x_i} \tag{A.3}$$

where

$$H_{P,i} = \sum_{N=1}^{NB(P)} \alpha_N v_{N,i}^* + b_i^* \tag{A.4}$$

Let us assume that corrections $v_i^{'}$ and $p^{'}$ should be superimposed on the velocity and pressure respectively, so as to satisfy the continuity equation,

$$\begin{aligned} v_i &= v_i^* + v_i^{'} \\ p &= p^* + p^{'} \end{aligned} \tag{A.5}$$

Subtracting eq. A.3 from A.2 and assuming that corrections of the source are negligible. the following equation is derived for the correction fields,

$$\alpha_P v_{P,i}^{'} = \sum_{N=1}^{NB(P)} \alpha_N v_{N,i}^{'} - \frac{\partial p^{'}}{\partial x_i} \tag{A.6}$$

By further assuming that the first term on the right-hand side of A.6 is negligible, compared to the pressure gradient, a more simplified expression results in

$$v_{P,i}^{'} = -\frac{1}{\alpha_P}\frac{\partial p^{'}}{\partial x_i} \tag{A.7}$$

Then, by combining eqs. A.7 and 2.2, we arrive at

$$\frac{\partial v_j}{\partial x_j} = 0 \Rightarrow \frac{\partial v_j^{'}}{\partial x_j} = -\frac{\partial v_j^*}{\partial x_j} \tag{A.8}$$

By substituting eq. A.7 into eq. A.8 we get

$$\frac{\partial}{\partial x_j}\left(\frac{1}{\alpha_P}\frac{\partial p^{'}}{\partial x_j}\right) = \frac{\partial}{\partial x_j}\left(\frac{1}{\alpha_P}H_{P,j} - \frac{1}{\alpha_P}\frac{\partial p^*}{\partial x_j}\right) \Rightarrow \frac{\partial}{\partial x_j}\left(\frac{1}{\alpha_P}\frac{\partial p}{\partial x_j}\right) = \frac{\partial}{\partial x_j}\left(\frac{1}{\alpha_P}H_{P,j}\right) \tag{A.9}$$

which is a Poisson equation for pressure. Integrating this equation over a cell P with N_f faces yields

$$\sum_{f=1}^{N_f} \overline{\hat{v}_{f,j}} S_{f,j} = \sum_{f=1}^{N_f} \frac{1}{\overline{\alpha_f}}\left(\frac{\partial p}{\partial x_j}S_j\right)_f \tag{A.10}$$

where

$$\hat{v}_{P,j} = \frac{1}{\alpha_P}H_{P,j} \tag{A.11}$$

Note that all of the above quantities are defined at the cell faces and are computed by interpolating the equivalent values of the adjacent cell centres with the exception of the normal directional derivative of pressure on the RHS of eq. A.10.

The final pressure field is obtained by solving eq. A.10. Subsequently, the velocity field is corrected by

$$\begin{aligned} v_{P,i} &= v^*_{P,i} + v^{'}_{P,i} \Rightarrow \\ v_{P,i} &= \hat{v}_{P,i} - \frac{1}{\alpha_P}\frac{\partial p^*}{\partial x_i} - \frac{1}{\alpha_P}\frac{\partial p^{'}}{\partial x_i} \Rightarrow \\ v_{P,i} &= \hat{v}_{P,i} - \frac{1}{\alpha_P}\frac{\partial p}{\partial x_i} \end{aligned} \tag{A.12}$$

As a final step, the volume flux $\dot{m}_f$ is computed as

$$\dot{m}_f = v_{f,j}S_{f,j} = \overline{\hat{v}_{f,j}}S_{f,j} - \frac{1}{\overline{\alpha_f}}\left(\frac{\partial p}{\partial x_j}S_j\right)_f \tag{A.13}$$

Εθνικό Μετσόβιο Πολυτεχνείο
Σχολή Μηχανολόγων Μηχανικών
Τομέας Ρευστών
Μονάδα Παράλληλης ΥΡΔ & Βελτιστοποίησης

Συνεισφορά στη Συνεχή Συζυγή Μέθοδο με Εφαρμογές στη Βελτιστοποίηση Μορφών σε Τυρβώδεις Ροές

Εκτενής περίληψη μεταπτυχιακής εργασίας
''ΔΠΜΣ Υπολογιστική Μηχανική''

Θεμιστοκλής Σκαμάγκης

Επιβλέπων: Κ. Χ. Γιαννάκογλου, Καθηγητής ΕΜΠ

Αθήνα, Ιανουάριος 2019

Εισαγωγή

Η μεταπτυχιακή εργασία αποσκοπεί στη διερεύνηση και επαλήθευση του κώδικα βελτιστοποίησης, βασισμένου στη μέθοδο συζυγών μεταβλητών, που αναπτύσσεται από την ΜΠΥΡΒ σε τυρβώδεις ροές, οι οποίες επιλύονται σε κατάλληλα αραιά πλέγματα κάνοντας χρήση συναρτήσεων τοίχου. Έμφαση δίνεται στην ακρίβεια των παραγώγων ευαισθησίας και την αποτελεσματικότητα στην εύρεση βέλτιστου σχήματος, τόσο σε προβλήματα εξωτερικής όσο και εσωτερικής αεροδυναμικής. Δευτερεύων σκοπός είναι η συνεισφορά στον κώδικα συζυγούς μεθόδου με στόχο τη βελτίωση της ακρίβειας των παραγώγων ευαισθησίας.

Διατύπωση Συζυγών Εξισώσεων

Αφετηρία για την εξαγωγή των συζυγών εξισώσεων είναι η μαθηματική διατύπωση του πρωτεύοντος προβλήματος, δηλαδή των εξισώσεων ροής μαζί με το μοντέλο τύρβης Spalart-Allmaras, οι οποίες είναι

$$R^p = -\frac{\partial v_j}{\partial x_j} = 0 \tag{Α′.14α′}$$

$$R_i^v = v_j \frac{\partial v_i}{\partial x_j} - \frac{\partial}{\partial x_j}\left[(\nu + \nu_t)\left(\frac{\partial v_i}{\partial x_j} + \frac{\partial v_j}{\partial x_i}\right)\right] + \frac{\partial p}{\partial x_i} = 0\ , \qquad i = 1, 2(, 3) \tag{Α′.14β′}$$

$$R^{\widetilde{\nu}} = v_j \frac{\partial \widetilde{\nu}}{\partial x_j} - \frac{\partial}{\partial x_j}\left[\left(\nu + \frac{\widetilde{\nu}}{\sigma}\right)\frac{\partial \widetilde{\nu}}{\partial x_j}\right] - \frac{c_{b2}}{\sigma}\left(\frac{\partial \widetilde{\nu}}{\partial x_j}\right)^2 - \widetilde{\nu}\, P\left(\widetilde{\nu}\right) + \widetilde{\nu}\, D\left(\widetilde{\nu}\right) = 0 \tag{Α′.14γ′}$$

$$R^{\Delta} = \frac{\partial\left(c_j \Delta\right)}{\partial x_j} - \Delta \frac{\partial^2 \Delta}{\partial x_j^2} - 1 \tag{Α′.14δ′}$$

όπου v_i η ταχύτητα του ρευστού, ν είναι η συνεκτικότητα, ν_t η τυρβώδης συνεκτικότητα και p η στατική πίεση διαιρεμένη με την πυκνότητα του ρευστού. Η ανεξάρτητη μεταβλητή για την οποία επιλύεται το μοντέλο τύρβης είναι η $\widetilde{\nu}$ και συνδέεται με την τυρβώδη συνεκτικότητα μέσω $\nu_t = \widetilde{\nu} f_{v_1}$ (βλ. κεφάλαιο 2). Η μεταβλητή Δ είναι η απόσταση του κέντρου ενός κελιού από τον πλησιέστερο τοίχο. Η εξίσωση Α′.14δ′ είναι η εξίσωση Hamilton-Jacobi [3] όπου $c_j = \frac{\partial \Delta}{\partial x_j}$. Η παρουσίαση της διατύπωσης του συζυγούς συστήματος εξισώσεων ακολουθεί μια γενικευμένη μεθοδολογία. Επειδή οι αντικειμενικές συναρτήσεις, που αφορούν στα προβλήματα που παρουσιάζονται σε αυτή την εργασία, ορίζονται ως επιφανειακά ολοκληρώματα, σε συγκεκριμένα (κατά περίπτωση) όρια του χωρίου, υιοθετείται η παρακάτω έκφραση

$$F = \int_S F_{S,i} n_i dS \tag{Α′.15}$$

όπου n_i το μοναδιαίο κάθετο με φορά προς τα έξω διάνυσμα στην επιφάνεια S και $F_{S,i}$ όλοι οι όροι που δεν περιέχουν γεωμετρικές ποσότητες. Στη συνέχεια, καταστρώνεται μια έκφραση για την επαυξημένη αντικειμενική συνάρτηση F_{aug}, δεδομένου ότι τα

υπόλοιπα των εξισώσεων Α′.14 είναι μηδέν μετά την επίλυση της ροής,

$$F_{aug} = F + \int_V u_i R_i^v dV + \int_V q R^p dV + \int_V \widetilde{\nu_a} R^{\widetilde{\nu}} dV + \int_V \Delta_\alpha R^\Delta dV \tag{Α′.16}$$

Ξεκινώντας με τη διαφόριση της εξίσωσης Α′.16 και εν συνεχεία, θέτοντας τους πολλαπλασιαστές των μεταβολών των ροϊκών μεταβλητών ως προς τις μεταβλητές σχεδιασμού ίσους με μηδέν, προκύπτουν οι συζυγείς πεδιακές εξισώσεις

$$R^q = -\frac{\partial u_j}{\partial x_j} = 0 \tag{Α′.17α′}$$

$$\begin{aligned} R_i^u = {} & u_j \frac{\partial v_j}{\partial x_i} - \frac{\partial (u_i v_j)}{\partial x_j} - \frac{\partial}{\partial x_j}\left[(\nu + \nu_t)\left(\frac{\partial u_i}{\partial x_j} + \frac{\partial u_j}{\partial x_i}\right)\right] + \frac{\partial q}{\partial x_i} \\ & - \frac{\partial}{\partial x_l}\left(\widetilde{\nu_a}\widetilde{\nu}\mathcal{C}_Y \frac{1}{Y} e_{mjk}\frac{\partial v_k}{\partial x_j} e_{mli}\frac{\partial}{\partial x_l}\right) + \widetilde{\nu_a}\frac{\partial \widetilde{\nu}}{\partial x_i} = 0 \end{aligned} \tag{Α′.17β′}$$

$$\begin{aligned} R^{\widetilde{\nu_a}} = {} & \frac{\partial \nu_t}{\partial \widetilde{\nu}}\frac{\partial u_i}{\partial x_j}\left(\frac{\partial v_i}{\partial x_j} + \frac{\partial v_j}{\partial x_i}\right) - \frac{\partial (\widetilde{\nu_a} v_j)}{\partial x_j} + \frac{1}{\sigma}\frac{\partial \widetilde{\nu_a}}{\partial x_j}\frac{\partial \widetilde{\nu}}{\partial x_j} - \frac{\partial}{\partial x_j}\left[\frac{\partial \widetilde{\nu_a}}{\partial x_j}\left(\nu + \frac{\widetilde{\nu}}{\sigma}\right)\right] \\ & + 2\frac{c_{b2}}{\sigma}\frac{\partial}{\partial x_j}\left[\widetilde{\nu_a}\frac{\partial \widetilde{\nu}}{\partial x_j}\right] + \widetilde{\nu_a}\widetilde{\nu}C_{\widetilde{\nu}} + \widetilde{\nu_a}\widetilde{\nu}(-P + D) = 0 \end{aligned} \tag{Α′.17γ′}$$

$$R^{\Delta_\alpha} = -2\frac{\partial}{\partial x_j}\left(\Delta_\alpha \frac{\partial \Delta}{\partial x_j}\right) + \widetilde{\nu}\widetilde{\nu_a}C_\Delta \tag{Α′.17δ′}$$

Οι αντίστοιχες οριακές συνθήκες παρουσιάζονται στο κυρίως κείμενο (στην αγγλική γλώσσα) και παραλείπονται για λόγους συντομίας. Η τελική έκφραση των παραγώγων ευαισθησίας είναι η

$$\begin{aligned} \frac{\delta F_{aug}}{\delta b_n} = {} & \int_V \left(FI_{jk}^L + FI_{jk}^T\right)\frac{\partial}{\partial x_j}\left(\frac{\delta x_k}{\delta b_n}\right) dV \\ & + \int_{S_{W_p}} F_{S_{W_p},i}\frac{\delta n_i}{\delta b_n} dS + \int_{S_{W_p}} F_{S_{W_p},i} n_i \frac{\delta (dS)}{\delta b_n} + T_{WF} + T_G \end{aligned} \tag{Α′.18}$$

όπου S_{W_p} είναι το παραμετροποιημένο όριο. Ο όρος T_{WF} στο δεξί μέλος της εξ. 3.55 προέρχεται από τη διαφόριση των συναρτήσεων τοίχου. Οι όροι T_G και T_{WF} είναι,

$$\begin{aligned} T_G = {} & -\int_{S_{W_p}}\left(-u_k n_k + \frac{\partial F_{S_{W_p},k}}{\partial \tau_{lz}} n_k n_l n_z\right)\tau_{ij}\frac{\delta (n_i n_j)}{\delta b_n} dS - \int_{S_{W_p}} \frac{\partial F_{S_{W_p},k}}{\partial \tau_{lz}} n_k t_l^I t_z^I \tau_{ij}\frac{\delta (t_i^I t_j^I)}{\delta b_n} dS \\ & - \int_{S_{W_p}} \frac{\partial F_{S_{W_p},k}}{\partial \tau_{lz}} n_k t_l^{II} t_z^{II} \tau_{ij}\frac{\delta (t_i^{II} t_j^{II})}{\delta b_n} dS - \int_{S_{W_p}} \frac{\partial F_{S_{W_p},k}}{\partial \tau_{lz}} n_k \left(t_l^{II} t_z^I + t_l^I t_z^{II}\right)\tau_{ij}\frac{\delta (t_i^{II} t_j^I)}{\delta b_n} dS \end{aligned} \tag{Α′.19}$$

$$
\begin{aligned}
T_{WF} = & \int_{S_{W_p}} C_{\Delta}^{WF} \left(-u_i t_i^I + \frac{\partial F_{S_{W_p},k}}{\partial \tau_{ij}} n_k t_i^I n_j + \frac{\partial F_{S_{W_p},k}}{\partial \tau_{ij}} n_k t_j^I n_i \right) \frac{\delta \Delta^P}{\delta b_n} dS \\
& + \int_{S_{W_p}} 2 v_\tau C_v^{WF} \frac{v_i^P}{|\vec{v}|} \left(-u_i t_i^I + \frac{\partial F_{S_{W_p},k}}{\partial \tau_{ij}} n_k t_i^I n_j + \frac{\partial F_{S_{W_p},k}}{\partial \tau_{ij}} n_k t_j^I n_i \right) \frac{\delta v_i^P}{\delta b_n} dS \\
& + \int_{S_{W_p}} \left(-u_i t_i^I + \frac{\partial F_{S_{W_p},k}}{\partial \tau_{ij}} n_k t_i^I n_j + \frac{\partial F_{S_{W_p},k}}{\partial \tau_{ij}} n_k t_j^I n_i \right) \tau_{ij} \frac{\delta \left(n_j t_i^I \right)}{\delta b_n} dS \qquad \text{(A}'.20\text{)}
\end{aligned}
$$

Ακρίβεια των Παραγώγων Ευαισθησίας

Η επικύρωση του συζυγούς επιλύτη έγινε σε μία αεροτομή NACA4415. Το πλέγμα αποτελείται από 2×10^5 κελιά, η γωνία της επ΄άπειρον ροής είναι $\alpha = 3^o$ και ο αριθμός Reynolds $Re = 6 \times 10^6$. Η παραμετροποίηση της γεωμετρίας έγινε με ογκομετρικές B-splines και το πλέγμα ελέγχου φαίνεται στο Σχήμα Α΄.1. Οι παράγωγοι ευαισθησίας που υπολογίστηκαν με τη συζυγή μέθοδο συγκρίνονται με παραγώγους αναφοράς που έχουν υπολογιστεί με πεπερασμένες διαφορές. Η ίδια εργασία έγινε σε δύο πλέγματα, ένα με $y^+ = 10$ και ένα με $y^+ = 50$ (ο αριθμός των κελιών παραμένει περίπου 2×10^5 και στα δύο πλέγματα). Η αντικειμενική συνάρτηση είναι η δύναμη άνωσης που ασκείται στην αεροτομή. Τα αποτελέσματα παρουσιάζονται στο Σχήμα Α΄.2.

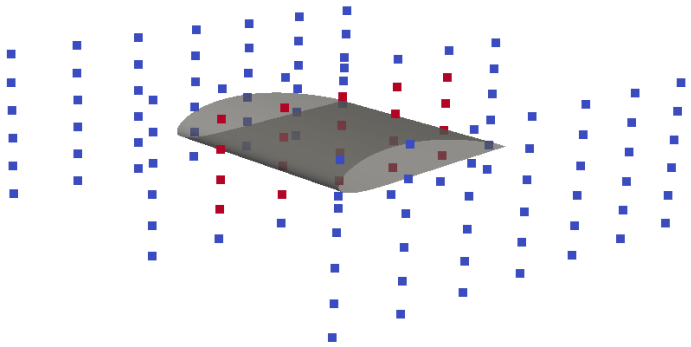

Σχήμα Α΄.1: *Παραμετροποίηση πλέγματος γύρω από την αεροτομή με ογκομετρικές B-splines. Τα σημεία ελέγχου με κόκκινα χρώμα είναι ενεργά και επιτρέπεται η κίνηση τους ενώ αυτά που είναι σηματοδοτούμενα με μπλε χρώμα παραμένουν σταθερά. Η ροή είναι αμιγώς 2Δ καθώς δεν γίνεται επίλυση της ταχύτητας ως προς τη z συνιστώσα. Τα ενεργά σημεία ελέγχου δεν μετακινούνται κατά τη z κατεύθυνση. Παρότι το πλέγμα ελέγχου είναι 3Δ δεν συμβαίνει στρέβλωση της επιφάνειας της αεροτομής κατά τη z διεύθυνση γεγονός που εξασφαλίζεται από τη συμμετρία των συναρτήσεων βάσης.*

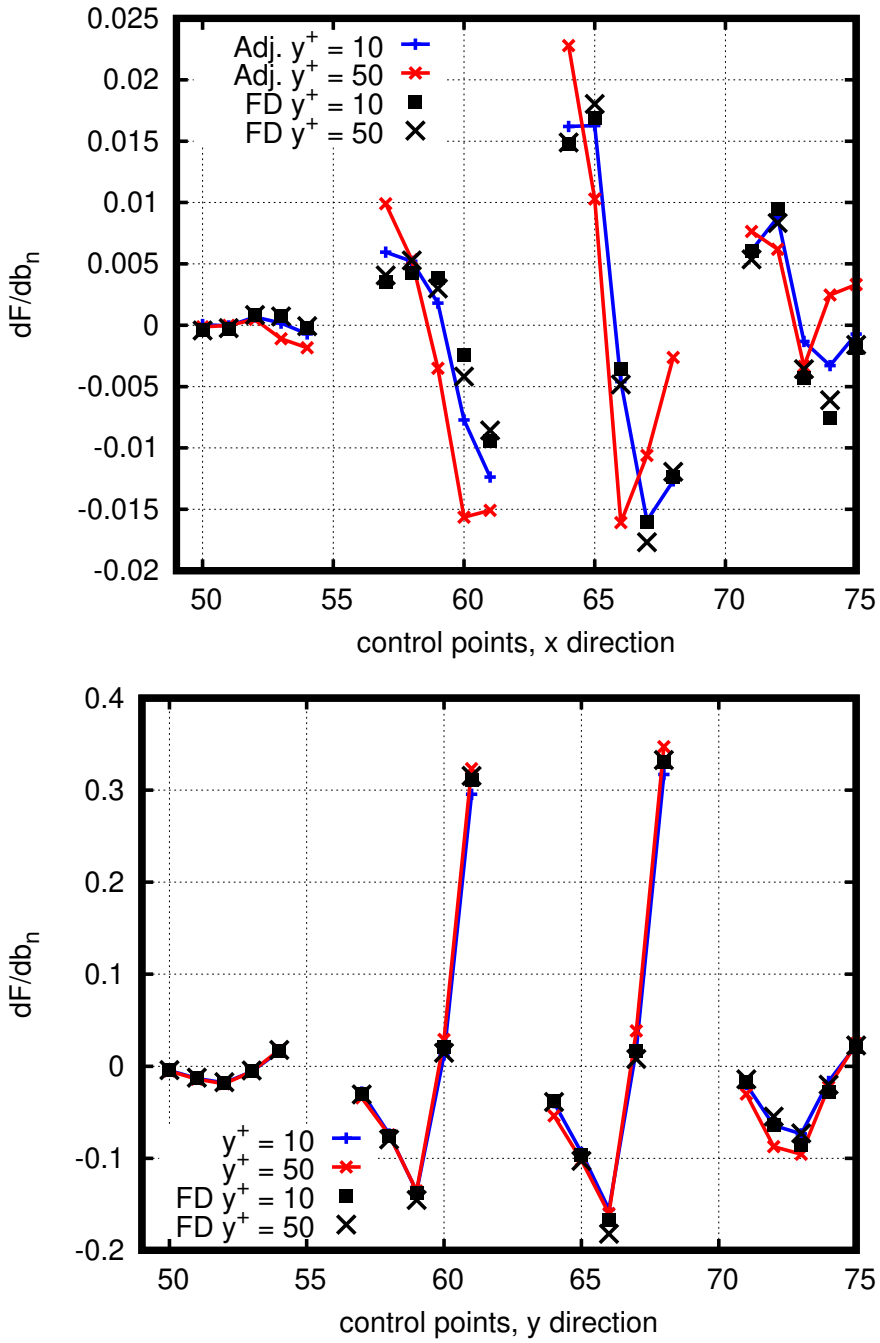

Σχήμα Α′.2: *NACA4415, $Re = 6 \times 10^6$, a=3º. Σύγκριση παραγώγων ευαισθησίας για δύναμη άνωσης υπολογιζόμενες με τη συζυγή μέθοδο, για y^+=10 και y^+=50. Η σύγκριση γίνεται με παραγώγους αναφοράς που έχουν υπολογιστεί με πεπερασμένες διαφορές. Τα σημεία ελέγχου μετακινούνται προς στις κατευθύνσεις x (άνω) και y (κάτω). Στο αριστερό πλέγμα, η ακρίβεια των παραγώγων ευαισθησίας είναι χειρότερη.*

Βελτιστοποίηση Μορφής με Χρήση της Συζυγούς Μεθόδου σε Εξωτερική Αεροδυναμική

Η αεροτομή NACA4415 βελτιστοποιήθηκε με χρήση της συζυγούς μεθόδου με στόχο την μέγιστη δύναμη άνωσης για y^+=10. Η πορεία της σύγκλισης φαίνεται στο Σχήμα Α΄.3 ενώ στο σχήμα Α΄.4 συγκρίνονται η αρχική και η τελική μορφή της αεροτομής. Παρατηρώντας το πεδίο της πίεσης (βλ. Σχήμα Α΄.5), είναι φανερό ότι η άνωση προκαλλείται από το πίσω μέρος της αεροτομής, γεγονός που σημαίνει ότι σε μία βιομηχανική περίπτωση θα έπρεπε να επιβληθεί επιπλέον περιορισμός ως προς τη ροπή γύρω από τον άξονα που είναι κάθετος στο επίπεδο της επιφάνειας που απεικονίζεται στο Σχήμα Α΄.4. Αντίστοιχη βελτιστοποίηση έγινε και για ελαχιστοποίηση της οπισθέλκουσας, η παρουσίαση της οποίας παραλείπεται εδώ για λόγους συντομίας.

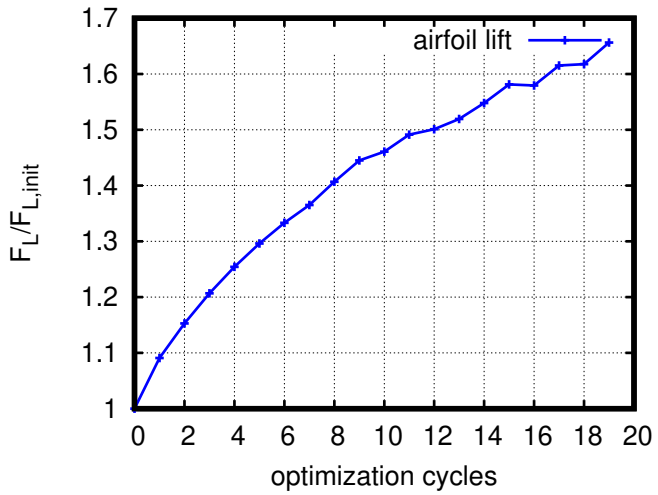

Σχήμα Α΄.3: *NACA4415, $y^+ = 10$, $Re = 6 \times 10^6$, a=3°. Μεγιστοποίηση ανωστικής δύναμης - Πορεία σύγκλισης της αντικειμενικής συνάρτησης. Το κέρδος από τη βελτιστοποίηση σχήματος είναι περίπου 65%. Η τιμή της αντικειμενικής συνάρτησης κανονικοποιείται βάσει της αρχικής της τιμής.*

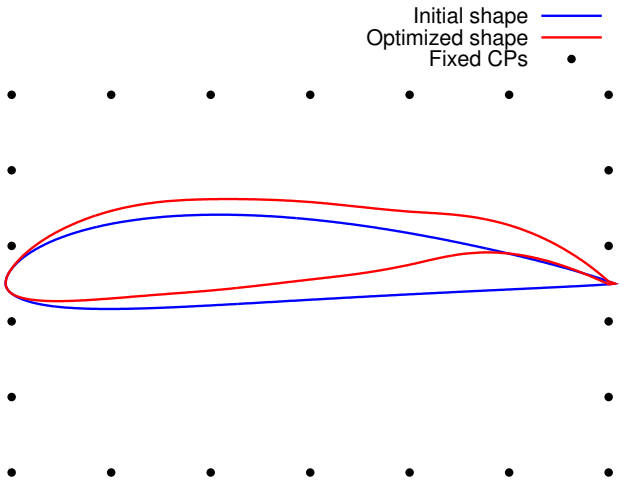

Σχήμα Α′.4: *NACA4415,* $y^+ = 10$, $Re = 6 \times 10^6$, a=3^o. *Αρχική (μπλε) και βέλτιστη (κόκκινο) επιφάνεια αεροτομής. Οι θέσεις των σημείων ελέγχου φαίνονται για την αρχική και τελική διάταξη.*

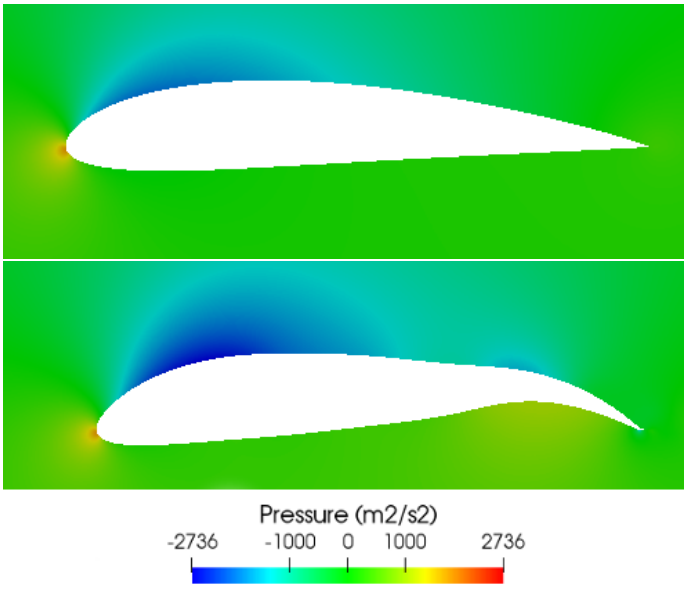

Σχήμα Α′.5: *NACA4415,* $y^+ = 10$, $Re = 6 \times 10^6$, a=3^o. *Κατανομή πίεσης γύρω από την αεροτομή στην αρχική (άνω) και βέλτιστη (κάτω) γεωμετρία. Η αύξηση στη δύναμη άνωσης προέρχεται από το πίσω μέρος της αεροτομής.*

Βελτιστοποίηση Μορφής με Χρήση της Συζυγούς Μεθόδου σε Εσωτερική Αεροδυναμική

Πραγματοποιήθηκε ελαχιστοποίηση ολικών απωλειών πίεσης σε τρεις διαφορετικές περιπτώσεις, ενός 2Δ αγωγού σχήματος U, ενός 3Δ αγωγού σχήματος S και ενός HVAC αγωγού. Χάριν συντομίας, παρουσιάζονται τα αποτελέσματα μόνο από τη βελτιστοποίη-

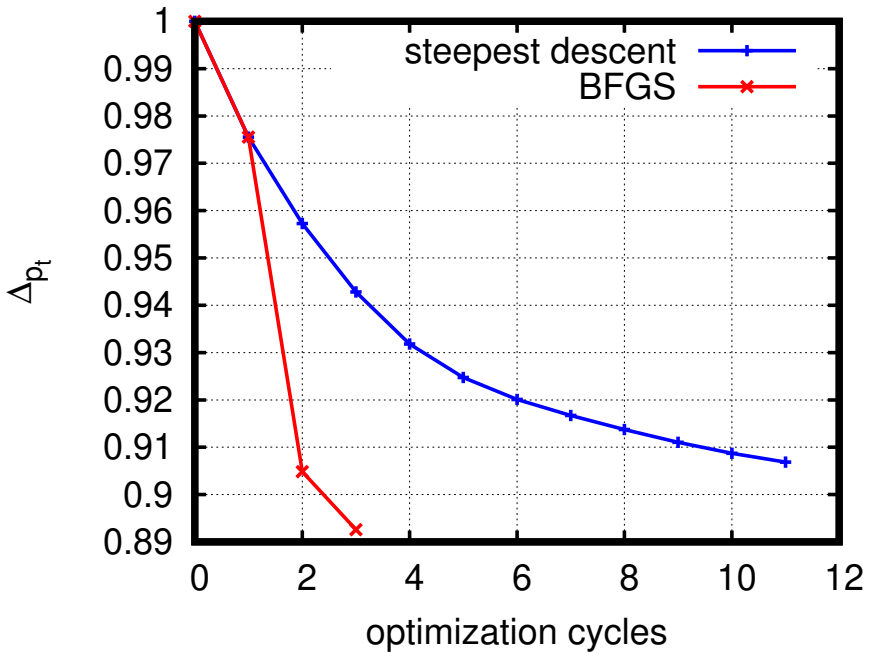

Σχήμα Α′.6: *HVAC duct,* $Re = 13800$. *Πορεία σύγκλισης της αντικειμενικής συνάρτησης* Δ_{P_t}. *Οι δύο μέθοδοι βελτιστοποίησης συγκρίνονται ως προς την ταχύτητα σύγκλισης. Η BFGS ελαχιστοποιεί την αντικειμενική συνάρτηση γρηγορότερα από ότι η μέθοδος της απότομης καθόδου (steepest descent).*

ση που εφαρμόστηκε στον HVAC αγωγό. Η σύγκλιση της αντικειμενικής συνάρτησης παρουσιάζεται στο Σχήμα Α′.6. Για τη βελτιστοποίηση χρησιμοποιήθηκαν δύο μέθοδοι, η μέθοδος της απότομης καθόδου και η BFGS, μια σύντομη περιγραφή των οποίων γίνεται στο υποκεφάλαιο 3.7. Η σύγκριση της αρχικής και της τελικής γεωμετρίας παρουσιάζεται στο Σχήμα Α′.7.

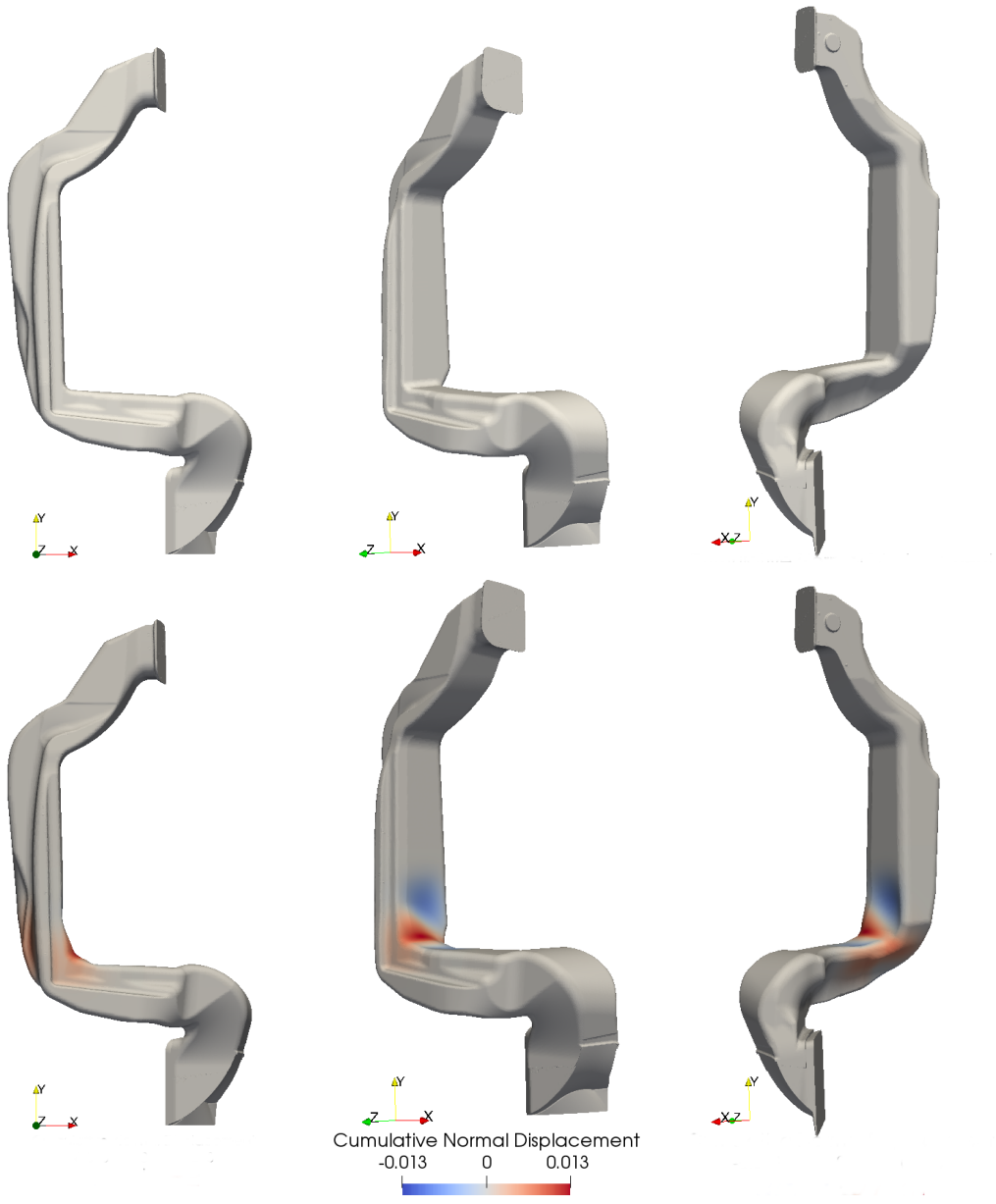

Σχήμα Α′.7: *HVAC duct, Re* = 13800. *Αρχική (άνω) και βέλτιστη (κάτω) γεωμετρία. Η αθροιστική κάθετη μετατόπιση υποδεικνύει τη διεύθυνση κατά την οποία μετακινείται η επιφάνεια του αγωγού, είτε προς το εξωτερικό (κόκκινο) είτε προς το εσωτερικό (μπλε).*

Συνεισφορές στην Περαιτέρω Ανάπτυξη του Κώδικα

Επιπλέον των έως τώρα παρουσιαζόμενων αποτελεσμάτων έγινε μία διερεύνηση των δυνατοτήτων επέκτασης του υφιστάμενου κώδικα με απώτερο σκοπό την βελτίωση της ακρίβειας των παραγώγων ευαισθησίας. Η πρώτη διερεύνηση αφορούσε στην εφαρμογή μίας πρώτης τάξης ακρίβειας προεκβολής της πίεσης από το κέντρο του κελιού δίπλα στον τοίχο επάνω στον τοίχο. Το OpenFOAM χρησιμοποιεί μηδενικής τάξης ακρίβειας προεκβολή (εξ. 5.1) και, στη βιβλιογραφία [16], έχει αναφερθεί πως, ανάλογα με τις συνθήκες ροής, αυτό μπορεί να επιφέρει δυσκολίες στη σύγκλιση των συζυγών εξισώσεων λόγω υψηλών τιμών ATC κοντά στον τοίχο [16]. Η οριακή συνθήκη που εφαρμόστηκε περιγράφεται από τη σχέση

$$p_b = p_c + \left.\frac{\partial p}{\partial x_i}\right|_c \Delta_i \tag{A′.21}$$

όπου p_b είναι η πίεση επάνω στον τοίχο, p_c η τιμή της πίεσης στο βαρύκεντρο του κελιού, που έχει ως οριακή ‘‘φάτσα’’ τον τοίχο, και Δ_i το διάνυσμα που ενώνει το κέντρο του κελιού c με τον τοίχο. Τα αποτελέσματα από την εφαρμογή αυτής της οριακής συνθήκης ως προς την ακρίβεια των παραγώγων ευαισθησίας και που αφορούν παραγώγους της δύναμης άνωσης αναδεικνύονται στο σχήμα A′.8. Τα αποτελέσματα προέρχονται από την παραμετρική μελέτη που περιγράφεται αναλυτικότερα στο κεφάλαιο 5 και εφαρμόστηκαν στην αεροτομή NACA4415 για $y^+ = 10$.

Παράλληλα, διερευνήθηκε η επίδραση του παρακάτω όρου, επονομαζόμενου ως T_{SD}, ο οποίος περιλαμβάνεται στην έκφραση των παραγώγων ευαισθησίας και προέρχεται από τη διαφόριση των συναρτήσεων τοίχου

$$T_{SD} = \int_{S_{Wp}} \left(-u_i t_i^I + \frac{\partial F_{S_{Wp},k}}{\partial \tau_{ij}} n_k t_i^I n_j + \frac{\partial F_{S_{Wp},k}}{\partial \tau_{ij}} n_k t_j^I n_i \right) \tau_{ij} \frac{\delta \left(n_j t_i^I \right)}{\delta b_n} dS \tag{A′.22}$$

Αρχικά είχε υποτεθεί πως ο όρος αυτός θα έχει σχεδόν μηδενική συνεισφορά στις παραγώγους ευαισθησίας (βλ. κεφάλαιο 5) όμως σε γεωμετρίες των οποίων το παραμετροποιημένο όριο παρουσιάζει αυξημένη καμπυλότητα, όπως η περίπτωση του αγωγού σχήματος U, θα μπορούσε αυτή η υπόθεση να μην ισχύει. Η υπόθεση αυτή επανεξετάστηκε και τα αποτελέσματα παρουσιάζονται στο σχήμα A′.9

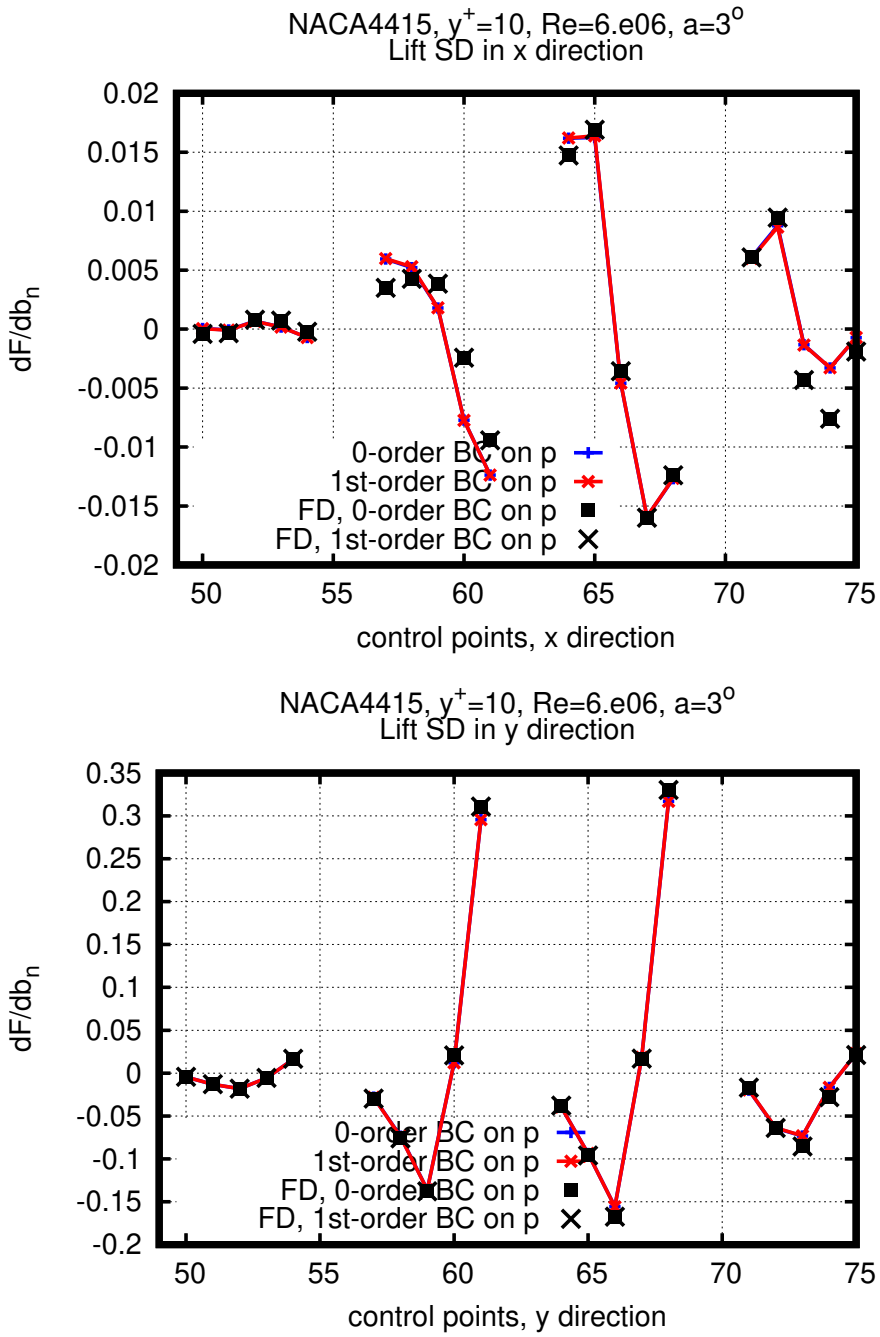

Σχήμα Α'.8: *NACA4415,* $y^+ = 10$, $Re = 6 \times 10^6$, *a=3º. Παράγωγοι ευαισθησίας που έχουν υπολογιστεί με τη συζυγή μέθοδο. Το πρωτεύον πρόβλημα έχει λυθεί χρησιμοποιώντας μηδενικής τάξης (μπλε) και πρώτης τάξης (κόκκινο) προεκβολή για την πίεση. Παράγωγοι ευαισθησίας που έχουν υπολογιστεί με πεπερασμένες διαφορές και λειτουργούν ως ένα επίπεδο αναφοράς ακολουθούν το ίδιο μοτίβο. Το πεδίο συζυγούς πίεσης έχει υπολογιστεί χρησιμοποιώντας προεκβολή μηδενικής τάξης. Τα σημεία ελέγχου αφορούν τη* x *διεύθυνση (άνω) και τη* y *διεύθυνση (κάτω).*

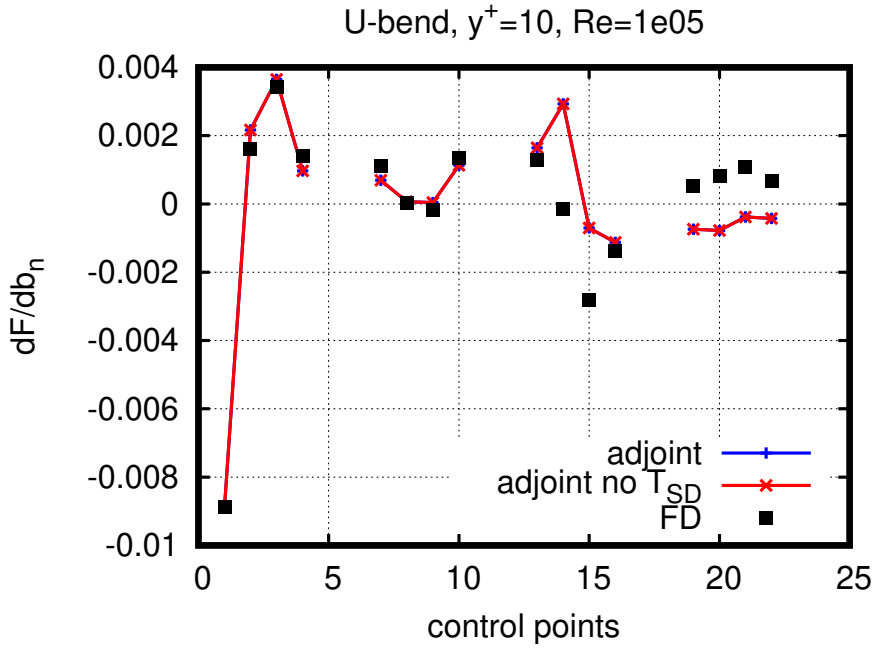

Σχήμα Α′.9: *U-bend,* $y^+ \approx 10$*,* $Re = 1 \times 10^5$*. Αξιολόγηση της συνεισφοράς του όρου* T_{SD} *στον υπολογισμό των παραγώγων ευαισθησίας.*

Συμπεράσματα

Το πρώτο τμήμα της εργασίας αφιερώθηκε στην επικύρωση του κώδικα ως προς την ακρίβεια των παραγώγων ευαισθησίας και τη δυνατότητα εκτέλεσης επιτυχημένων βρόχων βελτιστοποίησης σε τυρβώδεις ροές που επιλύονται σε αραιά πλέγματα. Οι μελέτες περίπτωσης που εξετάστηκαν ήταν: η ελαχιστοποίηση οπισθέλκουσας και η μεγιστοποίηση του συντελεστή άνωσης σε μία NACA4415 και η ελαχιστοποίηση ολικών απωλειών πίεσης Δ_{P_t} σε έναν 2D αγωγό σχήματος U, έναν 3D αγωγό σχήματος S και έναν HVAC αγωγό. Στην NACA4415, η ακρίβεια των παραγώγων ευαισθησίας φθίνει από y^+=10 σε y^+=50. Η βελτιστοποίηση έγινε σε πλέγμα με y^+=10 και ήταν επιτυχής για τις δύο αντικειμενικές συναρτήσεις, άνωση και οπισθέλκουσα.

Στις περιπτώσεις εσωτερικής αεροδυναμικής που εξετάστηκαν, ο κώδικας κατάφερε με επιτυχία να παράξει γεωμετρίες στις οποίες η απώλειες ολικής πίεσης μειώθηκαν. Στις 3Δ περιπτώσεις, το κέρδος από τη βελτιστοποίηση ήταν 25% στον αγωγό σχήματος S και 9% ή 11% στον HVAC αγωγό, ανάλογα με τη μέθοδο βελτιστοποίησης που χρησιμοποιήθηκε, ήτοι απότομη κάθοδος ή BFGS. Παρατηρήθηκε δυσκολία στη σύγκλιση των συζυγών εξισώσεων μετά από ορισμένους κύκλους βελτιστοποίησης, η οποία δυσκολία οφείλεται κατά πάσα πιθανότητα στην εμφάνιση μη-μόνιμων πεδίων ροής.

Στο δεύτερο μέρος της εργασίας έγινε διερεύνηση της δυνατότητας επέκτασης του κώδικα με στόχο τη βελτίωση της ακρίβειας των παραγώγων ευαισθησίας. Η οριακ-

κή συνθήκη που εφαρμόστηκε για την πρώτης τάξης ακρίβειας προεκβολή της πίεσης στον τοίχο εξετάστηκε ως προς την επίδραση που έχει στην ακρίβεια των παραγώγων ευαισθησίας. Προκύπτει όμως συμπερασματικά πως δεν έχει επίδραση στην ακρίβεια αυτών. Το ίδιο ισχύει και για τον όρο T_{SD} που, όπως συζητήθηκε, έχει μηδαμινή επίδραση στη διαμόρφωση της τιμής των παραγώγων ευαισθησίας.

Βιβλιογραφία

[1] Nadarajah, S. K. and A., Jameson: *A comparison of the continuous and discrete adjoint approach to automatic aerodynamic optimization.* AIAA Paper 2000-0667, AIAA 38th. Aerospace Sciences Meeting and Exhibit, Reno, NV, 2000.

[2] Giles, M.B. and Pierce., N.A.: *An intoroduction to the adjoint approach to design.* Flow, Turbulence and Combustion, 65:393–415, 2000.

[3] Papoutsis-Kiachagias, E.: *Adjoint methods for turbulent flows, applied to shape and topology optimization and robust design.* PhD thesis, Lab. of Thermal Turbomachines, N.T.U.A., Athens, 2013.

[4] Kavvadias, I.: *Continuous adjoint methods for steady and unsteady turbulent flows with emphasis on the accuracy of sensitvity derivatives.* PhD thesis, Lab. of Thermal Turbomachines, N.T.U.A., Athens, 2015.

[5] Ζυμάρης, Α.: *Συζυγείς μέθοδοι για το σχεδιασμό μορφών με βέλτιστη αεροδυναμική συμπεριφορά σε στρωτές και τυρβώδεις ροές.* Διδακτορική διατριβή, Εργαστήριο Θερμικών Στροβιλομηχανών, Ε.Μ.Π., Αθήνα, 2010.

[6] Zymaris, A.S., Papadimitriou, D.I., Giannakoglou, K.C., and Othmer, C.: *Continuous adjoint approach to the spalart-allmaras turbulence model for incompressible flows.* Computers & Fluids, 38(8):1528–1538, 2009.

[7] Zymaris, A.S., Papadimitriou, D.I., Giannakoglou, K.C., and Othmer, C.: *Adjoint wall-functions: A new concept for use in aerodynamic shape optimization.* Journal of Computational Physics, 229(13):5228–5245, 2010.

[8] Papoutsis-Kiachagias, E.M., Zymaris, A.S., Kavvadias, I.S., Papadimitriou, D.I., and Giannakoglou, K.C.: *The continuous adjoint approach to the $k-\epsilon$ turbulence model for shape optimization and optimal active control of turbulent flows.* Engineering Optimization, 47(3):370–389, 2015.

[9] *OpenFOAM User's Guide*. 2014.

[10] Spalart, P. and Allmaras, S.: *A one-equation turbulence model for aerodynamic flows.* AIAA Paper 1992-439, 30th Aerospace Sciences Meeting and Exhibit, Reno, Nevada, USA, January 6–9 1992.

[11] Spalding, D. B.: *A single formula for the law of the wall.* Journal of Applied Mechanics, 28:455–457, 1961.

[12] Papadimitriou, D.I.: *Adjoint formulations for the analysis and design of turbomachinery cascades and optimal grid adaptation using a posteriori error analysis.* PhD thesis, Lab. of Thermal Turbomachines, N.T.U.A., Athens, 2007.

[13] Papoutsis-Kiachagias, E.M., Asouti, V.G., Giannakoglou, K.C., Gkagkas, K., Shimokawa, S., and Itakura, E.: *Multi-point aerodynamic shape optimization of cars based on continuous adjoint.* Structural and Multidisciplinary Optimization, 59(2):675–694, 2019.

[14] Nocedal, J. and Wright, S.J.: *Numerical Optimization.* Springer, 1999.

[15] Karoni, K.: *Aeroacoustic Prediction and Adjoint-based Shape Optimization.* MSc Thesis. Lab. of Thermal Turbomachines, N.T.U.A., 2018.

[16] Karpouzas, K.G.: *A Hybrid Method for Shape and Topology Optimization in Fluid Mechanics.* PhD thesis, Lab. of Thermal Turbomachines, N.T.U.A., Athens, 2019.